Determination of heavy metals at the electrochemically reduced graphene oxide mercury film electrode (ERGO-HgF-PGE) using Adsorptive Stripping Voltammetry

UNIVERSITY *of the* **WESTERN CAPE**

By

Nelia Abraham Sanga

BSc (Hons) Chemistry (University of Western Cape)

A thesis submitted in fulfilment of the requirements for the degree of

Magistrate Scientiae in Chemistry

Supervisor: Prof. Nazeem Jahed

Co-supervisor: Prof. Emmanuel. I. Iwuoha

Co-supervisor: Dr. Keagan Pokpas

May 2020

i

Cupferron

Graphene

Pencil graphite electrode (PGE)

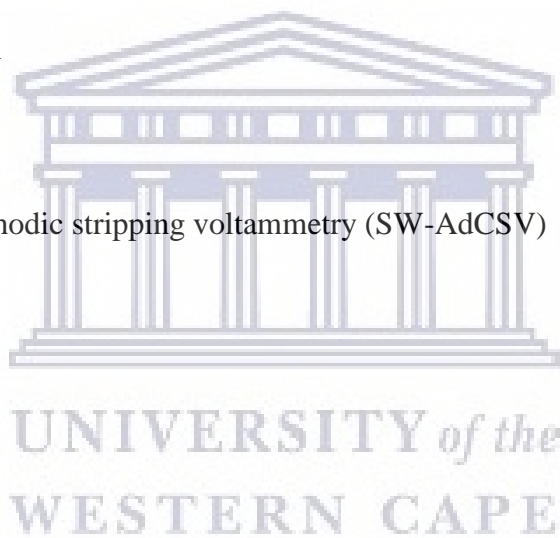Electrochemically reduced graphene oxide pencil graphite electrode (ERGO-PGE)

Thin mercury film

Trace metal analysis

Simultaneous determination

Cd^{2+}, Cu^{2+}, Pb^{2+} and Zn^{2+}

Square wave adsorptive cathodic stripping voltammetry (SW-AdCSV)

Water sample

Abstract

This work reports the use of a pencil graphite electrode (PGE) as inexpensive and sensitive electrochemical sensing platform fabricated by using electrochemically reduced graphene oxide (ERGO) in conjunction with an *in-situ* plated thin mercury film. For the first time the ERGO-HgF-PGE sensor is proposed for simultaneous detection of cadmium (Cd^{2+}), copper (Cu^{2+}), lead (Pb^{2+}) and zinc (Zn^{2+}) using N-Nitroso-N-phenylhydroxylamine (cupferron) as complexing agent by square-wave adsorptive cathodic stripping voltammetry (SW-AdCSV). The technique is based on the adsorption of cupferron- metal ion complexes onto the surface of the ERGO-HgF-PGE at 0.1 V for 60 s carried out in 0.1 M acetate buffer solution (pH 4.6). The synthesized graphene oxide (GO) and graphene nanosheets (GNs) were characterized using different analytical techniques such as FT-IR which confirms the presence of oxygen moieties embedded in the graphitic structure and further demonstrated by UV-Vis, validating the synthesis of GO. HR-TEM analysis confirmed the exfoliation of graphite to form single and few-layer graphene nanosheet (GNs). The structure and morphologies of GO were examined by XRD and HR-SEM, respectively. Moreover, instrumental parameters such as deposition time, amplitude and frequency were investigated and optimized for maximum electrode response including the influence of pH, supporting electrolytes, mercury concentration and cupferron concentration. Well-defined peaks were observed under optimal experimental conditions with detection limits of 0.17 μg.L^{-1} for Cd^{2+}, 0.02 μg.L^{-1} for Cu^{2+}, 0.17 μg.L^{-1} for Pb^{2+} and 0.14 μg.L^{-1} for Zn^{2+} at a deposition time of 60 s. The SW-AdCSV was applied successfully to the determination of trace heavy metals in tap water with satisfactory results below the United States Environmental Protection Agency (US-EPA) maximum contaminant level for zinc (5 mg.L^{-1}), cadmium (0.003 mg.L^{-1}), lead (0.02 mg.L^{-1}) and copper (0.05 mg.L^{-1}) in drinking water.
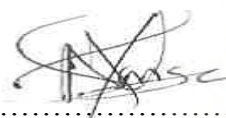
Declaration

I declare that *Determination of heavy metals at the electrochemically reduced graphene oxide mercury film electrode (ERGO-HgF-PGE) using Adsorptive Stripping Voltammetry* is my own work, that has not been submitted for any degree or examination at any universities and that all the sources I have used or quoted have been properly indicated and acknowledged by complete references.

Nelia Abraham Sanga   **May 2020**

Signed……………………………………………….

iv

Acknowledgments

I give thanks to the Lord GOD almighty for his amazing grace, love, protection and the gift of life and abundance blessings in my life. I will keep on trusting you GOD for my future. Thank you, Lord.

I would like to express my sincere and deepest gratitude to my supervisor **Prof. Nazeem Jahed** for the opportunity given to work with him on this project, his guidance and support throughout the entire project.

I owe my special thanks and sincere appreciation to my co-supervisor **Prof. Emmanuel. I. Iwuoha** for giving me this opportunity, his financial support and helping me to further my studies.

I am extremely grateful to **Dr. Keagan Pokpas** for sharing his knowledge, experience, invaluable advice and patience was of great value for my progress during the entire study.

I would like to express my deepest gratitude to my parents, **Mr. Bryn Russell**, granny **Geraldine** and my family for believing in me, their moral support, encouragement, prayers and love.

I would like to thank my fiancé **Sazi Selby Thwala** for always being there for me academically and emotionally.

I thank my colleagues **Zandile Leve, Kelechi Nwambaekwe** and **Kevin Tambwe** for the ideas shared, emotional support and encouragement during the entire study. Furthermore, I thank chemistry department and sensor labs, for allowing me to widen my horizons in chemistry field.

Acronyms and Abbreviations

AAS	Atomic absorption spectrometry
ABS	Acetate buffer solution
AdSV	Adsorptive stripping voltammetry
AE	Auxiliary electrode
Ag\AgCl	Silver silver chloride
Au	Gold
ASV	Anodic stripping voltammetry
BiFE	Bismuth film electrode
C	Carbon
CE	Counter electrode
CNT	Carbon nanotube
Cup	Cupferron
CPE	Carbon paste electrode
CSV	Cathodic stripping voltammetry
CV	Cyclic voltammetry
CVD	Chemical voltammetry deposition
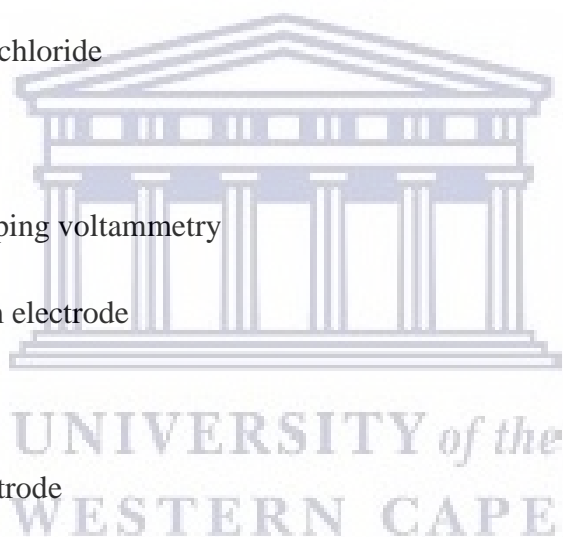
DL   Detection limit

DPV   Differential pulse voltammetry

EPA   Environmental protection agency

ERGO   Electrochemical reduced graphene oxide

FAAS   Flame atomic absorption spectrophotometry

FT-IR   Fourier transformed spectroscopy

GCE   Glassy carbon electrode

GE   Gold electrode

GFAAS   Graphite furnace atomic absorption spectroscopy

GO   Graphene oxide

Gr   Graphene

GNs   Graphene nanosheets

Hg   Mercury

HMDE   Hanging mercury drop electrode

HRTEM   High resolution transmission electron microscopy

HRSEM   High resolution scanning electron microscopy

ICP-OES   Coupled plasma optical emission spectrometry

HgFE   Mercury film electrode

L   Ligand

vii
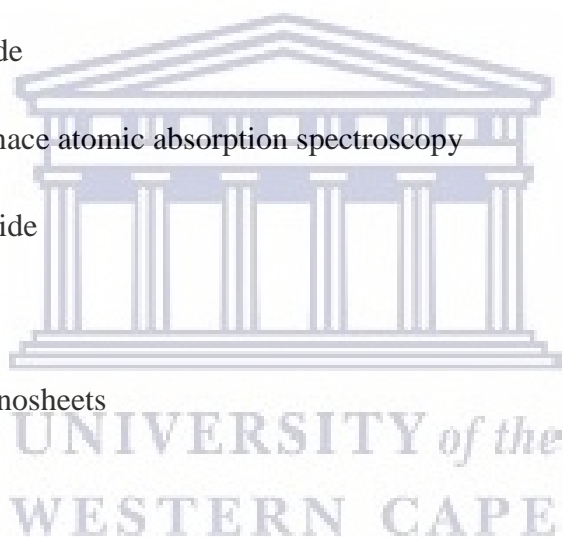
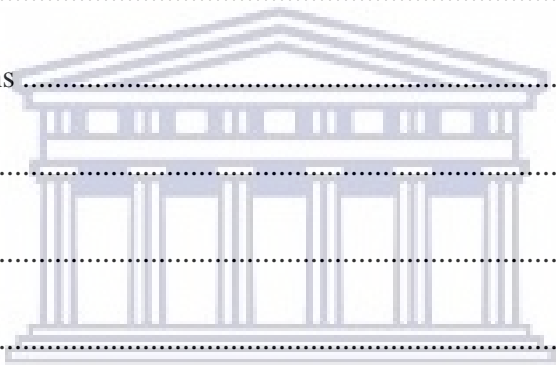|	
LCD	Liquid crystal display
LED	Light emitting diode
LOD	Limit of detection
LOQ	Limit of quantification
NCBiFE	Nafion coated bismuth film
N. D	Not determined
OLED	Organic light emitting diode
PGE	Pencil graphite electrode
PPB	Parts per billion
Pt	Platinum
RE	Reference electrode
Red-Ox	Reduction oxidation
RGO	Reduced graphene oxide
RPM	Revolution per minutes
RSD	Relative standard deviation
SbFE	Antimony film electrode
SCE	Saturated calomel electrode
SEM	Scanning electron microscopy
SHE	Standard hydrogen electrode

viii
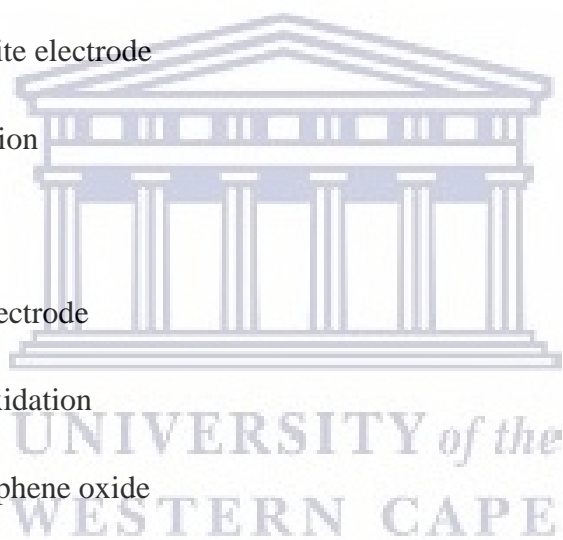
SV	Stripping voltammetry
SWSV	Square wave stripping voltammetry
TEM	Transmission electron microscopy
TMFE	Thin mercury film electrode
WE	Working electrode
WHO	World health organization
XRD	X-ray diffraction
0D	Zero dimensional
1D	One dimensional
2D	Two dimensional
3D	Three dimensional

Contents

xi

xiv

List of Figures

xvi

xviii

UNIVERSITY *of the*

WESTERN CAPE

List of Tables

CHAPTER ONE

1. Introduction

This chapter provides a brief background on heavy metal pollution in the environment, its exposure to mainstream water samples and therefore its effects on human health. Herein, the use of various electrochemical techniques and their associated literature, which have commonly been used in trace metal analysis, are discussed. A brief overview of the problem statement, aim, objectives, research questions, hypothesis and methodological approach are presented. The chapter goes further and briefly covers the novelty of the research study and thesis layout.

1.1 Background of the study

1.1.1 Heavy metal pollution and poisoning

Environmental pollution from heavy metals has been one of the most serious issues in the world, with ever increasing demand for these metals in many areas, such as agriculture, industry, rapid population growth as a result of urbanization, medical and technological advances over the years, thus increasing their exposure in the environment [1, 2]. Heavy metals in water can be caused by either natural processes (weathering and erosion of bed rocks and ore deposits) or anthropogenic activities (mining, industries, irrigation of wastewater and agriculture activities) [3]. Poor disposal of industrial effluents, domestic and agricultural waste, into water bodies further increases heavy metal pollution [4, 5]. Owing to their high toxicity and bio-accumulative nature in the environment even at trace levels, it's enough to endanger human health and biotic life [6]. The need for clean drinking water is crucial for human survival [7], and past studies have shown that drinking water is highly contaminated by heavy metals which are usually linked to human poisoning. Consequently, organizations such as the World Health Organization (WHO), have set the maximum permissible limits for heavy metals in drinking water namely, zinc (5 mg.L^{-1}), cadmium (0.003 mg.L^{-1}), lead (0.01 mg.L^{-1}) and copper (2 mg.L^{-1}) [8–10] among others. According to the United States environmental protection agency (US-EPA) permissible levels of zinc (5 -15 mg.L^{-1}), cadmium (0.003 mg.L^{-1}), lead (0.02 mg.L^{-1}) and copper (0.05 -1.50 mg.L^{-1})

1

are used to control water pollution [6, 11]. Human poisoning from water is often caused by an excess intake of heavy metals such as cadmium, chromium, manganese, arsenic and lead [12, 13]. However, few heavy metals are significant to human body growth namely copper, cobalt and zinc [12].

Cadmium is a toxic metal classified as a group one carcinogen [14, 15]. It, however has been desirable in the manufacturing of batteries, as well as in the aerospace, electroplating, automotive and metallurgy industries and thus the incorrect disposal of cadmium-containing products has been a major problem resulting in an increase in heavy metal pollution [16]. Cadmium is able to accumulate, even at lower concentrations within the human body [17, 18] and may cause illnesses such as Anemia by interacting with iron and decreasing hemoglobin levels, kidney stones, lung cancer and Itai Itai disease, which was prominent in Japan in 1960s as a result of Japanese ingestion of cadmium-contaminated rice [14, 19]. For this reason, the permissible level of cadmium in drinking water is 0.003 mg.L^{-1} as set by the World Health Organization (WHO) [11]. The total intake of cadmium should not exceed 1 μg.kg^{-1} of body weight per day [20]. Lead is a carcinogen metal that occurs naturally in the earth's crust. Lead poisoning in human bodies as well as environmental pollution is the consequence of sources such as mining, smelting, battery manufacturing, soldering, painting, cable sheathing, ceramics and fertilizers [21]. Almost every organ in the human body can be affected by lead, including bones, kidneys, reproductive system, intestines and the nervous system, due to its high bio-accumulative nature [22]. The maximum permissible level of lead in drinking water is 0.05 mg.L^{-1} according to the WHO [11]. Excessive consumption of lead has been known to result in miscarriage, kidney failure, mental retardation, stomach cancer, Anemia and infertility [8, 11, 23]. Zinc too is a natural metal present in water, food and soil [24] and is one of the most vital nutrients found throughout the human body. Among many advantageous properties, zinc has shown to be essential for growth, a healthy immune system, good metabolism, poor wound healing, taste and smell [2]. Deficiencies or low levels of zinc has been commonly associated with anorexia, neurosensory disorder, dermatitis, growth and mental retardation [14]. While, excessive concentrations of zinc may cause illnesses such as hypogonadism, prostate cancer, infertility and impotence [25]. Zinc deficiency was first identified in 1961, when Iranian males were diagnosed with zinc deficiency

symptoms such as hypogonadism and growth retardation [26]. Copper is an essential nutrient for many biological processes in the human body as a component of metallo-enzymes has been associated with hemoglobin formation, carbohydrate metabolism, the cross-linking of collagen, elastin, and hair keratin, and the antioxidant defense mechanism [27, 28]. Copper poisoning is mainly due to the consumption of food and drinking water, which may be attributed either to the leaching of copper from pipes (smelting, mining or copper-producing industries) into drinking water, or copper cookware as copper leeks from worn-out utensils into cooked food and to medicines such as birth control pills that increase the copper levels in the body [29–31]. High amounts of copper may lead to Anemia, Leukemia, kidney failure, and liver damages have been associated with copper build-up in the liver which may result in a genetic condition known as Wilson's disease, which was first identified in 1912 [32, 33]. The maximum contaminant level for copper is 2 mg.L^{-1} according to the WHO [9].

In this study, heavy metals such as zinc, copper, lead and cadmium present in tap water were investigated by adsorptive cathodic stripping voltammetry using reduced graphene oxide to electrochemically modify a pencil graphite electrode along with an *in-situ* plated mercury film and cupferron chelating agent. Heavy metal pollution has stirred a lot of attention due to the serious environmental and human health threats. The need to develop highly sensitive, reliable, fast, simple, reproducible and inexpensive analytical techniques for the detection and monitoring of trace heavy metals at very low concentrations in water is therefore crucial. Various analytical techniques have been used previously in literature for the detection of trace heavy metal ions.

1.1.2 Analytical techniques for heavy metal analysis

Commonly used analytical techniques in the detection of trace and ultra-trace levels of heavy metals includes graphite furnace atomic absorption spectrometry (GFAAS) [34], inductively coupled plasma optical emission spectrometry (ICP-OES) [35] and x-ray fluorescence (XRF) [36]. Although these spectroscopic techniques provide high sensitivity and selectivity unfortunately they are costly, requires highly skilled personnel, time consuming, and unsuitable for *in-situ* analysis [35–38]. Electrochemical techniques such as adsorptive stripping voltammetry (AdSV), anodic stripping voltammetry (ASV) and cathodic stripping voltammetry

3

(CSV) are considered promising heavy metal detection techniques due to high sensitivity, low detection limits, on site analysis, ease of miniaturization, cost effectiveness and the ability to determine multiple analytes [36, 37, 39, 40]. AdCSV offers lower limit of detection in the $ng.L^{-1}$ to $\mu g.L^{-1}$ range and standard addition than ASV [43, 44]. In this work, adsorptive cathodic stripping voltammetry (AdCSV) was developed for simultaneous detection of Cu^{2+}, Cd^{2+}, Zn^{2+} and Pb^{2+}-cupferron complexes at the electrochemically reduced pencil graphite electrode with an *in-situ* plated mercury thin film electrode (ERGO-HgF-PGE) in tap water samples. AdCSV is based on the adsorption of Zn^{2+}, Cu^{2+}, Cd^{2+} and Pb^{2+} after complexation with the cupferron complexing agent, followed by the reduction of the cupferron complexes by applying a negative going potential on the surface of ERGO-HgF-PGE. Previously reports showed successfully determination of Zn^{2+} [45], Cu^{2+} [46], Cd^{2+} [47] and Pb^{2+} [48] by AdCSV on a hanging mercury drop electrode (HMDE).

The choice of the working electrode is significant for a successful stripping process. Working electrodes have been widely used for the detection of heavy metals namely gold electrode (GE) [49], glassy carbon electrode (GCE) [50, 51], carbon paste [52, 53] and pencil graphite electrode (PGE) [54]. Among the various carbon-based electrodes, PGEs have been very effective in numerous investigations due to their remarkable properties such as being environmentally friendly, inexpensive, offering excellent sensitivity, high selectivity, good electrical conductivity, lower background current and good reproducibility [55, 56]. A number of studies have recently been reported on the use of PGEs for the determination of anticancer drugs [57], vitamin B_{12} [58], heavy metals [54, 55] and DNA [59]. In addition, mercury-based electrodes have been extensively used as working electrode material for AdSV such as mercury film electrode (HgFE) and the hanging mercury drop electrode (HMDE) owing to their exceptional sensitivity, reproducibility and large negative potential window [2, 39]. There have been a lot of restrictions on the use of HgFEs because of the high toxicity of mercury. Alternative conductive materials such as antimony (Sb), bismuth (Bi), lead (Pb), gold, carbon and silver (Ag) have been used as films while boron-doped diamond has also been used as an alternative to mercury-based electrodes due to their lower toxicity [1, 39]. The overall performance of these non-mercury electrodes has not been as effective as HgFEs, due to their low cathodic potential limit, multiple

4

peaks or large background.

1.1.3 Graphene

Graphene is a distinctive two-dimensional (2D) carbon allotrope, with a one-atom-thick planar sheet of carbon atoms densely packed in a honeycomb crystal lattice [60–62]. It can be wrapped up into 0D fullerene, rolled into 1D nanotube or stacked into 3D graphite [60, 61]. Since its discovery by K. S. Novoselov and A. K. Geim in 2004 [61], graphene has stirred-up a lot of research interest due to its exceptional and unique physical, electrical and mechanical properties. Countless studies have been conducted to explore the prospective applications of this wonder material. Graphene and reduced graphene oxide have been used as a surface modifier in many sensor applications, such as the use of graphene-based electrodes in detection of heavy metal in water. From our research group Pokpas *et al* first reported the use of nafion graphene dimethylglyoxime modified glassy carbon electrode (NGr-DMG-GCE) for the detection of nickel (Ni^{2+}). The use of graphene improved the sensitivity of the sensor due to the enhanced active surface area associated with its use and therefore showed better detection capabilities to nickel detection in water samples [51]. Tekenya *et al* further showed the use of the electrochemically reduced graphene oxide *in-situ* plated mercury film on the determination of nickel (Ni^{2+}) in the presence of dimethylglyoxime on a pencil graphite electrode [54]. The high surface area to volume ratio of graphene has improved many devices in energy storage and quick charging capacity [63]. Graphene has also exhibited high electric conductivity, transparency and has influenced optical electronics applications such as the manufacturing of transparent conducting electrodes that are crucial for touchscreens, liquid crystal displays (LCDs) and organic light emitting diodes (OLEDs) applications since the use of indium tin oxide (ITO) is costly and limited supply in the world [64].

1.2 Novelty of research study

The ever-increasing demand for heavy metals in various industrial applications and the growth in urbanization has had a huge impact on the exposure of highly toxic heavy metals into the environment. For this reason, the detection of trace heavy metals has become a priority

5

worldwide. In this paper a highly selective, simple, fast and sensitive square-wave adsorptive cathodic stripping voltammetric (SW-AdCSV) technique is reported and applied for the simultaneous determination of Zn^{2+}, Cu^{2+}, Cd^{2+} and Pb^{2+} in tap water samples at an electrochemically reduced graphene oxide pencil graphite electrode (ERGO-PGE) in conjunction with *in-situ* electroplated thin mercury film in the presence of cupferron complexing agent. To the best of our knowledge, this is the first report on the simultaneous detection of four metal ions (Zn^{2+}, Cu^{2+}, Cd^{2+} and Pb^{2+}) using cupferron as a complexing agent for complexation and adsorption of cupferron complexes on the electrochemically reduced graphene oxide pencil graphite electrodes in conjunction with an *in-situ* plated mercury film. Nearly all previous reports in literature performed trace metal detection with cupferron complexing agent on either a hanging mercury drop electrode (HMDE) or a nafion-coated bismuth film electrode (NCBiFE). Cd^{2+} [47, 65–67], Cu^{2+} [68], Pb^{2+} [48], Zn^{2+} [45, 47] were among the metal ions detected. Herein, a pencil graphite electrode is used as the working electrode for the adsorption of metal ion-chelating agent complexes on the electrochemically reduced graphene oxide pencil graphite electrode (ERGO-PGE) prepared using cyclic voltammetric reduction of graphene oxide in 0.1 M acetate buffer solution (pH 4.6) in combination with an *in-situ* plated thin mercury film for the simultaneous determination of Zn^{2+}, Cu^{2+}, Cd^{2+} and Pb^{2+}. ERGO and mercury films have been used to greatly improve the selectivity and sensitivity of the electrochemical sensor (ERGO-HgF-PGE). Further a square-wave adsorptive cathodic stripping voltammetry technique is developed for simultaneous detection of trace metal ions in tap water to provide a new, fast, cheap and extremely sensitive electrochemical sensor as an alternative to expensive sensors such as glassy carbon electrodes and hanging mercury drop electrode.

1.3 Aim

This study seeks to develop an ERGO-HgF-PGE as a fast, cheap and sensitive electrochemical sensor for the simultaneous detection of Zn^{2+}, Cu^{2+}, Cd^{2+} and Pb^{2+} in the presence of cupferron chelating agent in tap water samples using the adsorptive cathodic stripping voltammetry technique.

1.4 Objectives

The following objectives are to be achieved in order to carry out the research study:

- To study and comprehend the adsorptive stripping voltammetry technique.
- To synthesize graphite oxide using a modified Hummers method.
- To characterize graphene oxide using Fourier transform infrared spectroscopy, X-ray diffraction, Ultraviolet-visible spectroscopy, electrochemical impedance spectroscopy, High resolution transmission electron microscopy, High resolution scanning electron microscopy.
- To modify the surface of a pencil graphite electrode (PGE) through the electrochemical reduction of graphene oxide followed by the *in-situ* plating of a mercury film to form the ERGO-HgF-PGE.
- To investigate the electrochemically reduced mercury film pencil electrode (ERGO-HgF-PGE) responses towards the simultaneous detection of copper (Cu^{2+}), cadmium (Cd^{2+}), zinc (Zn^{2+}) and lead (Pb^{2+}) using cupferron ligand.
- To investigate the ERGO-HgF-PGE responses towards the cupferron complexing agent.
- To optimize instrumental parameters and determine the optimal instrumental parameters of the ERGO-HgF-PGE for copper (Cu^{2+}), cadmium (Cd^{2+}), zinc (Zn^{2+}) and lead (Pb^{2+}).
- To develop an analytical procedure for the determination of heavy metals in water samples using the ERGO-HgF-PGE.

1.5 Research questions

The aim of the study was to provide answers to the following questions:

- Could a pencil graphite electrode be a desirable electrochemical sensing platform for the detection of metal ions?
- Would ERGO, in conjunction with mercury thin films be able to enhance the sensitivity of the electrode in detection of Cu^{2+}, Cd^{2+}, Zn^{2+} and Pb^{2+} by AdCSV?
- Would the formation of cupferron-metal complexes in the presence of cupferron

7

chelating agent offer high selectivity and suitable electrode preconcentration for the trace metals investigated?

1.6 Hypothesis

Using electrochemically reduced graphene oxide together with an *in-situ* plated mercury film and cupferron chelating agent on the surface of the pencil graphite electrode can increase sensitivity and selectivity to detect trace heavy metals in tap water samples.

1.7 Research approach

In order to realize the aim and objectives of the research, the following experimental protocol was followed:

- Synthesis of graphite oxide by a modified Hummers method
- Preparation of graphene oxide colloidal solution
- Characterization of graphite, graphite oxide and graphene oxide
- Electrochemical characterization of the ERGO-PGE
- Adsorptive stripping voltammetry analysis
- Optimization of experimental conditions and instrumental parameters
- Analytical performance of the ERGO-HgF-PGE
- Recovery studies of test solutions
- Repeatability, reproducibility and stability
- Interference studies
- Analytical application to real water samples

1.8 Scope and delimitations

Pentel HB pencil lead 0.5 mm in diameter and length 60 mm bought from a local bookstore was used as a working electrode due to its advantages like inexpensive, eco-friendly, good stability and reproducibility. Tap water samples were collected from our laboratory for the detection of trace heavy metals present in tap water at the University of Western Cape in the municipal region

8

of Bellville in Cape Town, South Africa.

Figure 1.1 Location of the study area (water sampling region).

1.9 Thesis layout

The thesis is divided into seven chapters and is structured as follows:

Chapter one: Introduction

Chapter one sets out to provide the overall concept of the research study. A brief introduction to the pollution of heavy metals and the effect of heavy metal poisoning on human health is detailed. This section further summarizes various stripping techniques used for the determination of heavy metals to date as well as outlines the novelty of the research study by providing the aim and objectives to be achieved, the research approach.

Chapter two: Literature review

This chapter is based on a literature review of the relevant aspects of the research study, which focuses on the context of graphene, its properties and characterization techniques. It also provides information on the cupferron complexing agent and other complexing agents previously used for the formation of metal ion-chelating agent complexes. A detailed review of the mercury

9

film, pencil graphite electrode, and other reported electrodes involved in adsorptive stripping voltammetry are further provided. In addition, various voltammetry stripping techniques and their operating principles were further clarified.

Chapter three: Material and experimental method

This chapter provides a detailed summary of the instruments used in the research study, the experimental methods, chemicals and materials used to achieve the objectives presented in chapter one. The procedures involved in graphite oxide synthesis, characterization techniques, the electrochemical analysis, preparation of sample and standard solutions are also included in this chapter.

Chapter four: Morphology and structural characterization of graphite, graphite oxide and the ERGO-PGE.

The chapter describes the structural and morphological features of graphite, prepared graphite oxide through modified Hummers method and the electrochemically reduced graphene oxide pencil graphite electrode (ERGO-PGE) using various spectroscopic and microscopic techniques. The inclusion of oxygen within the graphitic structure are confirmed by Fourier transform infrared spectroscopy (FT-IR), electronic transitions of the samples are examined by Ultraviolet visible spectroscopy (UV-Vis) and the crystalline structure is determined by X-ray diffraction (XRD) analysis, while microscopic techniques such as High resolution transmission electron microscopy (HRTEM) confirms the exfoliation of graphene nanosheets and High resolution scanning electron microscopy (HRSEM) studies the surface morphologies of the unmodified and graphene modified PGE.

10

Chapter five: Preparation and electrochemical characterization of the ERGO-PGE

In this chapter, 1 mg.mL^{-1} graphene oxide colloidal solution is electrochemically reduced on the pencil graphite electrode (PGE) surface using cyclic voltammetry. The electrochemical properties of the fabricated ERGO-PGE are determined in acetate buffer solution, $[Fe(CN)_6]^{-3/-4}$ as redox probe by using cyclic voltammetry as well as the electrochemical impedance spectroscopy (EIS). The electrochemical parameters such as the surface coverage (Γ), electroactive surface area (A), the diffusion coefficient (D) and charge transfer resistance (Ω) are calculated.

Chapter six: The determination of metal ion- cupferron complexes on the ERGO-HgF-PGE and bare-PGE

Focusing on the investigation of simultaneous detection of cadmium (Cd^{2+}), copper (Cu^{2+}), zinc (Zn^{2+}) and lead (Pb^{2+}), optimization of instrumental parameters, recovery studies and calibration curves conducted on test solutions of known concentrations, real water sample analysis performed at the ERGO-HgF-PGEs as well as the interference study.

Chapter seven: Conclusions and Future work

This chapter summarizes the findings and highlights the novelty of the research study, sets out recommendations for further investigations and future work. The list of references used throughout the research study is presented as a separate section at the end of the thesis.

11

CHAPTER TWO

LITERATURE REVIEW

2. Introduction

This chapter presents a critical review of stripping voltammetry techniques for trace metal detection, various working electrodes and complexing agents used previously in literature relevant to the research study. A detailed background of graphene, its synthetic routes, microscopic and spectroscopic characterization techniques are also covered.

2.1 Voltammetry

Voltammetry, an electrochemical technique in which the current is measured as a function of the voltage obtained at the electrode and is widely used for variety of applications such as trace and ultra-trace metal ions, organic and inorganic materials [70, 71]. The main advantages of voltammetry are its remarkable sensitivity, selectivity, fast, low-cost instrumentation and minimal sample preparation [71]. Unlike potentiometric measurements which utilize two electrode system, voltammetric measurements are usually performed in an electrochemical cell consisting of three electrode systems, namely a working electrode (WE), a reference electrode (RE) and an auxiliary electrode (AE) or a counter electrode (CE) as shown in Figure 2.1. In addition, the nitrogen purge tube is used to remove dissolved oxygen, the stirrer bar is used to mix the solution and allow the mass transport of the analytes [72].

The working electrode is where the reaction of interest occurs. They are often made of inert metals classified as solid electrodes (platinum (Pt), gold (Au), silver (Ag)) or carbon materials (graphite, glassy carbon, carbon-paste electrodes) and liquid electrodes include hanging mercury drop electrodes [73]. A reference electrode, including saturated calomel electrode (SCE), silver/silver chloride (Ag/AgCl) electrode and standard hydrogen electrode (SHE) is often employed. Typically, they have a steady and known electrode potential that is used in the electrochemical cell as a point of reference for measuring the potential applied to the working electrode [74, 75]. Platinum electrode is usually preferred as auxiliary electrode due to its

12

inertness nature, high conductivity and stability. Counter electrodes control the current circuit in the cell system, it provides electrical current pathway to flow into an electrochemical cell without passing sufficient current through the reference electrode [74, 76]. The supporting electrolyte is an electrolyte solution that usually contains non-electro active ionic salt in a solvent present in the electrochemical cell. Thus, enabling the ability of electrolyte to carry electrical current due to high conductivity, usually supporting electrolytes must not get adsorbed on electrode surface, not form complexes with the analytes species of interest. A schematic representation of a three-electrode electrochemical cell system is presented as follows:
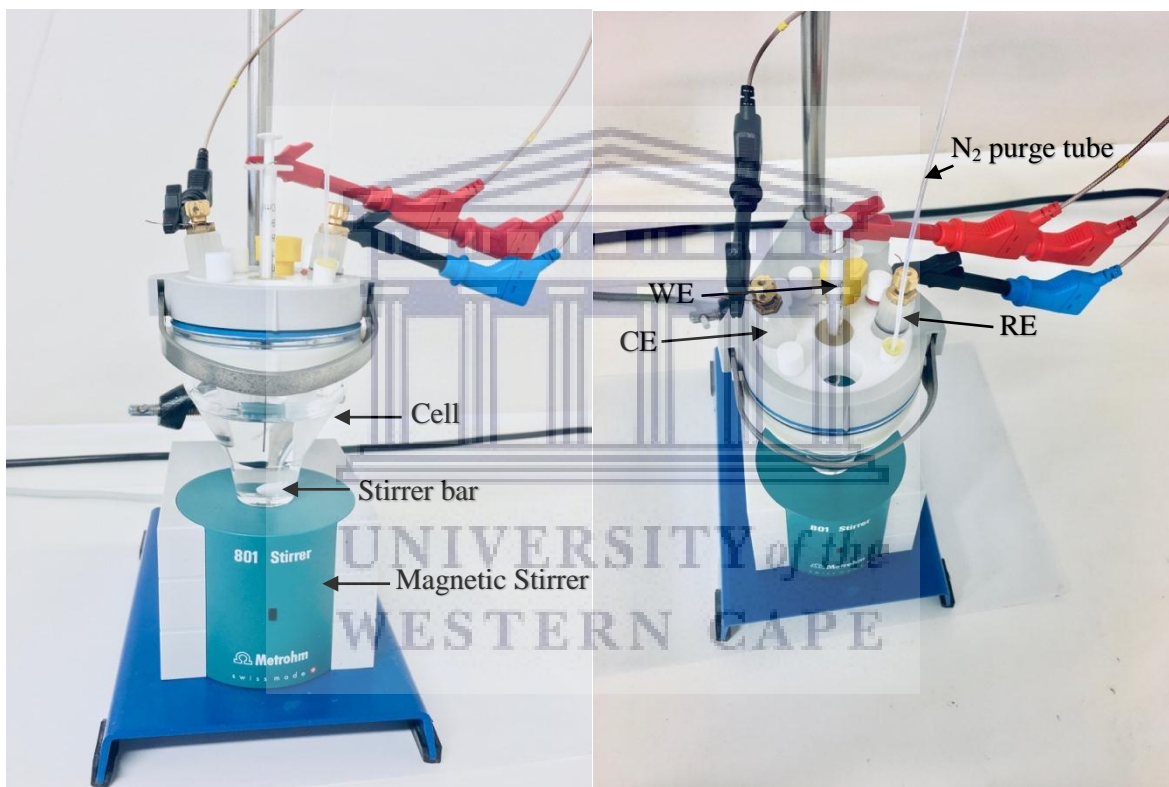
Figure 2.1 Schematic representation of a voltammetric electrochemical single cell and three electrodes system.

2.2 Stripping voltammetry

Stripping voltammetry is a very sensitive electroanalytical technique due to the pre-concentration step in which chemical species are accumulated and deposited on or into the electrode surface at

13

a constant potential. At the stripping step, the accumulated chemical species in the amalgam or film are stripped back into solution [70]. Stripping voltammetry allows analytical determinations of simultaneous of four to six trace and trace metals at low concentration sub-ppm level [76]. Stripping voltammetry involves three significant steps the pre-concentration step (accumulation step) which is based on the accumulation of analytes on the electrode surface, which is performed in a stirred solution under potential control for a certain period. The constant stirring of the solution enables the analytes to be transported massively to the electrode surface. In addition, when the analytes are deposited on or into amalgam-forming mercury electrodes, the stirring speed may not be too fast as the mercury film drops may deform and disrupt the film-forming process. Alloys are formed when bismuth, tin or antimony electrodes are used to accumulate alloy-forming metals electrolytically.

The pre-concentration step is responsible for the remarkable sensitivity of the stripping voltammetry. Rest period (equilibration time), the stirring of the solution is halted, and the solution can become inactive. The rest period extends to approximately 10 to 30 s so that the metal concentration in the amalgam ceases and reaches uniformity on the active surface of the electrode or on metal film where applied potential remains unchanged, ensuring that the metal is electro-deposited from the electrode surface is diffusion controlled and no convection transport of ions through the solution precedes the stripping step. After the pre-concentration step, the deposited analytes are stripped from the electrode surface back into the solution.

2.3 Stripping voltammetry techniques

Stripping processes for metal analysis typically involve oxidation or reduction of trace metals to its ionic form under conditions of diffusion control under an applied potential. By either applying adsorptive, anodic or cathodic potential sweeps, electrons are transferred because of the redox reactions and a resultant voltammogram is generated where the current is recorded as a function of the potential applied. Various types of stripping voltammetry such as anodic stripping voltammetry, cathodic stripping voltammetry and adsorptive stripping voltammetry have been used for trace metal analysis. In anodic stripping voltammetry (ASV), during deposition step analyte species are pre-concentrated onto the electrode surface with a constant stirring of the

14

solution and then stripped from the electrode surface to the solution by applying oxidizing potential. Most ASV technique have been successfully reported for the analysis of trace metals in conjunction with either HMDE or HgFE, which provides a high surface area to volume ratio resulting in increased sensitivity. While CSV, is based on the electrodeposition of analytes on the mercury electrode during the pre-concentration step by applying a positive current potential [42]. These techniques are not easily applicable for determination of numerous trace metals that cannot be deposited electrolytically, because of adsorption of interference of metal ions on the electrode surface that cause non-reproducible results [77]. However, AdCSV offers highly sensitive and selectivity owing to adsorption process other than electrolytic accumulation [78].

Therefore, as an alternative stripping approach for trace quantitation of Zn^{2+}, Cu^{2+}, Cd^{2+} and Pb^{2+} adsorptive cathodic stripping voltammetry (AdCSV) was used in the present study. Notably, almost all previous reports procedures for the determination of trace metals with cupferron complexing agent were conducted using AdCSV, this technique is one of the favorable analytical technique for individual and simultaneous determination of trace metals owing to its simplicity, high sensitivity and selectivity, low detection limits and low-cost instrumentation [1, 71, 73]. In AdCSV, an appropriate ligand is required to form a metal ion complex, which is then adsorbed and reduced on the electrode surface [42].

Previous reports in literature have successful detect trace metals with cupferron complexing agent using adsorptive cathodic stripping voltammetry (AdCSV), cupferron complexing agent used to form stable complexes, enhance sensitivity, good reproducibility and to obtain lower detection limits. The formation and stability of following cupferron complexes were extremely dependent upon pH and the nature of the buffer solution. A.A. Ensafi *et al* [68] reported the simultaneous determination of Cu^{2+} and Mo^{6+} in the presence of cupferron on HMDE. They explored that cupferron complexes were more stable in acidic media (acetate buffer, pH 3) owing to high AdSV sensitivity and good peak separation. While M. Grabarczyk *et al* [67] observed that Cd^{2+}-cupferron complex on HMDE was not able to form in acidic solution (acetate buffer, pH 4), however when they increased the pH of the buffer to 6.1 cupferron complex peak appeared. M. Grabarczyk *et al* [48] found that the formation of Pb^{2+}-cupferron complex on HMDE was extremely dependent upon pH of the buffer solution. N. Meepun *et al* [65]

15

determined Cd^{2+}-cupferron complex on a nafion coated glassy carbon bismuth film electrode (NC-GC-BiFE) in acetate buffer solution. Stable cupferron complex at pH 4 was formed with sharp and enhanced peak current of the cupferron complex. A more basic solution (borate buffer, pH 8.5) was used to form Zn^{2+}-cupferron complex on HMDE as reported by S. Abbasi et al [45]. In addition, the simultaneous detection of U^{6+} and Cd^{2+}-cupferron complexes on HMDE [43], simultaneous detection of Bi^{3+} and Pb^{2+}-cupferron complexes on a mercury film silver-based electrode (Hg(Ag)FE) [79] and Ga^{3+}-cupferron complex using an *in-situ* plated lead film electrode (PbFE) [80] were also pH dependent. In our research group, AdCSV was used to quantify Ni^{2+} on a nafion graphene dimethylglyoxime modified glassy carbon electrode (NGr-DMG-GCE) [51] and the determination of Ni^{2+} with dimethylglyoxime on the electrochemically reduced graphene oxide in conjunction with an *in-situ* mercury film electrode (ERGO-HgF-PGE) [54].

Moreover, the determination of trace metals with various complexing agents using AdCSV has also been reported in literature. Deswati *et al* reported the simultaneous determination of trace Zn^{2+} and Cd^{2+} with 1,2-dihyroxyanthraquinone or alizarin as a complexing agent [44], N. Thanh *et al* reported the use of oxine (8-hydroxyquinoline) complexing agent for simultaneous determination of Zn^{2+}, Cd^{2+} and Pb^{2+} on glassy carbon bismuth film electrode (GC-BiFE) [81] and the determination of Zn^{2+} and Cd^{2+} complexes with xylenol orange (xo) as complexing agent on HMDE was reported by A.A. Ensafi *et al* [78]. All reported complexing agents formed stable metal ion complexes owing to high complexing ability attributed to their highly conjugated structures and electron donating oxygen and nitrogen atoms.

Following steps are involved in AdCSV for trace metal analysis, the formation of complex ($M^{2+}L$) occurs spontaneously in a solution which involves metal cation (M^{2+}) and ligand (L) ,which is then adsorbed on the electrode surface.

$$M^{2+} + L \rightarrow M^{2+}L_{adsorption}$$

16
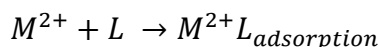
The adsorbed metal ion ligand complex is then stripped, and the metal cation is reduced to its metallic state by applying a negative (cathodic) potential scan from the electrode surface back to the solution.

$$M^{2+}L_{adsorption} \rightarrow M^0L_{solution} + 2e^-$$
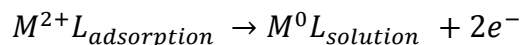
2.4 Complexing agent

The sensitivity and selectivity of various analytical techniques such as AdSV tend to rely upon either the working electrode or the selection of suitable ligands that more often form complexes with metal ions. These complexes must be able to form quickly in a solution and effortlessly adsorbed onto the surface of the working electrode, pH and the nature of the electrolyte solution are highly significant in forming stable complexes.

2.4.1 Cupferron

Cupferron is an organic compound (Ammonium salt of N-nitroso-phenyl-hydroxyl amine) that may appear to be white or light yellow in color. Cupferron is soluble in water, benzene, alcohol and ether. For the simultaneous determination of Cd^{2+}, Zn^{2+}, Cu^{2+} and Pb^{2+}, N-nitroso-phenyl-hydroxyl amine is proposed as a coordinating surface ligand to enhance the electrochemical responses of these metal ions by forming a complex when anion binds to the metal cations by means of two oxygen atoms therefore resulting in a five membered ring. In addition, cupferron has been used as chelating agent and as electrode modifier agent for voltammetric investigations resulting in well-defined adsorptive stripping peaks [24]. Despite its astounding sensitivity and selectivity, it has been accounted for electrochemical active stable complexes formation with different metals by expanding their adsorptivity onto the working electrode [21]. Moreover, previously reported papers demonstrated the use of cupferron as chelating agent using adsorptive stripping voltammetry to detect different metal ions such as uranium [78, 83], vanadium [83], gallium [84], europium [85], chromium [77], copper [46], molybdenum [87, 88], Iron[77], cadmium [15, 37, 89], lead [21], zinc [24], and aluminium [88].

17
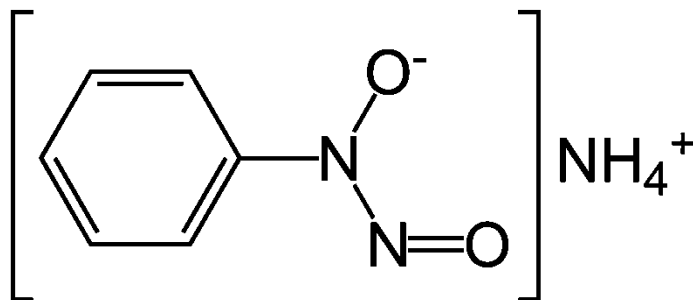
Figure 2.2 Chemical structure of cupferron ($C_6H_9N_3O_2$) [47].

2.5 Pulse voltammetry

In AdCSV measurements of trace metal analysis, stripping voltammograms are usually recorded using square-wave, differential pulse and cyclic modes. This can be described as follows:

2.5.1 Square-wave voltammetry (SWV)

SWV is a highly sensitive, versatile and rapid electrochemical technique used for quantitative analysis. It can be utilized for trace analysis and electro kinetic measurements of different electrode processes [89]. The SWV technique originated from Kalousek commutator and Barker's square-wave polarography and was extensively developed by the Osteryoungs [90]. SWV potential modulation consists of a staircase potential ramp combined with square shaped potential pulses, a symmetrical square-wave of constant amplitude is superimposed on the working electrode on a base staircase waveform and the difference between two current measurements in forward and reverse cycle is plotted versus the base staircase potential [91]. Square-wave pulse voltammetry was selected for further experiment due to high sensitivity and speed.

18
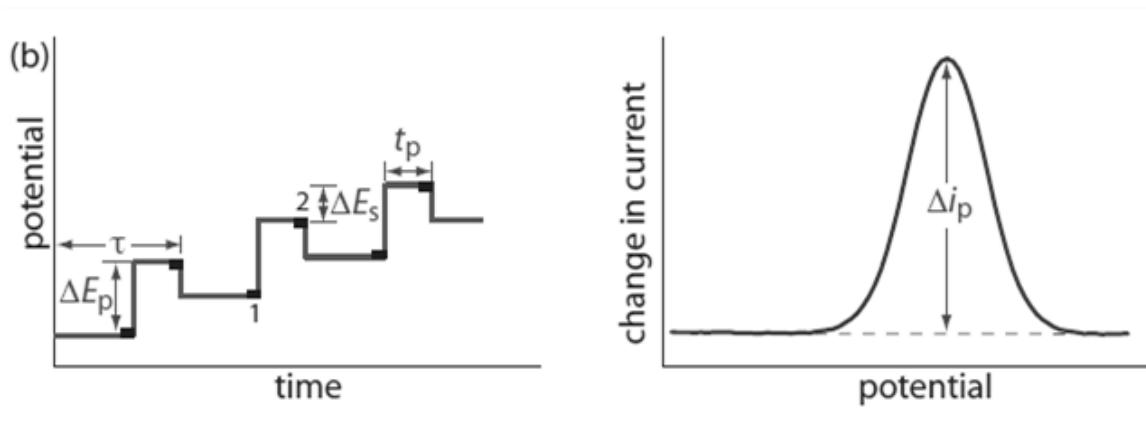
Figure 2.3 Schematic diagram of the possible staircase waveform and its current response [92].

2.5.2 Differential pulse voltammetry (DPV)

Barker and Gardner proposed the DPV technique which is a linear sweep voltammetry derivative in which a series of pulses scans the potential. However, each potential pulse in DPV is fixed with small amplitude ranging from 0.01 to 0.1 mV which is superimposed on either linear sweep or stair-steps based potential, the current difference obtained from each pulse between the two points is plotted against the applied potential [93]. DPV produces symmetric peaks for faradaic currents rather than sigmoidal waveform obtained by other techniques such as normal pulse voltammetry. DPV offers high sensitivity and more efficient resolution [72].
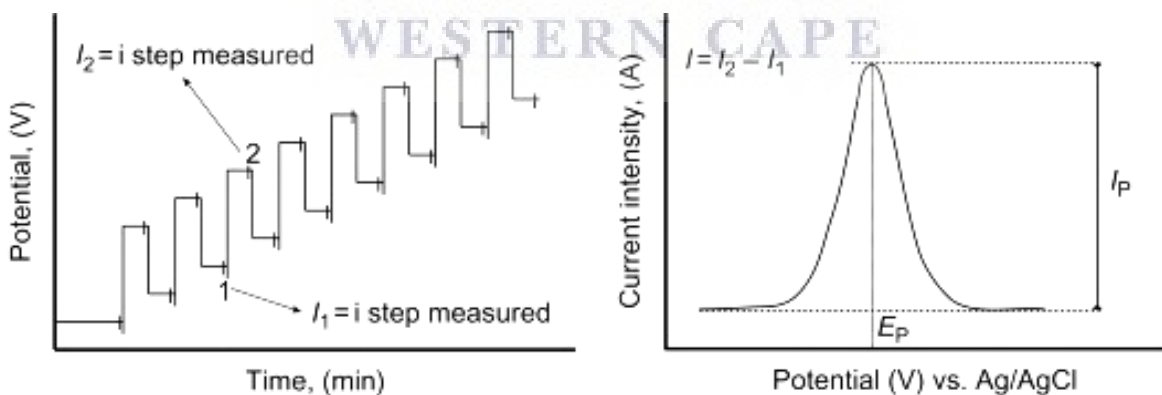
Figure 2.4 Schematic diagram of the potential waveform and its current response [93].

19

2.5.3 Cyclic voltammetry (CV)

Cyclic voltammetry is a powerful electro-analytical technique commonly used for qualitative determination of electrochemical behavior of various reactions such as the reduction and oxidation processes of various molecular species, to investigate chemical reactions initiated by electron transfer and redox coupled reactions. This technique is mostly based on measuring the potential applied between the working electrode and the reference electrode, while measuring the current between the working electrode and the auxiliary electrode [94]. The oxidation or reduction peak can be observed on a cyclic voltammogram depending on the nature of the electro-active species. Figure 2.5, shows the resulting scan of potential against time, using a triangular potential waveform and the corresponding voltammogram, the working electrode potential is ramped linearly versus time in an unstirred solution. Where the anodic peak current = I_{AP}, anodic peak potential = E_{AP} and during the reverse scan a cathodic peak current = I_{CP} and cathodic peak potential = E_{CP} are measured.
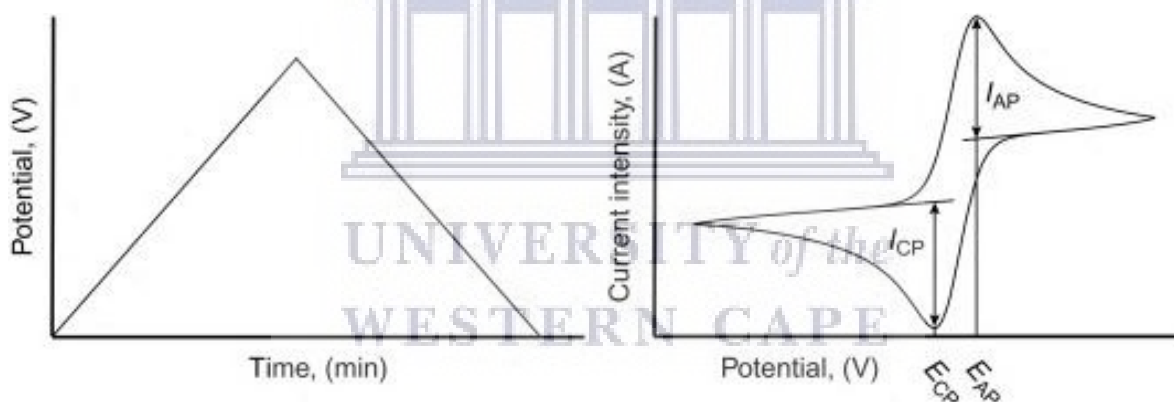
Figure 2.5 Schematic diagram of the triangular potential-time waveform and its current response [93].

2.6 Electrode materials for stripping voltammetry

Working electrodes (WE) are exceptionally critical and several factors are considered for choosing the right WE. The substrate should be fast, cheap, reproducible, wide potential window, favorable redox behavior with the analytes and good signal to noise ratio for fruitful and better

20

experimental results [73]. In this study pencil graphite electrode (PGE) was used as the working electrode in conjunction with *in-situ* thin mercury film in the determination of trace metals with cupferron in tap water. Almost all previously studies for the determination of trace Zn^{2+}, Cu^{2+}, Cd^{2+} and Pb^{2+} using cupferron ligand have been conducted on either the hanging mercury drop electrode (HMDEs) or glassy carbon electrode in conjunction with bismuth film electrodes (BiFEs).

2.6.1 The hanging mercury drop and bismuth film electrodes

The hanging mercury drop electrode (HMDEs) has received enormous attention in electro-analytical determination of trace Zn^{2+}, Cu^{2+}, Cd^{2+} and Pb^{2+} using cupferron ligand due to its elevated sensitivity, reproducibility, reliability and renewability [6, 97–102]. HMDEs involve the formation of a new electrode surface after the previous drop has fallen off which is then substituted by creation of a fresh new drop for the next experiment, resulting in a significant cleaning method that reduces interferences and less time consumption [97, 100, 103]. Previous reports have shown the use of HMDE in combination with adsorptive cathodic stripping voltammetry (AdCSV) in determining various trace metals such as Cd^{2+} [16, 37, 104], Zn^{2+} [104, 105] and Pb^{2+} [21] using cupferron as a complexing agent. However, HMDE has many setbacks such as its extremely costly to buy, high mercury toxicity, less reproducible drop size and premature drop during or between analysis [103, 106]. Bismuth film electrodes (BiFEs) has been used as an alternative substitute for mercury-based electrodes for the determination of various trace metals and organic compounds due to their negligible toxicity, ease preparation and partial insensitivity to dissolved oxygen [88, 99, 107–109]. The BiFEs behave correspondingly to TMFEs due to comparable electroanalytical performance as a broad potential window, formation of alloys with various trace metals and the ability to operate in highly alkaline media [99, 110–112]. The use of BiFEs has been reported in literature for various substrates such as pencil graphite electrodes, gold, carbon paste, glassy carbon, carbon fiber, noble metals, screen printed inks and platinum [51, 90, 111, 113, 114]. Furthermore, only negative potentials can be applied for BiFEs because positive potentials can completely oxidize and remove the bismuth film from the substrate surface. From literature, N. Meepun *et al* reported the use of nafion-coated bismuth film electrode on the determination of Cd^{2+} using cupferron complexing agent by AdCSV in

21

marine algae [65] which only negative potentials were implemented in stripping voltammetry. In addition, BiFEs can result to the narrowing of the cathodic potential range and air instability due to its natural oxidation. For these reasons, in the present study a thin mercury film electrode was used as an alternative electrode due to lower mercury consumption, improved sensitivity and selectivity.

2.6.2 Thin mercury film electrodes (TMFEs)

In this study for the determination of Zn^{2+}, Cu^{2+}, Cd^{2+} and Pb^{2+} with cupferron in tap water, an *in-situ* plated thin mercury film was used in combination with electrochemically reduced graphene oxide pencil graphite electrode (ERGO-PGE). A thin mercury film was used to improve the sensitivity and selectivity of the electrode due to large surface area to volume ratio, lower detection limit by reducing ionic metallic analytes that are readily dissolved in mercury to form amalgam, shorter diffusion distances for deposited metal, broad potential window, excellent mechanical stability and easy preparation [6, 97, 99, 100, 102, 115–117]. Thin mercury film electrodes (TMFEs) were plated using an *in-situ* process, where mercury is added directly into 0.1 M acetate buffer solution (pH 4.6) and coated on the surface of the ERGO-PGE. Mercury films are deposited on the ERGO-PGE surface in the form of small droplets rather than uniform films that led to a lower hydrogen overvoltage [114]. However, mercury toxicity has resulted to restricted use, significant attempts have been made to investigate alternative electrode materials [97]. Nonetheless, general performance of non-mercury electrodes including antimony, bismuth, gold were examined but not close to that of mercury owing to a low cathodic potential limit, short linear dynamic range, multiple peaks, low hydrogen evolution, small background contributions, poor precision and resolution [99]. Regardless of how toxic mercury is regarded, in this research only a negligible amount of mercury is used to modify the ERGO-PGE because only a small concentration of mercury is required to form a thin film layer, thereby minimizing its danger and disposal [99]. Mercury film was used for the simultaneous detection of Zn^{2+}, Cu^{2+}, Cd^{2+} and Pb^{2+} using cupferron ligand to enhance the sensitivity of the ERGO-PGE . In this study, the pencil graphite electrode (PGEs) is proposed as cheap and disposable substrate material for the simultaneous detection of trace metals in tap water samples.

22

2.7 The pencil graphite electrode (PGEs)

The need for highly sensitive, disposable, low cost and commercially accessible electrochemical sensor has been a concern. The electrochemical sensors like PGEs have been highly significant, effectively utilized in various applications such as cathodic and anodic stripping voltammetry for trace metal detection [88], vitamin B_{12} [58], anticancer drugs [57], DNA and RNA [59]. PGEs possesses many significance high electrochemical reactivity, low background current, high sensitivity, good reproducibility and inexpensive [118, 119]. In addition, pencil electrodes are sp^2 hybridized enabling high conductivity, good adsorption and surface modification. Moreover, the PGEs provides a readily renewable electrode surface that requires less electrode surface cleaning therefore lessen time consumption on electrode surface cleaning compare to other carbon-based electrodes such as glassy carbon electrodes (GCEs).

2.8 Carbon allotropes

Carbon is one of abundant chemical element [118], which occur either in an amorphous form (coke, carbon and coal) or in a natural allotropic crystalline form (diamond and graphite) [119]. Allotropes are different forms of one element with different chemical and physical properties. Diamond is a hardest and transparent three-dimensional (3D) mineral, while graphite is a multi-layered three-dimensional (3D) material weakly held together by van der Waal's forces. Weak interaction between graphite layers affects the sliding of graphite sheets over each other, thus allowing pencils to write on paper. Over the past years fascinating discoveries of other forms of carbon were uncovered, graphene (two dimensional 2D) [122, 123], carbon nanotubes (one dimensional 1D) [122] and fullerene (zero dimensional 0D) [123].

2.8.1 Graphene

Graphene is the thinnest, strongest and 2D crystal with single layer of one thick carbon atom densely packed and held together in a hexagonal honeycomb frame [124]. Graphene can be wrapped up to form a 0D fullerene, rolled up to 1D carbon nanotubes and stacked up on each other to form a 3D graphite [125]. The unique structure and exceptional properties of graphene have spurred curiosity to many scientists and researchers over the years, and responsible for

23

growing success on sensors, electronics, battery applications, solar cells, water purification and desalination [128, 129].
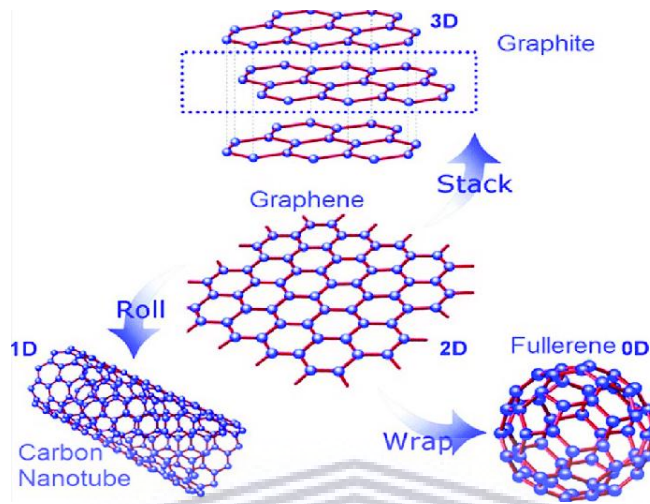
Figure 2.6 Carbon allotropes [124].

2.9 Graphene origin

Graphene was firstly reported by Schafhaeutl in 1840 [128] and Brodie in 1859 [129] but the isolation of this material was never archived until in 2004. In an attempt to explore the electrical properties of graphite two passionate physicists at Manchester University in England, Professor Andre Geim and Professor Konstantin Novoselov discovered graphene. A single layer of graphene was extracted from graphite flakes using the scotch tape (micro-mechanical) method. Adhesive tape was pressed to the silicon wafer oxide-coated layer. Repeated tape peeling resulted in tape isolating a thick carbon atom sheet of graphene, under an optical microscope the wafer was examined and a single layer of graphene was viewed [121]. For the first time in 2010, Andrei and Kostya won the noble prize in Physics for their outstanding work on graphene isolation [61]. The main advantage of this method is, its simplicity however only a small surface area of the single layer graphene film could be extracted.

24
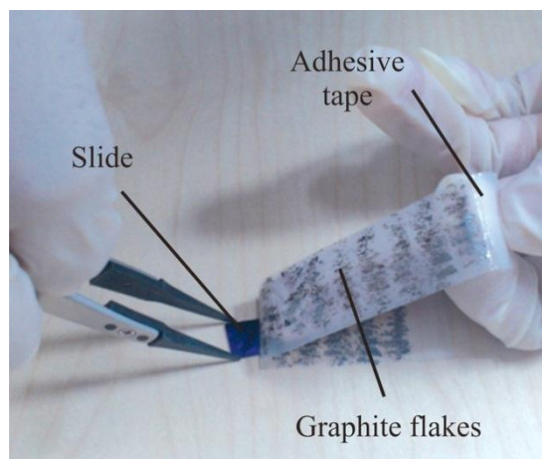
Figure 2.7 The scotch tape method for single layer graphene isolation [130].

2.10 Honeycomb graphene structure

Graphene is a flat 2D nanomaterial rather than cylindrical. Graphene sheets consists of carbon atoms tightly held together in a hexagonal honeycomb lattice. Each carbon atom is sp^2 hybridized and covalently bonded to three other carbon atoms. The distance between graphene carbon atoms is 0.142 nm (1.42 Å) and 0.335 nm (3.35 Å) accounts for the inter-planar spacing. These unique properties enable graphene to possess excellent electrical conductivity, large surface area, thermal and mechanical properties [131].
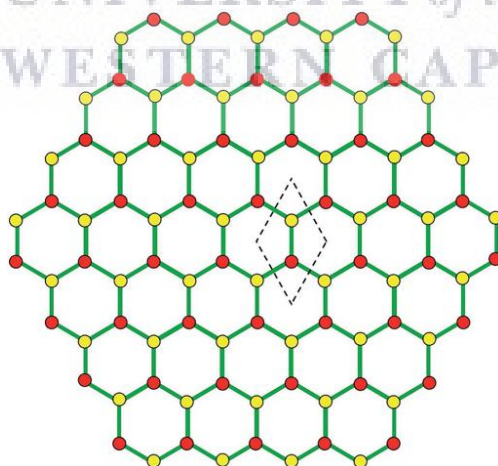
Figure 2.8 Single layer of graphene in a honeycomb lattice [132].

25

2.11. Graphene properties

2.11.1 Electrical conductivity

Graphene is a semimetal having holes and electrons as a carrier of charge, thereby improving its electrical conductivity. Each atom in graphene structure is bonded to three other carbon atoms leaving one electron known as pi (π) electrons available for electronic conduction. The 2D structure of graphene offers little resistance to the movements of pi electrons, thus improving electron delocalization when compared to graphite. The movement of electrons in graphene is much quicker than any other material at ambient temperature, its electron mobility is 15000 $cm^2.v^{-1}.s^{-1}$. Zero band gap (Dirac point) is a point where valence band and conductive band joined and are situated at six corners of the Brillouin zone [131]. As stated above, these are factors that make graphene electron mobility easier and faster.
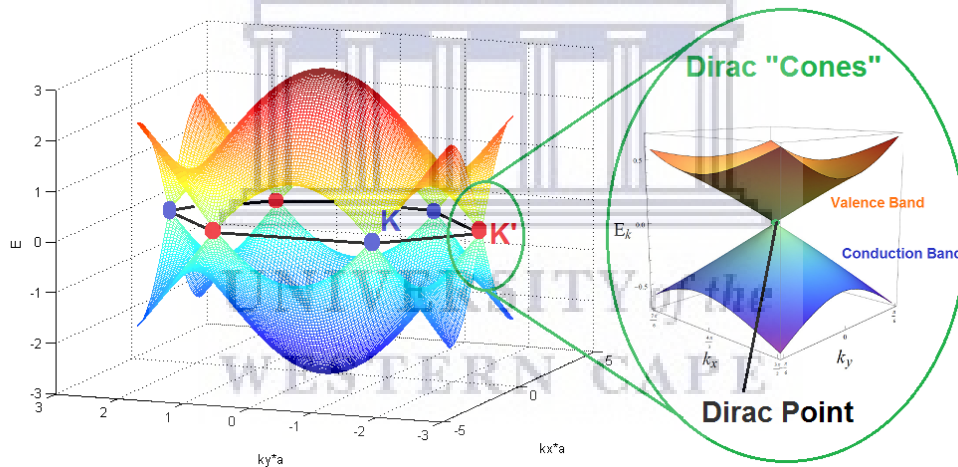
Figure 2.9 Three-dimensional electronic band structure of graphene with six corners of the Brillouin zone [133].

2.11.2 Mechanical property

Graphene is stronger than diamond and 200 times stronger than steel, this unrivaled strength is due to strong covalent bonds (42 $N.m^{-1}$ in length) between carbon atoms with a tensile strength of 130,000,000,000 giga-pascal. Unlike other strong materials, graphene is also elastic due to

26

each carbon atom is sp^2 hybridized throughout the crystal lattice thus enhancing its flexibility. Graphene can stretch to about 20 to 25 times its original length without carbon atoms breaking apart. Moreover, graphene is not only strong and elastic but is light and weigh less than a gram (0.77 mg.m^{-2}).

2.11.3 Optical property

Light absorption is another unique property of graphene since the discovery of a single layer of graphene as thinnest material being only one atom thick. Surprisingly graphene is transparent [134] thus enable inter-band transitions of electrons. Previous experiments verified graphene's ability to absorb some percent of white light (2.3%) [135]. Optical properties of graphene had tremendous success in electronic applications such as LCDs (liquid crystal displays) [135], touchscreens and solar panels. The following equation provides optical graphene absorption:

$$A = \pi\alpha \qquad (1)$$

Where: $\alpha = \frac{1}{137}$

A = optical absorption (2.3%)
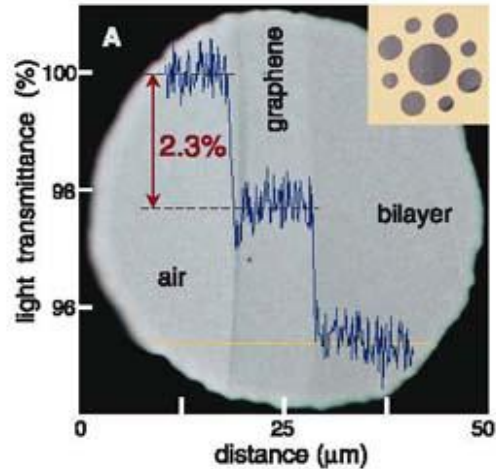
Figure 2.10 The intensity of white light transmitted from the exfoliated monolayer and bilayer of graphene [117].

2.11.4 Thermal property

Graphene has high thermal conductivity relative to other carbon allotropes such as carbon-nanotubes, graphite and diamond due to its two-dimensional structure that possess stable covalent bonding between carbon atoms as well as strong anisotropic bonding and low carbon atom mass. Thermal conductivity of graphene is estimated at 5×10^3 W.m^{-1}.K^{-1} which results from the presence of an elastic wave propagating through graphene lattice vibrational modes called phonons [61].

28

Table 1. Summary of graphene properties [136]

Graphene properties	values
Electron mobility	15000 cm^2.V^{-1}.s^{-1}
Thermal conductivity	5×10^3 W.m^{-1}.K^{-1}
Tensile strength	130 GPa
Thickness	0.34 nm
Specific Surface area	2630 m^2.g^{-1}
Transmittance	>95% for 2nm thick film
	>70% for 10nm thick film
Coefficient of thermal expansion	-6 $\times$ 10^{-4} K
Breaking through strength	42 Nm^{-m}
Elastic modulus	0.5 – 1 Tpa
Resistivity	10^{-6} Ω-cm

2.12 Synthetic routes of graphene

Graphene can be synthesized either by physical or chemical method depending on the exfoliation of pristine graphite into single layers of graphene sheets. Physical methods involve mechanical cleavage of graphite through the scotch tape method in which a single layer of graphene sheets were exfoliated for the first time. The main setback of this method is the high process temperature and inability to transfer single layer of graphene sheet on any other substrate [137]. Chemical vapor deposition (CVD) of graphene on metal substrate synthesis has been used as scalable and reliable production method of high-quality graphene. The method is based on the growth of graphene from metal-carbon melts followed by exfoliation of graphite using ultra

29

sonication. Although physical methods produce high quality graphene, it's not ideal for large-scale graphene synthesis [129, 140].

Chemical method is an alternative approach to the physical method, involving techniques such as Brodie, Staudenmaier, Hummers and Offeman used to synthesize graphite oxide (GO) in the presence of strong oxidants. The GO synthesis was first illustrated by Brodie in 1859, by mixing potassium chlorate ($KClO_3$) to graphite in the presence of fuming nitric acid (HNO_3) [129]. In 1898, Staudenmaier improved the Brodie's method by using sulfuric acid (H_2SO_4), HNO_3 and addition of different aliquots of $KClO_3$ throughout the reaction. The use of $KClO_3$ triggered explosions due to production of toxic gas (ClO_2), despite all this Staudenmaier created a more simplified technique for GO oxidation [139]. The Hummers method is one of the oldest techniques used to synthesize bulk graphene due to high efficiency and reaction safety. In 1958, Hummer and Offeman suggested an alternative method for GO synthesis, based on graphite oxidation using potassium permanganate ($KMnO_4$) or sodium nitrate ($NaNO_3$) in a concentrated sulfuric acid (H_2SO_4) [140]. The disadvantage of this method was the production of toxic gasses such as NO_2, N_2O_4 or ClO_2 and $NaNO_3$ which resulted in explosions. Many researchers have developed, new GO synthetic route by using modified Hummers method [141]. The tour Method is an improved Hummers method suggested by Tour's group at Rice University in 2010. The figure below shows the schematic chemical methods for the synthesis of GO from three different methods.

30
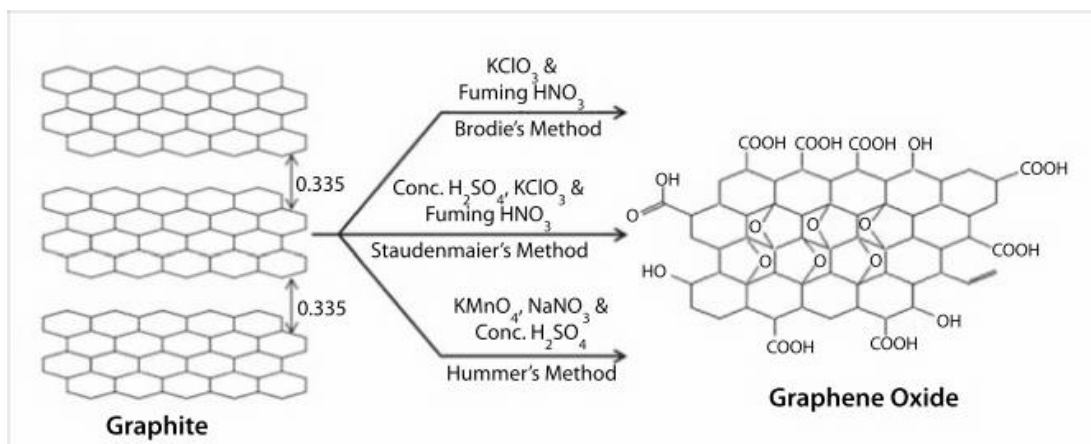
Figure 2.11 Illustration of Brodie, Staudenmaier and Hummers methods for GO synthesis [142].

2.13 Microscopic and spectroscopic techniques

A brief description of various spectroscopic and microscopic techniques used to characterize graphene oxide, graphite and graphite oxide is presented in this section. Spectroscopic technique used in this study include, Fourier transformed infrared spectroscopy (FT-IR), X-ray diffraction (XRD) and ultraviolet-visible spectroscopy (UV-Vis). While microscopic techniques include high resolution transmission electron microscopy (HRTEM) and high-resolution scanning electron microscopy (HRSEM) and information like structural configuration, morphology and formation of good quality single layers of graphene oxide were discussed.

2.13.1 Fourier transformed infrared spectroscopy (FT-IR)

Fourier transformed infrared spectroscopy (FT-IR) technique measures infrared radiation absorbed by graphite and synthesized graphite oxide at particular wavelengths from 4000 cm^{-1} to 400 cm^{-1} in the infrared region of the electromagnetic spectrum [143]. The obtained infrared spectrum confirmed the presence of oxygen functional groups such as hydroxyl, carboxyl, and epoxy groups present in the graphite oxide plane during the oxidation process. Previous reports in literature have proved successful conversion of pristine graphite to graphite oxide [144–146].

31

2.13.2 X-ray diffraction (XRD)

X-ray diffraction (XRD) was used to determine the crystallographic structure of graphite and graphene oxide. In XRD, a cathode ray tube produces X-rays by heating a filament to generate electrons and a high potential is used to accelerate electrons. The accelerated electrons bombard the samples by passing through them and their crystalline atoms, this phenomenon is referred to X-ray diffraction as the beam of incident X-rays diffracts in distinct directions [147]. Bragg's Law ($n\lambda = 2d\sin\theta$) explains the interference patterns of X-ray scattered by the crystal and used to measure the angle of diffraction [148]. Where λ = wavelength of x-ray, n = number of layers, d = interlayer spacing or d-spacing, θ = diffraction angle.

2.13.3 Ultraviolet visible spectroscopy (UV-Vis)

Ultraviolet-visible spectroscopy was used to characterize the spectroscopic absorption of light by graphite and graphene oxide due to the electronic transitions. UV-Vis spectrophotometer consists of a monochromator, a light source that can be either deuterium or tungsten lamp, a detector, reference and sample beams. A chopper splits the light from the source and forms two beams, the reference beam in the spectrophotometer travels from the light source to the detector without interacting with the sample. While the sample beam passing through the sample exposing it to ultraviolet light with a range of 190 to 350 nm and visible light of 350 nm to 800 nm wavelengths and the absorption spectrum is then obtained. The schematic of UV-Vis spectrophotometer is shown in Figure 2.12, this technique was used to confirm successful synthesis of graphene oxide.
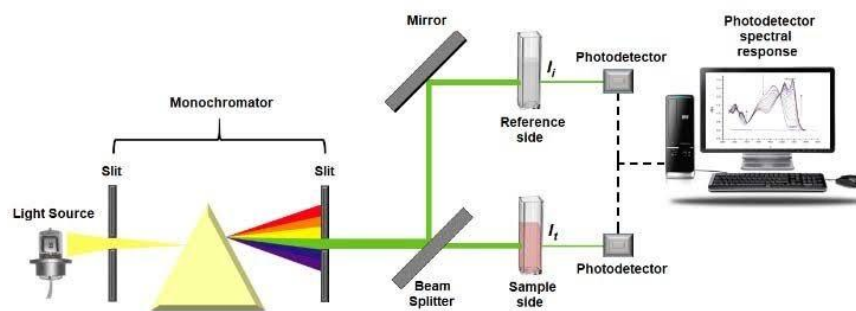
Figure 2.12 Schematic of UV-Vis spectrophotometer components [149].

32

2.13.4 High resolution transmission electron microscopy (HRTEM)

High resolution transmission electron microscopy (HRTEM) is one of powerful microscope which produces high resolution and two dimensional black and white images of various materials. HRTEM is used to characterize graphite and graphene oxide in order to determine morphology (size and shape), topography (texture and surface features) and crystal structure [150]. This technique works under the same fundamental principles as the light microscope but utilize electrons instead of visible light, glass lens is substituted with electromagnetic lens and image is viewed on fluorescent screen and not through an eyepiece. The first electron microscope was developed by Ernst Ruska with the assistance of Max Knolls in 1931, a high energy beam of electrons passes through and interacts with atoms of the samples to obtain properties of the sample such as crystallographic structure and morphology [153, 154]. At the tip of heated filament, the electron gun generates a monochromatic electron beam and the electrons are driven with high capacity of 40 to 100 kV. Electromagnetic lens with strong magnetic field guided through the column of the electron microscope, the sample is illuminated with the beam and image of the sample is created and monitored on a phosphorescent screen [153]. HRTEM is used to confirm the synthesis of graphene oxide.
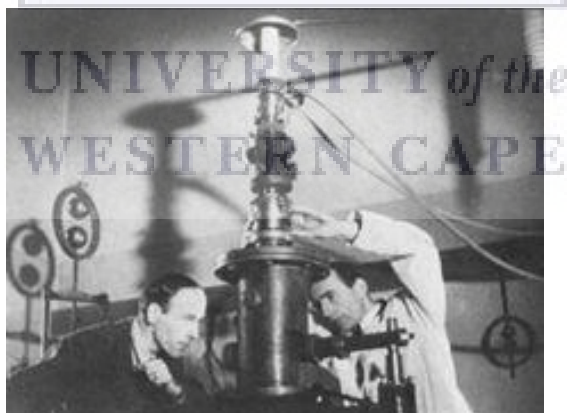
Figure 2.13 The first electron microscope prototype by E. Ruska and M. Knoll [151].

33

2.13.5 High resolution scanning electron microscopy (HRSEM)

High resolution scanning electron microscopy (HRSEM) is used to study the surface morphology and structure of the ERGO-PGE and bare-PGE. In HRSEM, when electron beam is generated by the tip of heated filament between 0.2 and 30 kV, electrons are accelerated by electromagnetic lenses through the HRSEM column and irradiate the surface of the samples under vacuum. The sample image is formed by detected secondary electrons emitted from the surface of the sample and the output signal is amplified by means of photomultiplier tubes [154]. In this study, HRSEM is used to confirm successful modification of pencil graphite electrode with electrochemically reduced graphene oxide.
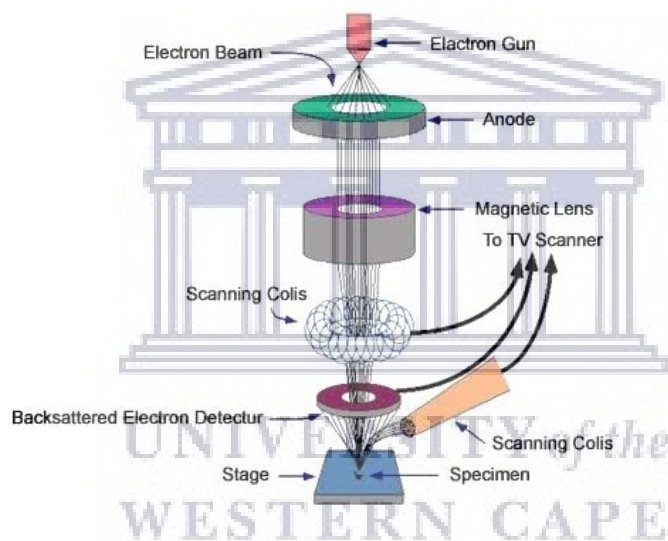
Figure 2.14 Schematic diagram of HRSEM [155].

CHAPTER THREE

Materials and experimental methods

3. Introduction

This chapter outlines detailed information of chemicals and materials used throughout the study. It also provides a detailed methodology on the development of the ERGO-HgF-PGE sensor, the synthesis of graphite oxide, preparation of graphene oxide colloidal solution (GO) and preparation of pencil graphite electrode. The electrode modification with electrochemically reduced graphene oxide (ERGO) and analytical procedure used to detect heavy metals in tap water samples is also outlined.

3.1. Chemicals and reagents

All chemicals were of analytical reagent grade and used without further purification. The atomic absorption standard solutions (AAS) of zinc (Zn^{2+}), copper (Cu^{2+}), cadmium (Cd^{2+}), lead (Pb^{2+}), nickel (Ni^{2+}), cobalt (Co^{2+}), gallium (Ga^{3+}) and arsenic (As^{3+}) were prepared from stock solution of 1000 mg.L^{-1} obtained from Fluka. Mercury (Hg) was purchased from Sigma-Aldrich and cupferron powder (nitrogen flushed, very hygroscopic, 25GR) was purchased from Acros-Organics these stock solutions were diluted as required. Graphite powder (<150µm, 99.99% trace metals basis), sodium acetate ($C_2H_3NaO_2$), sodium hydroxide (NaOH), acetic acid (CH_3COOH), potassium permanganate ($KMnO_4$), hydrochloric acid (HCl), sulfuric acid (H_2SO_4), hydrogen peroxide (H_2O_2) solution (contains inhibitor, 30 wt.% in H_2O, ACS reagent) and 99.99% ethanol were purchased from Sigma-Aldrich.

Acetate buffer solution (pH 4.6) was used as supporting electrolyte and prepared by mixing appropriate amounts of acetic acid (CH_3COOH) and sodium acetate ($C_2H_3NaO_2$) then further diluted with ultrapure distilled water (Millipore, Billerica, MA, USA) to give final concentration of 0.1 M acetate buffer. A Metrohm pH meter model, 827 was used to measure pH value of the prepared buffer solution. Ferricyanide solution was prepared by dissolving appropriate amount of

35

potassium ferricyanide ($K_3[Fe(CN)_6]$) in 0.1 M KCl used as redox probe for electrochemical measurements. Graphene oxide colloidal solution was ultrasonicated for an hour using a Misonix- S-4000, ultrasonic liquid processors (equipped with sonicator-horn).

3.2 Instrumentation

Cyclic voltammetry and square-wave cathodic stripping voltammetric measurements were carried out using a Metrohm Autolab PGSTAT 101 instrument in combination with Nova 1.11 software interfaced to a personal computer. A three-electrode system consisted of electrochemically reduced graphene oxide mercury film pencil graphite electrode (ERGO-MF-PGE) as the working electrode, an Ag/AgCl (saturated 3 M KCl) as the reference electrode and a platinum wire as an auxiliary or counter electrode. An electrochemical voltammetric cell was a standard 20 mL glass vial (Metrohm, Switzerland) and magnetic stirrer (801 Metrohm, Switzerland) was used during pre-concentration and cleaning steps. All electrochemical measurements were carried out at a room temperature.
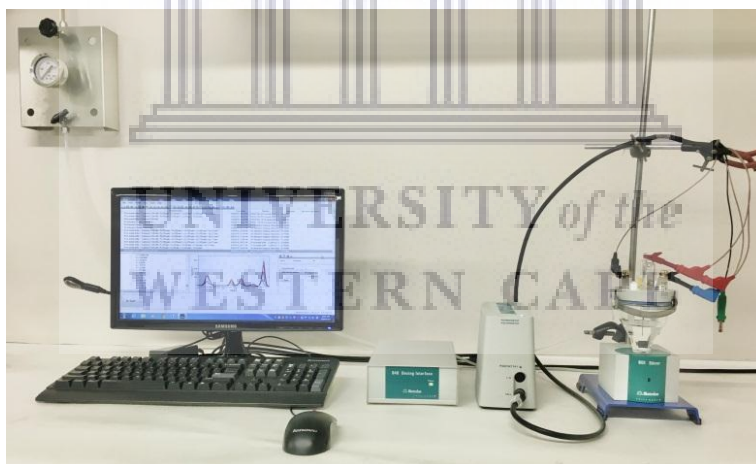
Figure 3.1 Metrohm Auto lab PGSTAT 101 and Magnetic stirrer 801.

36

3.3 Methods

3.3.1 Preparation of the standard solutions

The standard stock solution of acetate buffer was prepared by dissolving an accurate amount of sodium acetate (4.102 g) in ultrapure water and 2.9 mL acetic acid to make concentration of 0.1 M acetate buffer solution (pH 4.6) which was used in the preparation of graphene oxide colloidal solution. The stock solution was stable when stored in a refrigerator at 2 ℃ for about 2 weeks. Metal standard solutions were prepared from stock solution of 1000 mg.L^{-1} by dilution with 0.1 M hydrochloric acid (HCl) and then stored in a polyethylene vial. A 0.1 M solution of cupferron complexing agent was prepared by dissolving appropriate amount of cupferron (0.15515 g) in 10 mL of ultrapure water and stored in a refrigerator. Hydrochloric acid (HCl) was used for cleaning as well as removing metal ions from the electrodes and the electrochemical cell, 6 M HCl was prepared by diluting hydrochloric acid (99.7%) with ultrapure water.

3.4 Synthesis of graphite oxide

Graphite oxide was readily prepared by using a modified Hummers method [156], which involves the oxidation of graphite with strong oxidizing agents being potassium permanganate ($KMnO_4$) and sulfuric acid (H_2SO_4). 50 mL of concentrated H_2SO_4 was added into a clean dry conical flask (250 ml) and placed in an ice bath, the H_2SO_4 solution was stirred for few minutes and allowed to cool to 0 ℃. Followed by addition of 2 g graphite powder with constant magnetic stirring for 20 minutes, after the reaction mixture cooled to 0 ℃. Thereafter, 7 g of potassium permanganate was slowly added into the mixture to prevent formation of peroxides that might result in explosion, the flask was left to warm at room temperature. The reaction mixture was placed in a 35 ℃ water bath and stirred for 2 hours until the mixture turned dark green, indicating oxidation of graphite. The mixture was returned to an ice bath under constant stirring, 100 mL of ultrapure water was added and excess $KMnO_4$ was removed by adding approximately 5 ml of hydrogen peroxide (H_2O_2) gradually until effervescence ceases. Exothermic reaction occurred and the reaction mixture was removed from the ice bath and allowed to attain the room temperature. A yellow precipitated reaction mixture formed and filtered using the Buchner

37

funnel then washed three times with 10% hydrochloric acid (HCl) and ultrapure water. The resulting graphite oxide was collected in a beaker and thoroughly covered with a paper towel then dried for 48 hours in a desiccator.

3.5 Preparation of graphene oxide colloidal solution

The synthesized graphite oxide was used to prepare a graphene oxide (GO) colloidal solution. 500 mg of graphite oxide was placed in a beaker and 500 ml of 0.1 M acetate buffer solution (pH 4.6) added to make up 1 mg.mL^{-1} of GO colloidal solution. Followed by ultrasonication of GO colloidal solution for 1 hour, a clear brown colored solution was obtained. In conclusion, not all the oxygen functional groups are completely removed from the prepared graphene oxide and therefore, the more eminent term used instead of graphene oxide is the electrochemical reduction of graphene oxide (ERGO).

3.6 Preparation of the pencil graphite electrode (PGE)

The Pentel HB pencil lead with 0.5 mm diameter and 60 mm in length, purchased from the local bookstore was used as a working electrode for the investigation of Zn^{2+}, Cu^{2+}, Cd^{2+} and Pb^{2+} in tap water samples. The pencil rod was cut in half and inserted into a plastic syringe which was used as a holder and fixed vertically such that 1 cm of the pencil rod was exposed from the holder. The electrical connection on the pencil lead was achieved by soldering a copper wire on the reversed side of the pencil rod passing through the syringe.
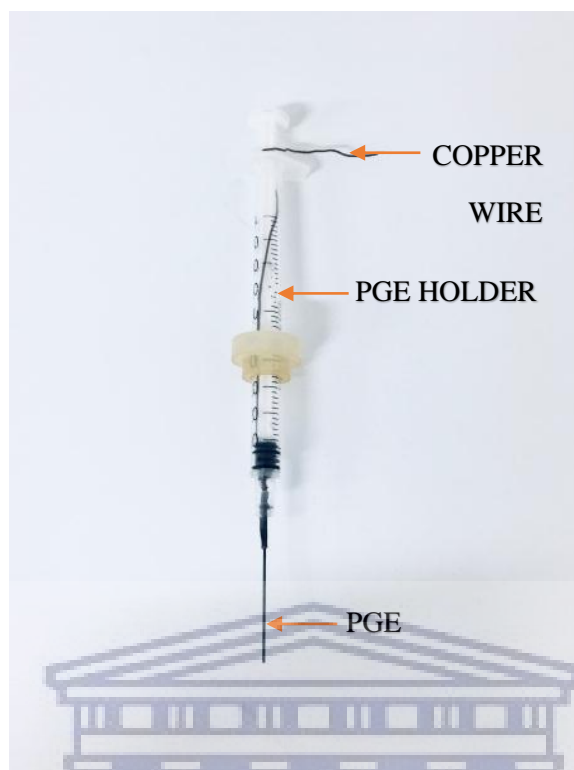
Figure 3.2 Pencil graphite electrode (PGE) and the holder.

3.6.1 Electrode cleaning and preparation of the ERGO-PGE

A clean electrode surface is crucial for good reproducibility and accuracy of the results. Thus, before analysis the pencil graphite electrodes were cut in half and thoroughly cleaned. A small amount of ethanol was placed onto a clean soft tissue paper and the electrode surface was gently wiped and then rinsed with ultrapure water. The PGE was electrochemically treated by immersing 1 cm of the electrode in 0.1 M acetate buffer solution (pH 4.6) in 20 mL electrochemical cell and then conditioned by using cyclic voltammetry. Conditioned electrodes were allowed to dry at room temperature for at least five minutes before use, thereafter 1 cm of conditioned pencil rod was immersed in an electrochemical cell containing 20 mL of 1 mg.mL^{-1} GO colloidal solution. Cyclic voltammetric reduction of GO onto the PGE surface was carried out in potential range between -1.5 and +0.3 V for 5 consecutive cycles. The instrumental parameters used were deposition time (120 s), scan rate (0.1 V), deposition potential (-0.7 V), and step potential (0.005 V). The electrochemically reduced graphene oxide pencil graphite

39

electrodes were allowed to dry in a refrigerator ($-4\,°C$) for 30 minutes before SW-AdCSV analysis.

3.6.2 Preparation of the ERGO-PGEs in multi-electrochemical cell

A multi-electrochemical cell was used to prepare eight pencil graphite electrodes, which were placed in eight holed cap connected with a copper wire throughout. Platinum wire was used as an auxiliary electrode and Ag/AgCl (3 mol.L^{-1} KCl) as a reference electrode placed on two holes made on the cap as seen in Figure 3.3. The multi-electrochemical system consisted of a stirrer bar and magnetic stirrer, which enable the pre-concentration step during the electrochemical reduction of GO on the PGEs surface. The eight electrodes were cleaned, conditioned and coated using the same procedure as previously explained on the preparation of the ERGO-PGE using a single cell (3.6.1). A multi-electrochemical cell helped to lessen time-consumption of coating electrodes using a single cell as well as to obtain reproducible results.
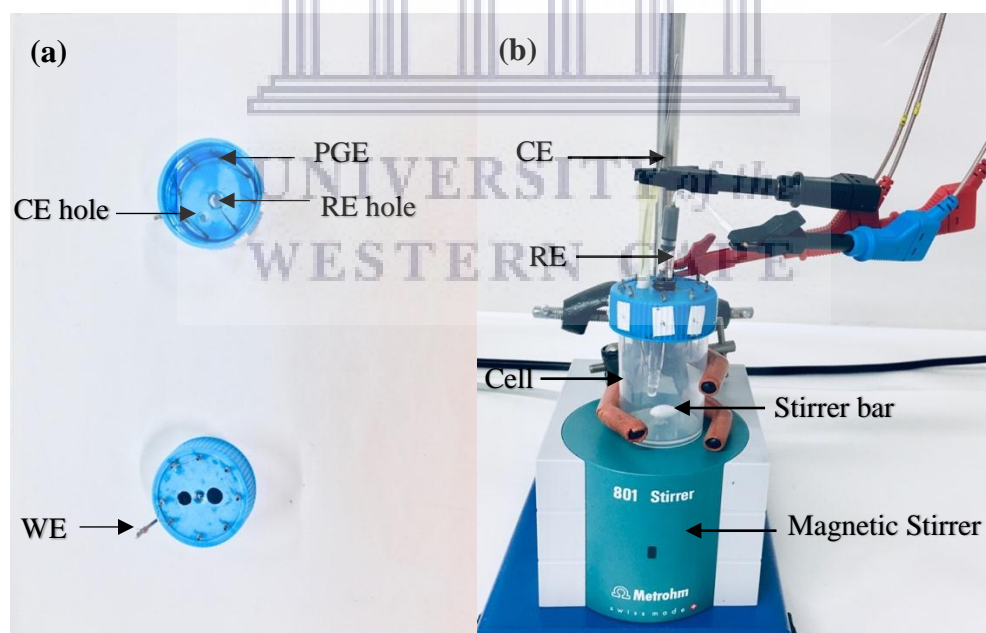
Figure 3.3 Schematic representation (a) multi-electrode cap, (b) multi-cell with three electrode systems.

40

3.7 Square-wave adsorptive cathodic stripping voltammetry analysis at the ERGO-HgF-PGE

Firstly, 6 M hydrochloric acid was used to clean the electrochemical system and washed thoroughly with ultrapure water in order to ensure complete removal of contaminants. 20 mL of 0.1 M acetate buffer (pH 4.6) solution is pipetted into an electrochemical cell and purged using a nitrogen gas for three minutes to remove dissolved oxygen, a nitrogen atmosphere is maintained over the solution throughout the analysis. Subsequently, 8 μL of cupferron (0.1 M in ultrapure water), aliquots of Zn^{2+}, Cu^{2+}, Cd^{2+} and Pb^{2+} standard solutions of 10 mg.L^{-1} stock solution, and 50 μL Hg (1000 ppm) are introduced into the cell. The stirrer was switched on and the mixture was stirred for 30 s to allow metal-cupferron complexes to form. The adsorption of cupferron complexes onto the ERGO-HgF-PGE was carried out at deposition potential of 0.1 V for 60 s from the stirred solution. At the end of the deposition time, the stirrer is switched off and the solution is allowed to quiescent for 10 s. The adsorptive cathodic stripping voltammogram is recorded from 0 V to -1.2 V in square-wave mode, with a 25 mV.s^{-1} scan rate, pulse amplitude (30 mV) and a frequency (35 Hz) for simultaneous analysis. All measurements were carried out at room temperature.

3.8 Quantitation

The method of standard addition was used to determine concentration of the analytes. For reproducibility purposes, each analysis was repeated for a minimum of three times. The concentrations of the analytes were calculated using the standard addition formula.

3.9 Sample preparation

Tap water was collected in our laboratory at the University of Western Cape in the municipal region of Bellville in Cape Town, South Africa after allowing water to run for 1 minute. 19 ml of tap water sample was added to 1 ml of 2 M acetate buffer solution (pH 4.6) pipetted into the electrochemical cell for the simultaneous analysis of Zn^{2+}, Cu^{2+}, Cd^{2+} and Pb^{2+}.

3.10 Voltammogram

All the voltammograms obtained in this study were baseline corrected and polynomial fixed order was used.

3.11 Spectroscopic techniques

3.11.1 Fourier transform infrared spectroscopy (FT-IR)

Fourier transform infrared (FT-IR) spectroscopy was used to confirm the presence of oxygen moieties present in the graphitic structure. FT-IR spectra of graphite and graphite oxide were obtained using a Perkin Elmer Spectrum, model spectrum Two LiTa (Liantrisant, UK) acquired in range 400 to 4000 cm^{-1} at room temperature. Sample preparation for the FT-IR analysis was done by mixing powder samples and potassium bromide (KBr) in a mortar, while grinding with a pestle. The mixture was placed in a pellet then pressed using a quick hand press (Sigma-Aldrich) into a round transparent KBr pellet. Potassium bromide was used as mulling agent, to remove moisture present in powdered samples and due to its large transmission window (transmittance is 100%).

3.11.2 Ultraviolet visible spectroscopy (UV-Vis)

The UV-Vis spectroscopic studies were carried out using Thermo-Fischer Scientific, model Genesys 10s UV-Vis spectrophotometer (Madison, USA) at wavelength of 200 to 600 nm range at room temperature. The ultrasonicated 1 mg.ml^{-1} GO colloidal solution and graphite dispersed in distilled water were placed in a 1 cm quartz cuvette, a clean soft tissue paper was used to wipe the cuvettes to remove fingerprint. Quartz cuvettes were used for UV-Vis measurements, because their transparent to the wavelengths higher than 180 nm, distilled water was used as a reference to give the baseline spectrum. The obtained absorption spectra of graphite and graphene oxide (GO) were used to study the electronic transitions in the samples.

3.11.3 X-ray diffraction (XRD)

XRD measurements of powdered graphite and graphene oxide were performed by using a Bruker AXS (Germany) D8-Advance diffractometer. The samples were placed onto a glass slide and

analyzed by using Cu-Kα radiation (λ Kα$_1$ = 1.54060 Å) as a radiation source with 40 kV in a 2θ range from 0.5° to 130°. A Lyn-Eye was used to record the diffraction data, the XRD patterns of graphite and graphene oxide were used to study interlayer distances and the graphitic structure.

3.11.4 Electrochemical impedance spectroscopy (EIS)

EIS measurements were carried out using a Zahner-Elektrik Electrochemical Workstation IM6e from Zahner- Elektrik GmbH & CoKG (Kronach, Germany) to characterize the bare-PGE and ERGO-PGE using 2.5 mM $[Fe(CN)_6]^{-3/-4}$ in a 0.1 M KCl as redox probe. Z-view software was used to obtain Randles equivalent circuit and information such as charge transfer resistance and electrical conductivity of the electrode.

3.12 Microscopic techniques

3.12.1 High resolution transmission electron microscopy (HRTEM)

High resolution transmission electron microscopy (HRTEM) measurements were carried out using a Tecnai G2 F20X-Twin MAT field emission transmission electron microscope from FEI (Eindhoven, Netherlands) under an acceleration voltage of 200 kV. The samples were prepared by grinding and dispersing little amount of graphite or graphite oxide powder in ethanol by ultrasonication, the suspensions were drop casted on standard copper grids. The grid was allowed to dry at room temperature before HRTEM analysis.

3.12.2 High resolution scanning electron microscopy (HRSEM)

The surface morphology of the bare-PGE and ERGO-PGE were investigated using an Auriga high resolution scanning electron microscopy (Auriga HRSEM) instrument equipped with electronic data system (EDS) (Woburn, USA). The ERGO-PGEs were prepared by electroreduction of graphene oxide (GO) on the surface of the PGE using cyclic voltammetry (CV), while the bare-PGEs were conditioned using CV before HRSEM measurements.

43

CHAPTER FOUR

4. Morphology and structural characterization of graphite, graphite oxide and ERGO

This chapter presents a detailed analysis of various microscopic and spectroscopic techniques used to characterize graphite, graphite oxide and the electrochemically reduced graphene oxide (ERGO) and their representative interpretation of attained results such as surface morphology and structural properties. Furthermore, electrochemical characteristics of the electrode surface are determined.

4.1 Fourier transformed infrared spectroscopy (FT-IR)

The FT-IR spectroscopic technique was used to determine various oxygen containing functional groups present in the graphite oxide sample. The FT-IR spectrum of pristine graphite shown in Figure 4.1(a) exhibited no significant oxygen-related peaks owing to their chemical inertness as reported by Bera *et al* [157], although weak stretches and bending bands were attributed to adsorbed water molecules [158]. The FT-IR spectrum of graphite oxide on the other hand showed clearly visible peaks between 400 and 4000 cm^{-1} wavelength. A broad and intense peak at 3328 cm^{-1} is ascribed to O-H stretching vibrations of adsorbed water molecules from potassium bromide (KBr) used during the sample preparations and alcohol (C–OH) groups [159]. The band at 2321 cm^{-1} was due to weak sp^2 and sp^3 of C-H stretching vibrations from the defects sites of the graphitic structure [160]. The carbonyl group, C=O (1738 cm^{-1}) and aromatic, C=C (1634 cm^{-1}) stretching vibrations were present due to the oxidation of the graphitic structure. The peak at 1401 cm^{-1} corresponds to C-OH stretching of alcohol group (deformation vibration), absorption peak at 1232 cm^{-1} and 869 cm^{-1} is characteristic to C-O-C stretching vibration of epoxy group and the band at 1054 cm^{-1} is assigned to C-O stretching of alkoxy group. Similar results were reported by N. Pan *et al* [161]. The peaks observed in graphite oxide spectrum confirms the inclusion of oxygen functional moieties such as epoxy, hydroxyl groups located on the basal plane of the graphite oxide [162, 164]. While carbonyl and carboxyl groups are presumably situated at the edges of graphite oxide as per Lerf Klinowski's model [163]. In conclusion, FT-IR spectrum of graphite oxide showed successful oxidation of pristine graphite

44

by potassium per manganate (KMnO$_4$) and sulphuric acid (H$_2$SO$_4$) through modified Hummers. Table 2 summarizes functional moieties present in graphite oxide. FT-IR was carried to confirm the synthesis of GO by confirming the presence of oxygen containing functionalities thus the FT-IR of PGE and ERGO was not carried out.
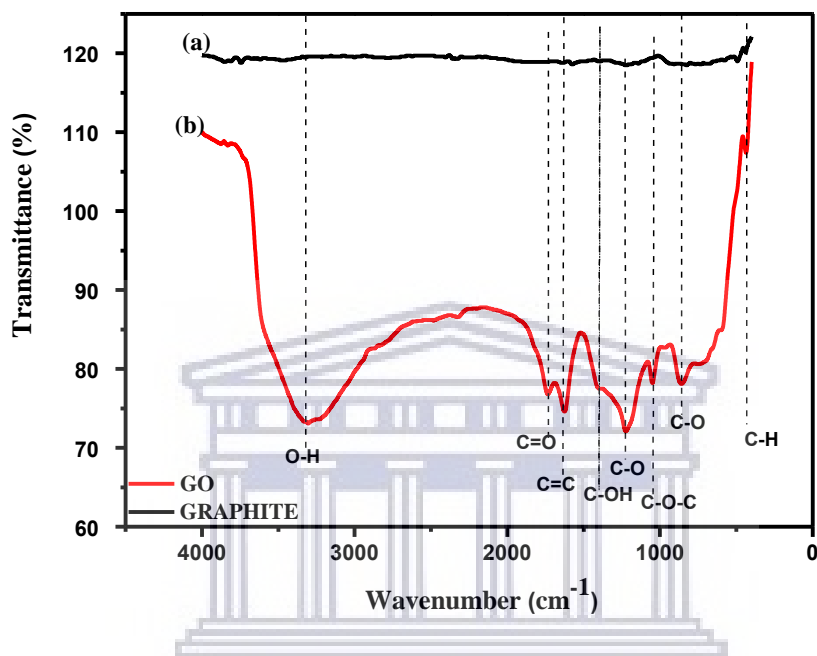
Figure 4.1 FT-IR spectra of (a) Graphite, (b) Graphite oxide (GO).

Table 2 Characteristics FT-IR absorption frequency of functional groups present in graphite oxide.

Absorption Frequency (cm^{-1})	Functional groups	Type of Vibration
3328 cm^{-1}	O-H	stretching
2321 cm^{-1}	C-H	stretching
1738 cm^{-1}	C=O	stretching
1634 cm^{-1}	C=C	stretching
1401 cm^{-1}	C-OH	stretching of alcohol group

45

1232 cm^{-1} and 869 cm^{-1}	C-O-C	stretching of epoxy group
1054 cm^{-1}	C-O	stretching of alkoxy group

4.2 Ultraviolet visible spectroscopy (UV-Vis)

The UV-Vis absorption spectroscopy was used to study the electronic transitions in graphite and graphene oxide after ultrasonication of 1 mg.mL^{-1} GO colloidal solution and ultrasonication of graphite dispersed in distilled water, as shown in Figure 4.2. The UV-Vis spectrum of pristine graphite, shows a strong and sharp absorption peak at 271 nm due to $\pi \to \pi^*$ transitions, owing to the excitation of π electrons of the graphitic structure [164]. On the other hand the UV-Vis spectrum for graphene oxide (GO) showed two significant absorption peaks, the maximum absorption peak at 230 nm was due to the $\pi \to \pi^*$ electronic transition of aromatic C=C bonds and the shoulder peak at 300 nm was assigned to the n $\to \pi^*$ transition of C=O in sp^3 regions of GO, indicating the presence of carbonyl groups on the edges of GO. The obtained results confirm the oxidation of graphite to GO during the electrochemical exfoliation. The absorption spectra obtained are coherent with previous reports in literature [163, 167–169]. The UV-Vis of PGE was not carried out as its difficult to work with solid samples, the UV-Vis of ERGO was not done because it was electrochemically reduced on to the surface of the PGE.
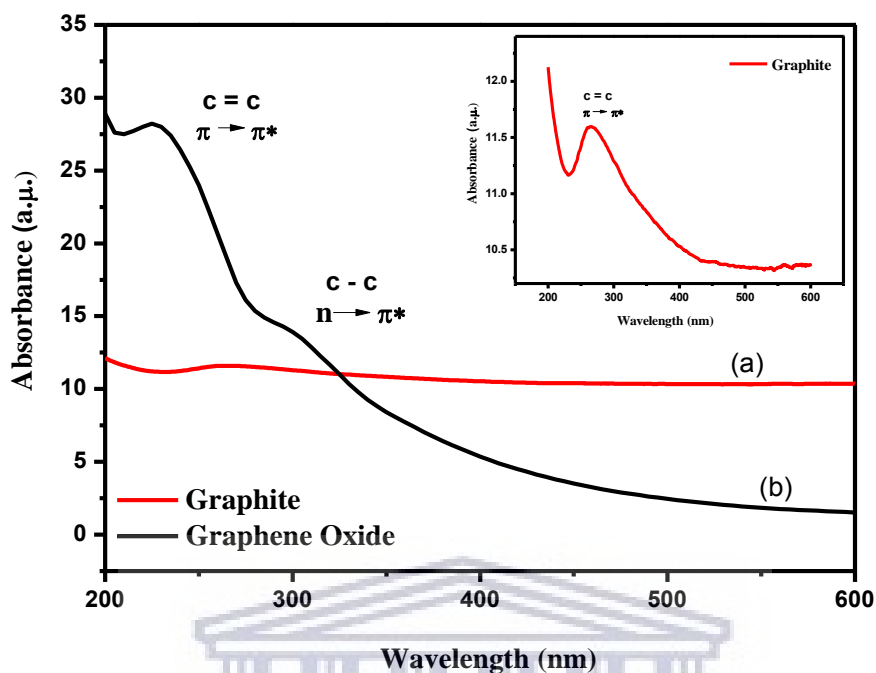
Figure 4.2 UV-Vis absorption spectra of (a) Graphite, (b) Graphene oxide.

4.3 X-ray diffraction spectroscopy (XRD)

The structural properties of powdered graphite and graphene oxide were characterized using XRD measurements [170, 171]. The XRD pattern of pristine graphite, shown in Figure 4.3(a) indicates that, graphite has a highly ordered carbon structure due to the presence of the strong peak at $2\theta = 26.5°$ which corresponds to (002) planes with d-spacing of 3.4 Å. In addition, the indexed peak (101) at 44.4° and (004) at 54.6° with d-spacing of 2.0 Å and 1.7 Å, respectively further confirming the crystalline nature of pristine graphite. Bragg's law equation (1) was used to calculate interlayer d spacing.

$$n\lambda = 2 \times d \times sin\theta \qquad (1)$$

Where λ = wavelength of x-ray, n = number of layers, d = interlayer spacing or d-spacing, θ = diffraction angle.

47

The XRD pattern for graphene oxide in Figure 4.3(b) shows a sharp and intense diffraction peak at $2\theta = 8.3°$ and weak shoulder peak at $2\theta = 42.2°$ with d-spacing of 10.6 Å and 2.1 Å respectively. These peaks correspond to (001) and (100) diffraction planes. The disappearance of the graphite peak at $2\theta = 26.5°$ and the appearance of GO peak at $2\theta = 8.3°$ shows that, graphite was strongly oxidized by a modified Hummers method. The increase of the d-spacing from 3.4 Å to 10.6 Å was due to the presence of oxygen functional groups such as hydroxyl, carboxyl and epoxy as well as water molecules inserted in the carbon layer structure [146]. Moisture present in graphene oxide could have resulted to a broad peak centered at $2\theta = 30°$ [172, 173]. The XRD patterns confirm the oxidation of pristine graphite to graphene oxide obtained results are consistent with previous reports in literature [148, 173–175].
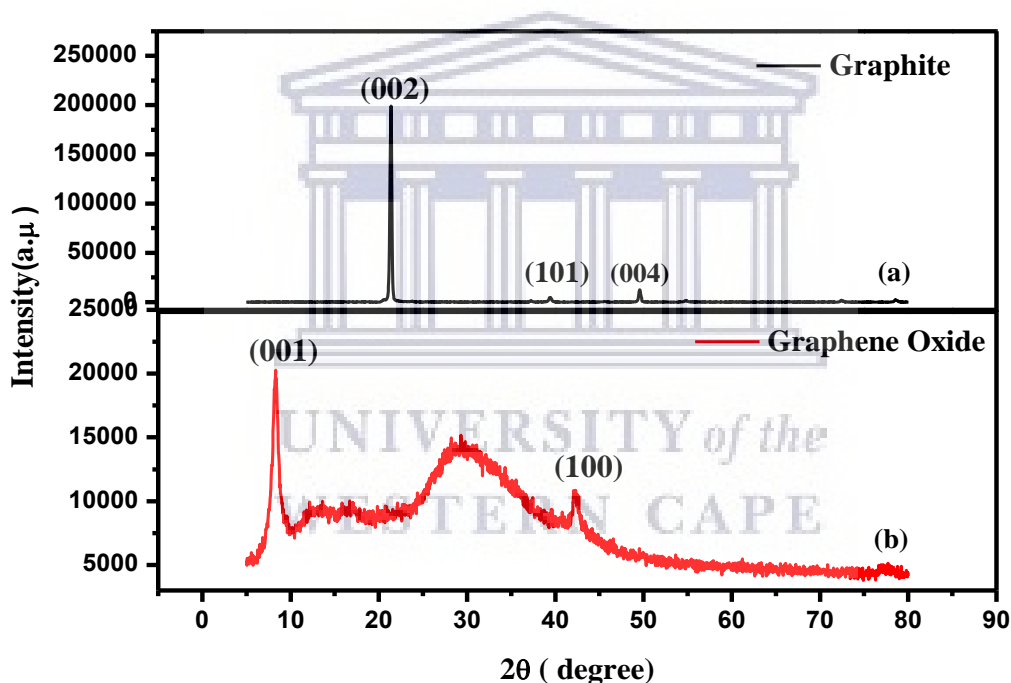
Figure 4.3 XRD patterns for (a) Graphite, (b) Graphene oxide.

Table 3 The peak position (2θ) and interlayer spacing (d) from the XRD results.

Sample	2θ	d spacing (Å)
Graphite	26.5°	3.4
	44.4°	2.0
	54.6°	1.7
Graphene oxide	8.3°	10.6
	42.2°	2.1

4.4 High resolution transmission electron microscopy (HRTEM)

The surface morphology of graphite and GO were studied using HRTEM analysis as shown in Figure 4.4 with their corresponding selected area electron diffraction (SAED). Samples (prepared in ethanol) were mounted on the standard holey-mesh copper grids and loaded into the microscope for measurements. Figure 4.4(a) showed that, the above sheet of graphite flake appears darker due to several layers of stacked graphite while lighter clear area suggested less stacked sheets of graphite. As clearly illustrated in Figure 4.4(b), sharp and straight edges indicated by the arrows resembling the fore edges of a closed book suggested that graphite has a highly ordered carbon structure. Moreover, Figure 4.4(c) illustrates the selected area electron diffraction pattern of graphite. It shows that the diffraction spots are arranged in a clearly visible hexagon symmetry which is characteristic to hexagonal lattice structure of graphite, obtained results are in agreement with reports from literature [176, 177].

In Figure 4.4(d) GO sheet appears large with smooth folded edges, which are characteristic features of single sheets of GO [176–179]. The dark area implies that several sheets of GO are stacked together, while the transparent area suggests a single or less stacked GO sheets and similar results have been reported in previous studies [9–13]. The morphology of GO sheet was associated with the presence of oxygen moieties such as carboxyl, hydroxyl and epoxy on the

49

GO sheets that changed the sp^2 hybridized carbon atoms (planar structure) to sp^3 (tetrahedral structure) [185, 186]. Few GO layers as indicated by the arrows shows the amorphous nature of GO as seen in Figure 4.4(e). The GO selected area electron diffraction (SAED) pattern shown in Figure 4.4(f) clearly differs from that of graphite. The diffraction patterns obtained from SAED measurements illustrate the polycrystalline structure of GO, the diffraction ring further confirm the amorphous nature of GO layers as previously reported by S. N. Alam *et al* [185]. Thus, the HRTEM analysis confirm the oxidation and exfoliation of GO as a single or few layers of graphene oxide.
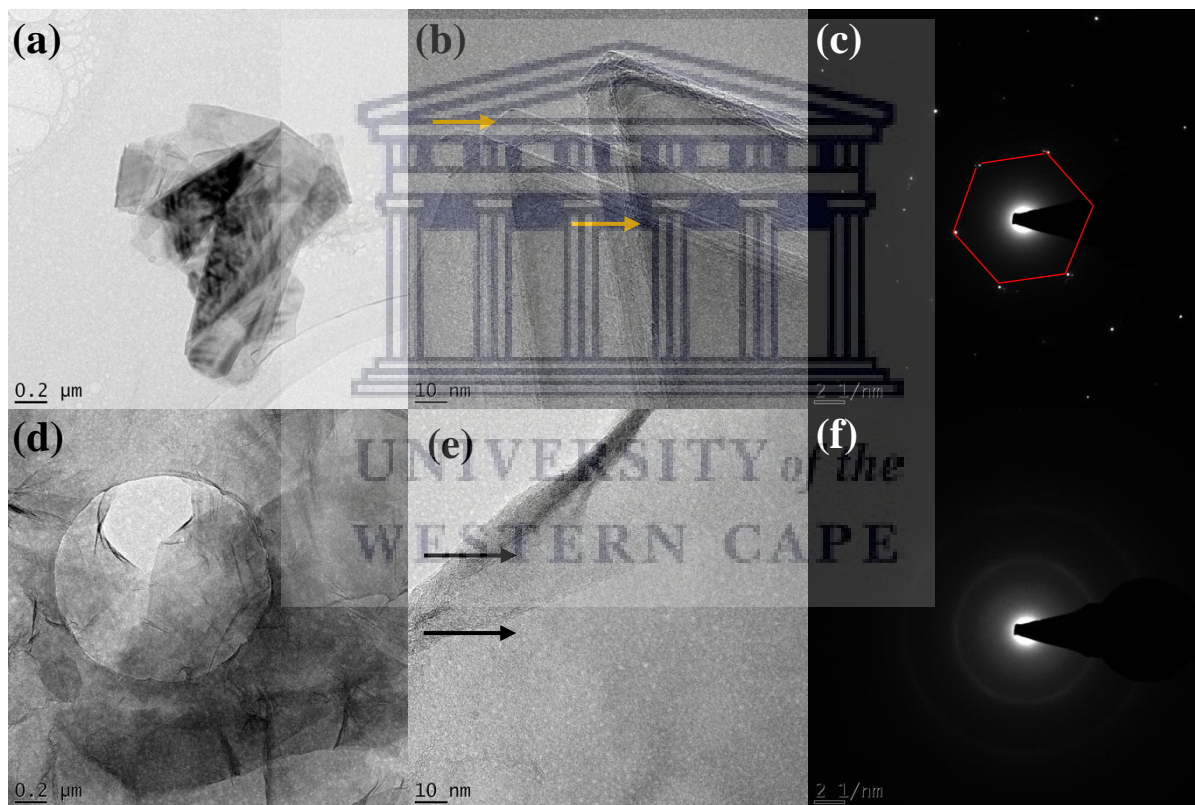
Figure 4.4 HRTEM images (a and b) of graphite and (c) corresponding SAED, HRTEM images (d and e) of GO and (f) corresponding SAED.

4.5 High resolution scanning electron microscopy (HRSEM)

Microscopic characterization of the pencil graphite electrode (PGE) and electrochemically reduced graphene oxide pencil graphite electrode (ERGO-PGE) were investigated using HRSEM analysis to study the surface morphology. At lower magnification (500 times) HRSEM images of the bare-PGE and ERGO-PGE in Figure (4.5a and 4.5b) respectively, shows changes in their electrode surfaces. The lateral surface roughness of the bare-PGE might have resulted from the extrusion method, during the manufacturing process of the pencil lead rods as illustrated in Figure 4.5(a) similar results have been reported by R. Navratil *et al* [186]. After the modification of the bare-PGE with ERGO, the electrode surface appeared coated with cauliflower shaped particles across the electrode surface presumably that the particles are ERGO. In addition, there are several stretches between the ERGO-PGE grooves indicating ERGO which can contribute to the conductivity of the electrode [187]. The HRSEM image of the bare-PGE (Figure 4.5c) at higher magnification (2000 times), shows the presence of impurities on the PGE surface that could be either clay or binder materials used to make the substrate. According to Esmaeel *et al*, almost all pencil graphite leads consist of (65%) graphite, (30%) clay and (5%) a binder (wax, resins, or high polymer) [188]. HRSEM image of the ERGO-PGE (Figure 4.5d) shows a multilayer ERGO sheets which appear tightly packed one to the other with a corrugated surface forming large, smooth, transparent and folded conductive films. Thus, HRSEM images confirm the electrochemically reduction of graphene oxide on the PGE surface.

51
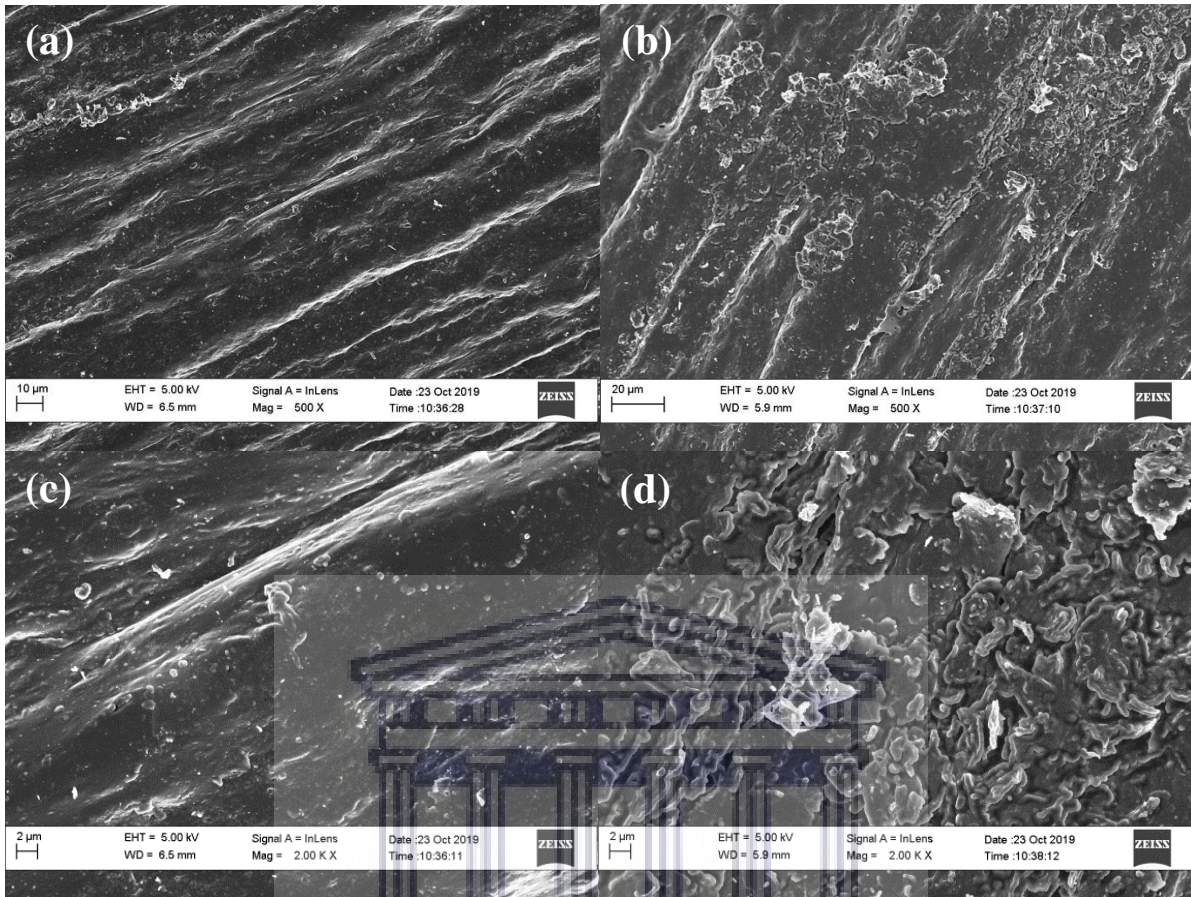
Figure 4.5 HRSEM images of the bare-PGE (a and c) and ERGO-PGE (b and d) shown at lower magnification 500 times (top) and higher magnification at 2000 times (bottom).

http://etd.uwc.ac.za/

5. Preparation and electrochemical characterizations of the ERGO-PGE

This chapter present detailed information on cyclic voltammetric responses of the ERGO-PGE and bare-PGE carried out in a ferro/ferricyanide [Fe (CN) $_6$]$^{-3/-4}$ redox probe and acetate buffer solution. The chapter further details the electron transfer properties of the ERGO-PGE and bare-PGE using the electrochemical impedance spectroscopy (EIS).

5.1 Electrochemical reduction of graphene oxide on the PGE surface

The electrochemical reduction of 1 mg.mL^{-1} graphene oxide (GO) colloidal solution on the pencil graphite electrode (PGE) surface was carried out by cyclic voltammetry in 0.1 M acetate buffer solution (pH 4.6) using 5 coating cycles range from -1.5 V to $+0.3$ V at a scan rate of 100 mV.s^{-1}. Two major peaks are observed in Figure 5.1, one anodic peak (i) and one cathodic peak (ii). The first anodic scan potential shows a large anodic peak current (i) around $+0.2$ V. The peak occurs as a result of oxidation of the PGE surface. The large anodic peak observed during the first cycle is gradually decreased with increasing number of coating cycles until it stabilizes. The reduction in anodic peak current may be attributed to blocking of the PGE surface with ERGO sheets [187]. The cathodic peak current (ii) at -1.2 V increases with the increasing number of coating cycles due to the electrochemical reduction of oxygen moieties (epoxide, carboxyl and hydroxide) on the surface of GO [189]. High resolution scanning electron microscopy (HRSEM) confirms the formation of GO film on the surface of the PGE shown in Figure 4.5(b).
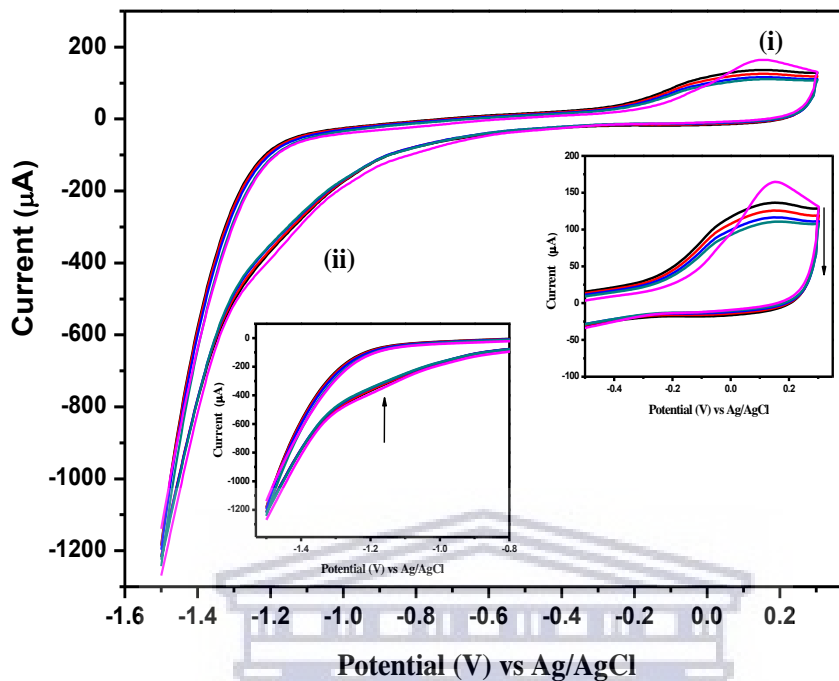
Figure 5.1 Repetitive cyclic voltammogram depicting the electrochemical reduction of 1 mg mL^{-1} GO (5 cycles) in 0.1 M acetate buffer solution (pH 4.6) on the PGE surface using the following instrumental parameters: scan rate 100 mV.s^{-1}, deposition time 120 s, frequency 50 Hz, amplitude 0.05 V and voltage step 0.005 V.

5.2 Electrochemical characterization of the ERGO-PGE and bare-PGE

The electrochemical response of the bare-PGE and ERGO-PGE were investigated by cyclic voltammetry at a scan rate of 100 mV.s^{-1} in 0.1 M acetate buffer solution (pH 4.6) over potential range of -0.3 V.s^{-1} to 0.8 V.s^{-1}. No measurable peaks were observed for either electrode over the observed potential range as shown in Figure 5.2. A higher current response was observed at the ERGO-PGE voltammogram (Figure 5.2, red-line) over the unmodified PGE, indicating large double layer capacitance compare to the bare-PGE (Figure 5.2, black-line) owing to high electron transfer rate and electrical conductivity of ERGO immobilized on the surface of the ERGO-PGE.

54
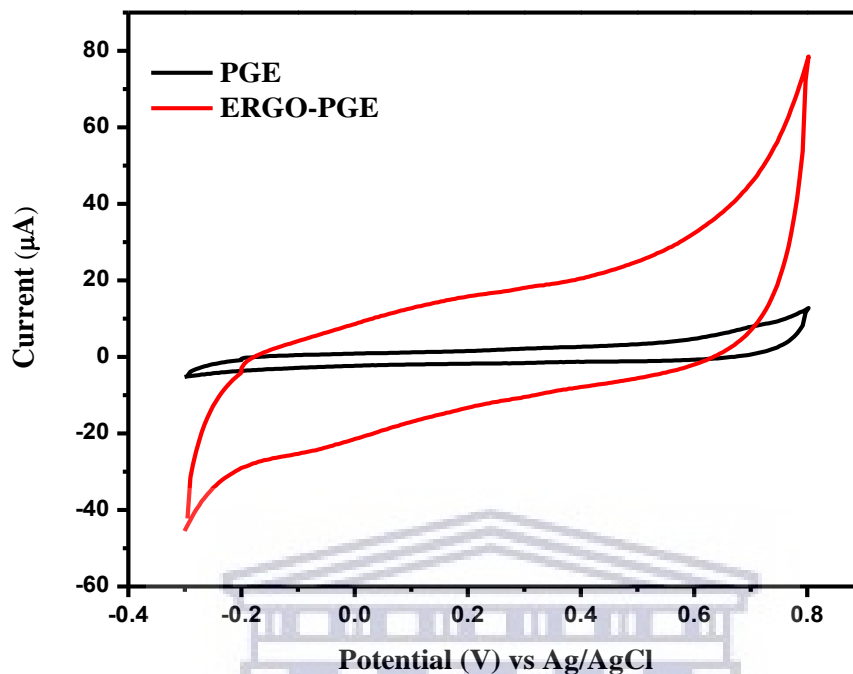
Figure 5.2 Cyclic voltammogram responses of the bare-PGE and ERGO-PGE in acetate buffer solution (0.1 M, pH 4.6) at the following instrumental parameters: scan rate 100 mV.s^{-1}, deposition time 120 s, frequency 50 Hz, amplitude 0.05 V and voltage step 0.005 V.

5.3 Electrochemical characteristic of the bare-PGE and ERGO-PGE using $[Fe(CN)_6]^{-3/-4}$ probe

Figure 5.3 compares cyclic voltammetric responses of the bare-PGE and ERGO-PGEs studied using $[Fe(CN)_6]^{-3/-4}$ as redox probe in a 0.1M KCl solution. The bare-PGE yielded peak currents of $I_{Pa} = 5.01$ x 10^{-6} A and $I_{Pc} = 3.99$ x 10^{-6} A which exhibited a pair of poor redox peaks for the $[Fe(CN)_6]^{-3/-4}$ redox couple, indicating a sluggish electron transfer at the electrode interface. While, ERGO-PGE yielded peak currents of $I_{Pa} = 4.82$ x 10^{-5} A and $I_{Pc} = 4.67$ x 10^{-5} A that showed a couple of well-defined, sharp and enhanced redox peaks. The ERGO-PGE peak currents were 10 times and 12 times bigger than the bare-PGE for anodic and cathodic peaks respectively, owing to improved electron transfer kinetics and electrical conductivity of ERGO

55

present on the electrode surface.

The anodic and cathodic peak potential of the ERGO-PGE were found to be $E_{Pa} = 0.258$ V and $E_{Pc} = 0.158$ V, while on the bare-PGE the anodic and cathodic peak potential were found to be $E_{Pa} = 0.409$ V and $E_{Pc} = 0.175$ V.

The anodic to cathodic peak potential separation (ΔE_P) was calculated using this formula:

$$\Delta E_P = E_{Pa} - E_{Pc} \qquad (1)$$

The calculated peak potential separation for the ERGO-PGE and bare-PGE were $\Delta E_P = 100$ mV and $\Delta E_P = 234$ mV respectively. The peak potential separation (ΔE_P) for the ERGO-PGE was smaller than the bare-PGE suggesting that ERGO improved the electron transfer kinetics, conductivity and high surface area to volume ratio of the ERGO-PGE. Above results confirm that ERGO as a modifier is a promising candidate for the electro-analysis and sensor applications.
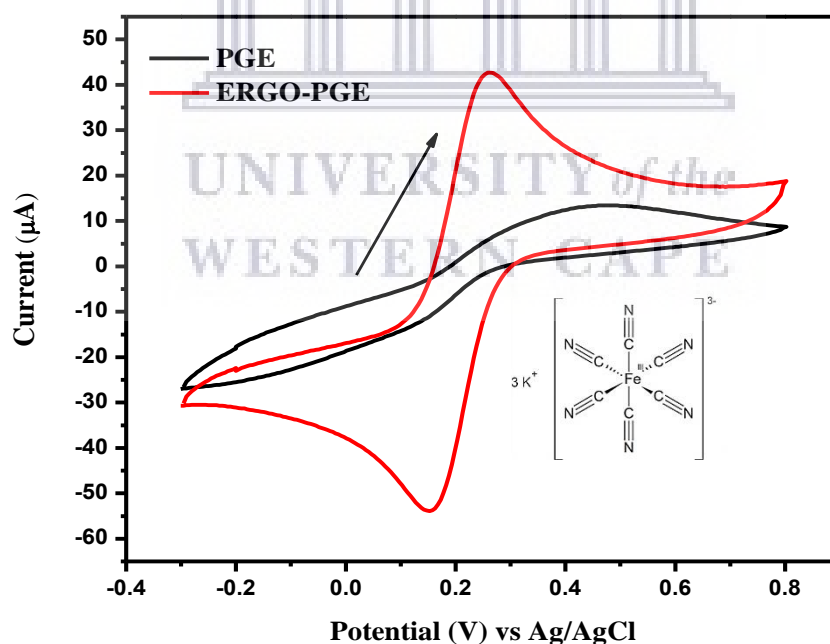
Figure 5.3 Cyclic voltammogram responses of the bare-PGE and ERGO-PGE in 2.5 mM $[Fe(CN)_6]^{-3/-4}$ in a 0.1 M KCl solution at a scan rate 100 mV.s^{-1}.

5.4 Electrochemical behavior of the bare-PGE and ERGO-PGE

The use of the ERGO to modify the surface of the pencil graphite electrode play a significant role on the electrode sensitivity thus the number of reduction cycles of GO on the electrode surface is crucial to achieve optimum electrochemical reduction cycles suitable for immobilizing ERGO on the PGE surface. Figure 5.4 shows the influence of various coating cycles (3, 5 and 10 cycles) on cyclic voltammetric responses of the ERGO-PGE and bare-PGE in 2.5 mM $[Fe(CN)_6]^{-3/-4}$ in a 0.1 M KCl solution. The redox peak currents varied with different number of coating cycles as shown in Figure 5.4. All three modified electrodes demonstrated improved current responses over the unmodified electrode. When 3 coating cycles was used, suppression of the ferri/ferro redox peak currents was observed due to insufficient amount of the reduced graphene oxide on the electrode surface. When increasing the number of coating cycles to 5 cycles, the redox peak currents of the ERGO-PGE increased owing to high electrochemical active-sites, conductivity and large surface area of ERGO. Upon increasing number of coating cycles to 10 cycles, a decrease in redox peak currents was observed, owing to high amount of ERGO on the electrode surface that formed thick ERGO film and hinders the current signals. Five electrochemical reduction cycles were chosen as optimum coating cycles for further experiments due to improved electrochemical response on the ERGO-PGE.

57
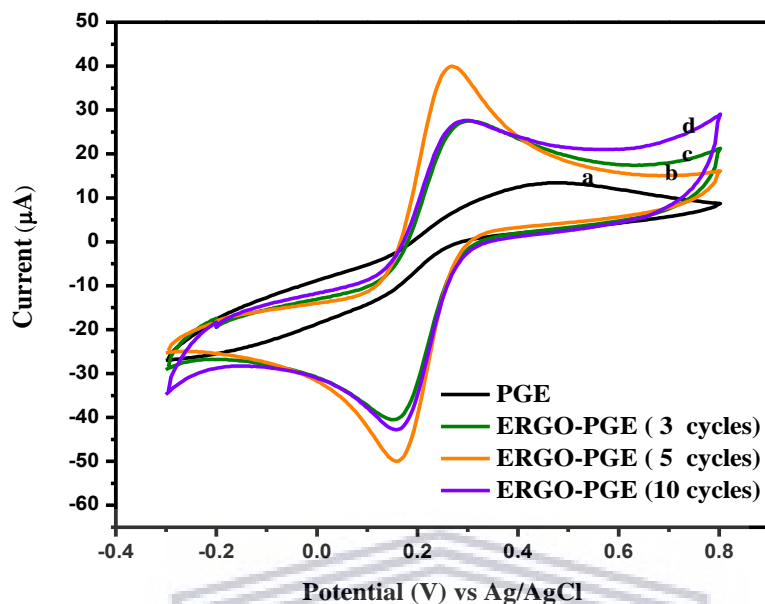
Figure 5.4 Cyclic voltammogram of (a) bare-PGE and ERGO-PGE prepared under different coating cycles (b) 5 cycles, (c) 3 cycles and (d) 10 cycles in 2.5 mM $[Fe(CN)_6]^{-3/-4}$ in a 0.1 M KCl solution.

5.5 Effect of scan rate on the bare-PGE and ERGO-PGE

Cyclic voltammograms of the ERGO-PGE and bare-PGE with their corresponding linear plots carried out in 2.5 mM $[Fe(CN)_6]^{3/-4}$ in a 0.1 M KCl as the redox probe over potential range of −0.2 to +0.6 V is shown in Figure 5.5(a-d). From the voltammogram of the ERGO-PGE shown in Figure 5.5(c) a steady increase in anodic and cathodic peak currents was observed when the scan rate varies from 10 mV.s^{-1} to100 mV.s^{-1}, indicating an increase in electro-catalytic activity and surface area to volume ratio of the electrode. In addition, the shape of the voltammogram is dependent on the scan rate used. The relationship between anodic and cathodic peak currents versus the square roots of the scan rate is linear indicating a diffusion controlled process, owing to the ERGO-PGE reversible reaction where $[Fe(CN)_6]^{-3/-4}$ ions move from electrolyte to the electrode surface through diffusion process [190]. In anodic scan, $[Fe(CN)_6]^{4-}$ is oxidized to $[Fe(CN)_6]^{3-}$ losing one electron and in cathodic scan $[Fe(CN)_6]^{3-}$ is reduced to $[Fe(CN)_6]^{4-}$.

58

$$[Fe(CN)_6]^{-4} \rightleftharpoons [Fe(CN)_6]^{-3} + e^- \qquad (2)$$
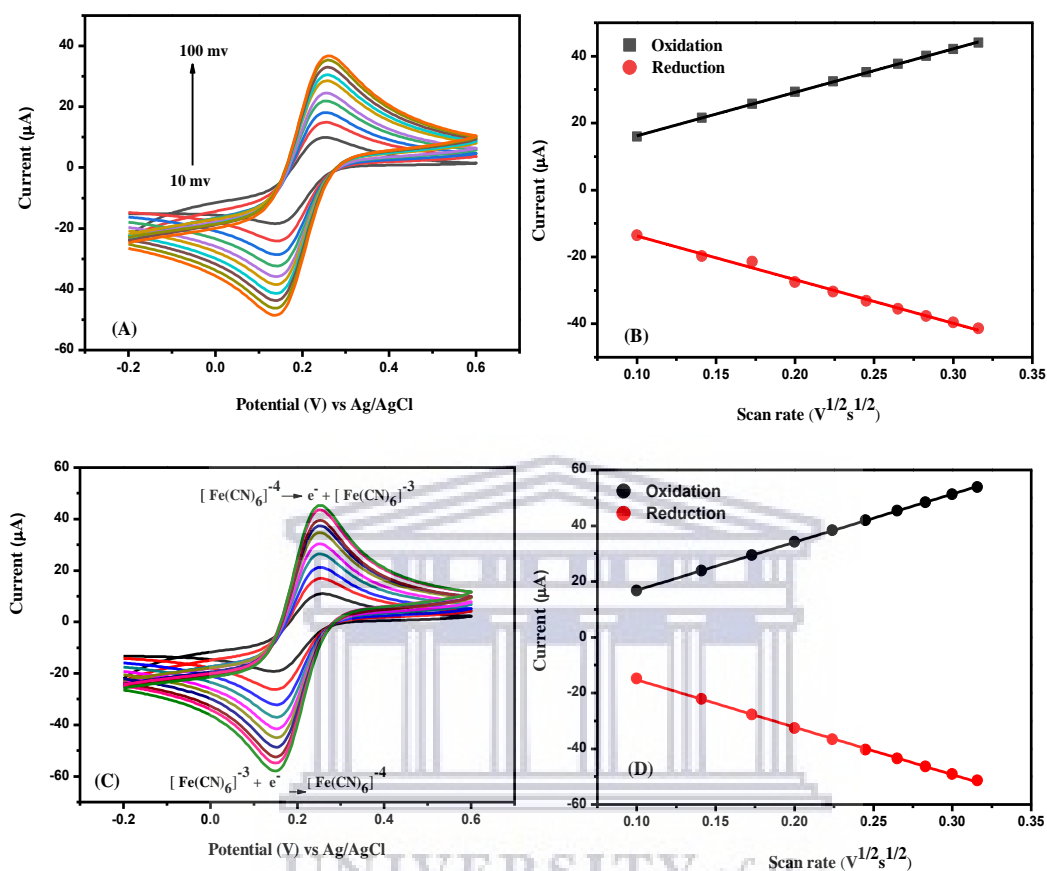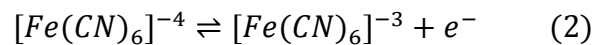
Figure 5.5 Cyclic voltammogram of 2.5 mM [Fe(CN)$_6$]$^{-3/-4}$ in a 0.1 M KCl solution at the (A-B) bare-PGE and (C-D) ERGO-PGE from 10 mV.s^{-1} to 100 mV.s^{-1} with their corresponding linear relation between anodic and cathodic peak currents versus the square root of scan rates.

Table 4. Linear equation and corresponding regression from the plot of current (I_p) versus square root of scan rate ($V^{1/2}.s^{1/2}$).

	Linear equation	Correlation coefficient (R^2)
ERGO-PGE		
I_{pa}	1.73×10^{-4} x $+ 4.40 \times 10^{-7}$	0.999
I_{pc}	-1.70×10^{-4} x $+ 1.75 \times 10^{-6}$	0.999
Bare-PGE		
I_{pa}	1.30×10^{-4} x $+ 3.19 \times 10^{-6}$	0.999
I_{pc}	-1.30×10^{-4} x $- 7.01 \times 10^{-7}$	0.993

5.5.1. Diffusion coefficient of the bare-PGE and ERGO-PGE

The Randles-Sevcik linear equation was used to determine diffusion coefficient of 2.5 mM $[Fe(CN)_6]^{-3/-4}$ in a 0.1 M KCl solution at the ERGO-PGE and bare-PGE. The Randles-Sevcik linear equation is expressed as follows:

$$I_P = 2.69 \times 10^5 \times n^{\frac{3}{2}} \times A \times D^{\frac{1}{2}} \times C \times v^{\frac{1}{2}} \quad (3)$$

Where, I_p is the peak current (Ampere), n is the number of electron transferred in the half-reaction for the redox couple ($n = 1$), A is the electrode surface area (cm^2), D is the diffusion coefficient of $[Fe(CN)_6]^{-3/-4}$ in solution ($cm^2.s^{-1}$), C is the concentration of the $[Fe(CN)_6]^{-3/-4}$ molecules ($mol.cm^{-3}$) and v is the scan rate ($V.s^{-1}$).

The electrode surface area of the pencil graphite electrode was calculated using the equation (4)

$$A = \pi r^2 + 2\pi rh \quad\quad (4)$$

Where, A is the electrode surface area (cm^2), π is the constant, r is the radius of the circle and h is the height of the electrode. The electrode surface area of the pencil graphite electrode was

60

calculated as 0.159 cm^2. The slope of the linear plot of peak current (I_p) versus square root of scan rate ($v^{\frac{1}{2}}$) was used to calculate the diffusion coefficient shown in Figure 5.5 (b) and 5.5 (d). The diffusion coefficients of the ERGO-PGE were calculated as 2.59×10^{-6} cm^2.s^{-1} and 2.53×10^{-6} cm^2.s^{-1} for anodic and cathodic. While, the diffusion coefficient of the bare-PGE was the same 1.46×10^{-6} cm^2.s^{-1} for anodic and cathodic peak currents. The diffusion coefficients obtained at the ERGO-PGE was 1.77 greater than the bare-PGE which indicated that, the use of the ERGO accelerates the charge transfer process between the $[Fe(CN)_6]^{-3/-4}$ probe and the electrode surface. Thereby improving the mass transfer of the $[Fe(CN)_6]^{-3/-4}$ ions from the solution to the ERGO-PGE surface suggesting the reaction is diffusion-controlled [54].

5.5.2. Electroactive surface area of the bare-PGE and ERGO-PGE

The electroactive surface area of the electrodes were calculated using the ideal value of the ferro/ferricyanide $[Fe(CN)_6]^{-3/-4}$ diffusion coefficient, 6.2×10^{-6} cm^2.s^{-1} [184]. Randles-Sevcik equation (3) can be rearranged to yield equation (5):

$$A = \frac{Slope\left(\frac{I_P}{v^{\frac{1}{2}}}\right)}{2.69 \times 10^5 \times n^{\frac{3}{2}} \times D^{\frac{1}{2}} \times C} \tag{5}$$

The electroactive surface area of the ERGO-PGE was calculated as 0.103 cm^2 and 0.102 cm^2 for anodic and cathodic peak current. While, the electroactive surface area of the bare-PGE was calculated as 0.078 cm^2 for anodic and cathodic peak currents. Thus, the electroactive surface area of the ERGO-PGE was 1.3 times bigger than the electroactive surface area of the bare-PGE due to high surface area to the volume ratio of ERGO.

5.5.3. Surface coverage of the bare-PGE and ERGO-PGE

The surface coverage of the electrochemically reduced graphene oxide on the PGE was calculated using the slope value from the plot of peak current (I_p) vs scan rate (υ) as shown in Figure 5.5.3, in accordance with the Brown-Anson model using the following equation [192].

$$I_P = \frac{n^2 F^2 \Gamma^* A \upsilon}{4RT} \qquad (6)$$

Where Ip, A and υ are the same as in equation (3), Γ^* is the surface concentration (mol.cm^{-2}), F is the Faraday constant (96 485 C.mol^{-1}), R is the molar gas constant (8.314 J.K^{-1}.mol^{-1}) and T is the temperature (298 K).
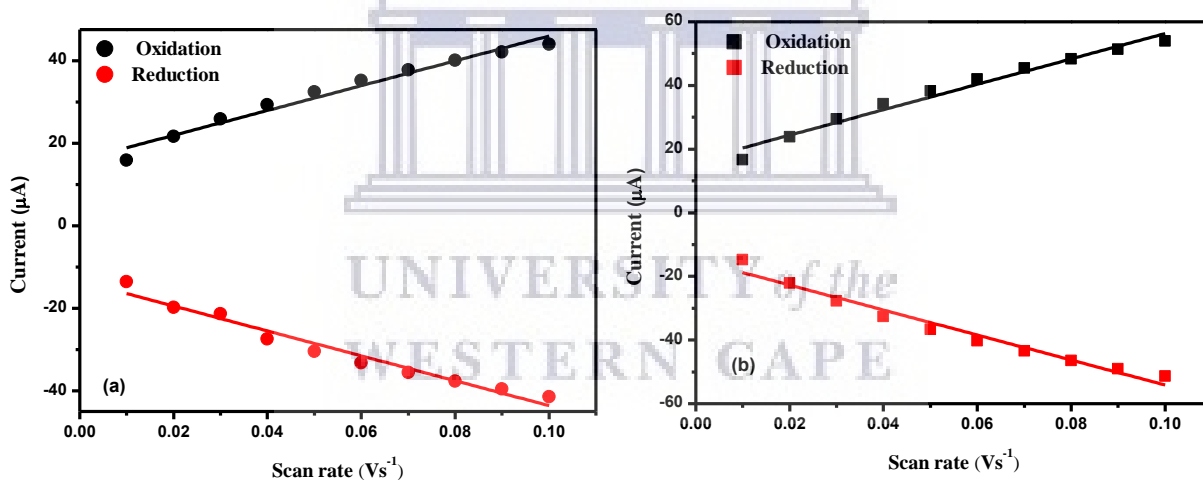
Figure 5.5.3 Plot of anodic and cathodic peak current (µA) versus scan rate (V.s^{-1}) for (a) bare-PGE and (b) ERGO-PGE.

Table 5. Linear equation and corresponding regression values from the plot of current (I_p) versus scan rate ($V.s^{-1}$).

	Linear equation	Correlation coefficient (R^2)
ERGO-PGE		
I_{pa}	3.99×10^{-4} x $+ 1.64 \times 10^{-5}$	0.98
I_{pc}	-3.93×10^{-4} x $- 1.49 \times 10^{-5}$	0.97
Bare-PGE		
I_{pa}	3.01×10^{-4} x $+ 1.59 \times 10^{-5}$	0.97
I_{pc}	-3.01×10^{-4} x $- 1.34 \times 10^{-5}$	0.97

The surface coverage of the ERGO-PGE was calculated to be 2.673×10^{-9} mol.cm^{-2} and 2.633×10^{-9} mol.cm^{-2} for anodic and cathodic while the surface coverage of the bare-PGE was found to be the same for anodic and cathodic and was calculated to be 2.02×10^{-9} mol.cm^{-2}. The higher values obtained at the ERGO-PGE confirm the use of the ERGO to modify the pencil graphite electrode surface has increased the electroactive species concentration of $[Fe(CN)_6]^{-3/-4}$ ions due to high sensitivity and specific surface area of ERGO.

5.6. Electrochemical impedance spectra (EIS)

Electrochemical impedance spectroscopy (EIS) is an efficient electrochemical tool used to gain insight into the electrochemical behaviour of the electrode interface such as charge transfer properties, electrical conductivity, capacitance of the bare-PGE and ERGO-PGE and further developing a circuit of the interface [195, 196]. The Nyquist plot of the bare-PGE and ERGO-PGE (Figure 5.6) was performed in 2.5 mM [Fe (CN)$_6$]$^{-3/-4}$ in a 0.1 M KCl solution over a frequency range of 0.1 Hz to 10^4 Hz when the electrodes were relatively steady. Moreover, the Nyquist plot usually contains a semicircular section at higher frequencies that quantifies the

63

charge transfer kinetics of the redox probe at the electrode-electrolyte interface and a linear portion at lower frequencies relates to diffusion control process of the reactive species and electrode conductivity [195]. Z-view software was used to evaluate EIS experimental results by fitting the Nyquist spectra of the bare-PGE and ERGO-PGE using the Randles equivalent circuit (inset, figure 5.6).

The equivalent circuit consisted of solution resistance (Rs), charge transfer resistance (R_{ct}), double layer capacitance (C_{dl}) and Warburg impedance (Z_w) [196]. From the Nyquist plot, the R_{ct} of the bare-PGE was found to be 686.6 Ω owing to a large depressed semicircle domain present at higher frequencies, indicating a limited charge transfer process at $[Fe(CN)_6]^{-3/-4}$ probe and the electrode interface due to poor electrical conductivity of the bare-PGE. On the other hand, the R_{ct} of the ERGO-PGE decreased dramatically to 319.8 Ω defined by small semicircle domain at higher frequencies, suggesting that ERGO improved the electrical conductivity and increased the reactive sites of the electrode. Thereby, reducing the interface resistance and increasing the charge transfer rate between the $[Fe(CN)_6]^{-3/-4}$ probe and the electrode interface [54, 199].

The slope of a linear portion of the electrodes were associated with Warburg impedance which corresponds to the diffusion of ions from the electrolyte to the electrode surface and conductivity of the electrode [197, 200]. The Warburg line of the ERGO-PGE at lower frequencies was almost straight line compare to the bare-PGE as shown in Figure 5.6, indicating high diffusion of $[Fe(CN)_6]^{-3/-4}$ ions towards the ERGO-PGE surface [172, 201]. In conclusion, the decrease in charge transfer resistance with an increase on the slope of the ERGO-PGE suggests that the presence of ERGO enhanced the electrical conductivity and transfer rate of the electron. This confirms that the ERGO-PGE is a promising candidate for sensor applications.
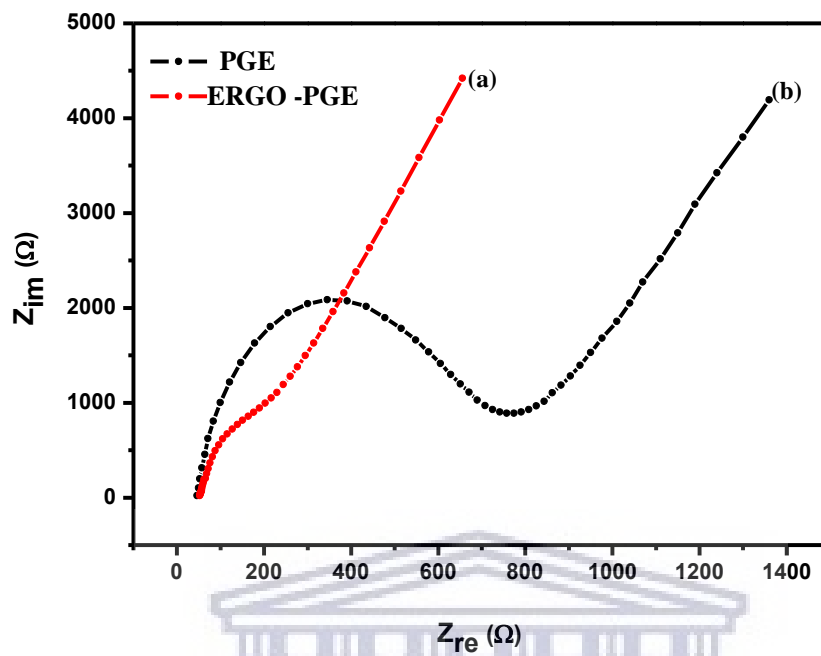
Figure 5.6 Nyquist plot of (a) bare-PGE, (b) ERGO-PGE in 2.5 mM $[Fe(CN)_6]^{-3/-4}$ in a 0.1 M KCl solution. The inset represents the equivalent electrical circuit.

CHAPTER SIX

6. The determination of metal ion- cupferron complexes on the ERGO-HgF-PGE and bare-PGE

In order to establish the most suitable experimental conditions for SW-AdCSV measurements, characteristic stripping responses of Cd^{2+}, Pb^{2+}, Cu^{2+} and Zn^{2+}-cupferron complexes at the ERGO-HgF-PGE were studied and various instrumental parameters were optimized . Cupferron was used as a selective complexing agent during the electrode pre-concentration for simultaneous detection of Cd^{2+}, Pb^{2+}, Cu^{2+} and Zn^{2+}. Proper attention was given to competition between the trace-metals and cupferron as well as competitive adsorption of the complexes.

6.1. Proposed mechanism for the formation of metal ion - cupferron complexes and electrochemical detection of Cd^{2+}, Pb^{2+}, Cu^{2+} and Zn^{2+}

The proposed mechanism for the formation of Cd^{2+}, Pb^{2+}, Cu^{2+} and Zn^{2+}complexes with cupferron is shown in schematic 6.1. Deprotonation of the N-nitroso-phenyl-hydroxyl amine achieved in a solution of suitable pH facilitates the reaction. The central metal ion is bonded to only two sites of the cupferron ligand which are two oxygen atoms forming a five membered ring. A 1:1 stoichiometric complex is achieved. For detection, an *in-situ* detection approach was employed. To the electrochemical cell, 8 μL of cupferron (0.1 M in ultrapure water), aliquots of Cd^{2+}, Pb^{2+}, $Cu^{2+}$and Zn^{2+} standard solutions of 10 mg.L^{-1} stock solution, and 50 μL of Hg (1000 ppm) are introduced into the cell. The stirrer was switched on and the mixture was stirred for 30 s to allow the metal ion-cupferron complexes to form. An oxidation potential of 0.1 V for 60 s was then applied while stirring the solution, this allowed for the formation of the mercury film onto the pencil graphite electrode with concomitant adsorption of the formed metal ion-cupferron complexes. The solution was allowed to become quiescent for 10 s followed by a recorded cathodic voltammetric scan from 0 V to -1.2 V in square-wave mode resulting in the reduction of the metal cations to the metal zero oxidation state and its subsequent stripping. Figure 6.2 shows well-defined stripping peaks for the reduction of Cd^{2+}, Pb^{2+}, $Cu^{2+}$and Zn^{2+}-cupferron complexes.

H. Cui *et al* proposed similar mechanism for the formation of Ti^{4+}-cupferron system on a bismuth-coated glassy carbon electrode [200].
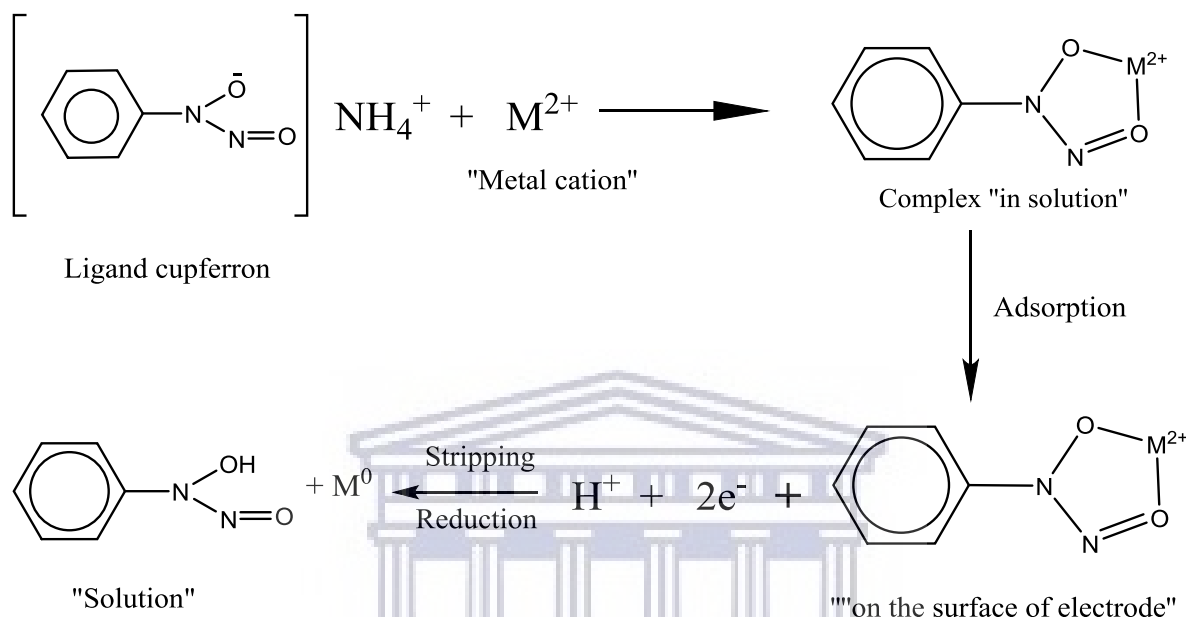
Schematic 6.1 Proposed mechanism for metal ion-cupferron complex formation and detection.

6.2. Effects of the electrochemically reduced graphene oxide on the voltammetric peak currents

Preliminary experiments were done to distinguish the particular features that characterize the behavior of metal ion -cupferron systems at the ERGO-HgF-PGE and bare-HgF-PGE in 0.1 M acetate buffer solution (pH 4.6) containing 50 $\mu g.L^{-1}$ of Cd^{2+}, Pb^{2+}, Cu^{2+} and 20 $\mu g.L^{-1}$ of Zn^{2+} as illustrated in Figure 6.2. Small peaks with low current responses are seen for the bare-HgF-PGE at 0.1 V after accumulation for 60 s. The ERGO-HgF-PGE exhibited well-resolved peaks and distinct reduction stripping peak currents of the adsorbed cupferron-complexes positioned at Cd^{2+} (- 0.649 V), Pb^{2+} (- 0.509 V), Cu^{2+} (- 0.140 V) and Zn^{2+} (-1.056 V). Two peaks were found for the possible reduction of active sites at the cupferron ligand, located at - 0.975 V and - 0.350 V, respectively. In literature only one cupferron reduction peak at - 0.350 V reported by A.

Koper *et al* and at - 0.975 V reported by S. Abbasi *et al* [16, 24] respectively. A signal increase of approximately 2, 5, 23 and 17 times at the ERGO-HgF-PGE was observed compare to the bare-HgF-PGE for stripping responses of Cd^{2+}, Pb^{2+}, Cu^{2+}, and Zn^{2+} respectively thus signaling exceptional electrocatalytic activity, good electron transfer promotion, high surface area to volume ratio owing to ERGO. The obtained results showed the use of the ERGO in conjunction with thin mercury film enhanced the selectivity and sensitivity of SW-AdCSV method [90, 203]. Further, indicating strong adsorptive capability and good conductivity of the ERGO-HgF-PGE towards the metal ion- cupferron complex reduction.
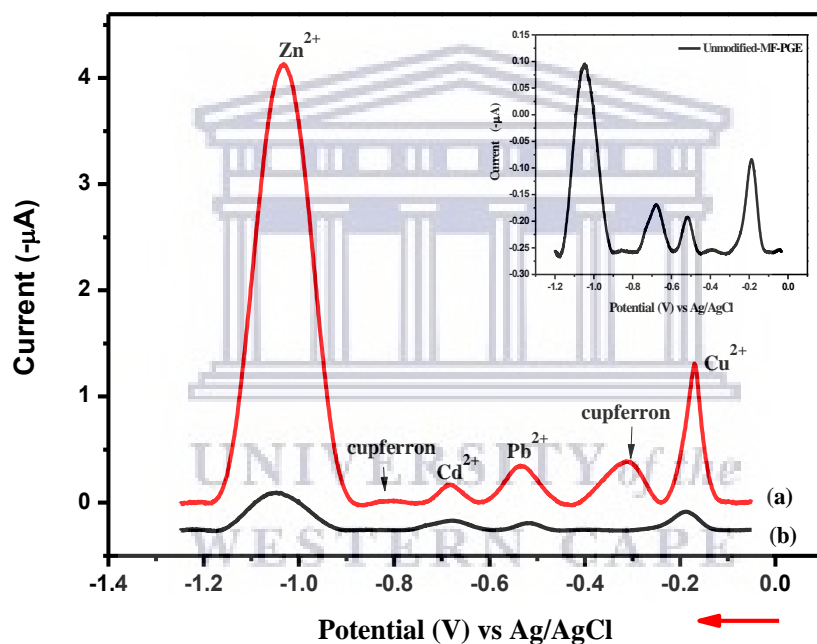
Figure 6.2 SW-AdCSV for simultaneous determination of 50 µg.L^{-1} Cd^{2+}, Pb^{2+}, Cu^{2+} and 20 µg.L^{-1} Zn^{2+} in 0.1 M acetate buffer solution (pH 4.6), 0.04 mM cupferron obtained at (a) ERGO-HgF-PGE, (b) bare-HgF-PGE.

6.3. Influence of cupferron complexing agent

Cupferron has been reported in literature to form stable complexes with various metal ions at different electrode substrates [20, 37, 78, 87, 204]. Figure 6.3, illustrates the influence of cupferron on SW-AdCSV of the adsorbed Cd^{2+}, Pb^{2+}, Cu^{2+} and Zn^{2+} complexes at the ERGO-HgF-PGE after accumulation of 60 s. In the absence of metal ions at the ERGO-HgF-PGE, only two peaks for cupferron reduction were observed at - 0.975 V and - 0.350 V as shown in Figure 6.3(a). This confirms that the two peaks shown are due solely to reduction of cupferron ligand. Four distinct cathodic peaks of Cd^{2+}, Pb^{2+}, Cu^{2+} and Zn^{2+} were observed at the ERGO-HgF-PGE upon the introduction of the trace metal ions as clearly illustrated in Figure 6.3(b). This was a promising result as it indicates the ability for adsorption of metals at the graphene mercury-film electrode. The inclusion of thin mercury film enhanced the electrode sensitivity as well as the presence of ERGO increased the electrode binding-sites that improved the electron transfer [203, 205]. In the absence of cupferron ligand we observe the removal of the cupferron reduction peaks, as expected. The addition of cupferron resulted in four well-resolved cathodic peaks of Cd^{2+}, Pb^{2+}, Cu^{2+} and Zn^{2+} in a solution containing trace metals and mercury film owing to strong adsorptive properties of cupferron ligand. An increase in stripping peak current for each metal stripping peak reduction was noted due to improved adsorption of metal ions at the electrode surface in the complexed form. Pb^{2+} demonstrated lowest affinity for the cupferron complex. The obtained results showed that cupferron is a suitable complexing agent with excellent peak separation for simultaneous determination of Cd^{2+}, Pb^{2+}, Cu^{2+} and Zn^{2+}.
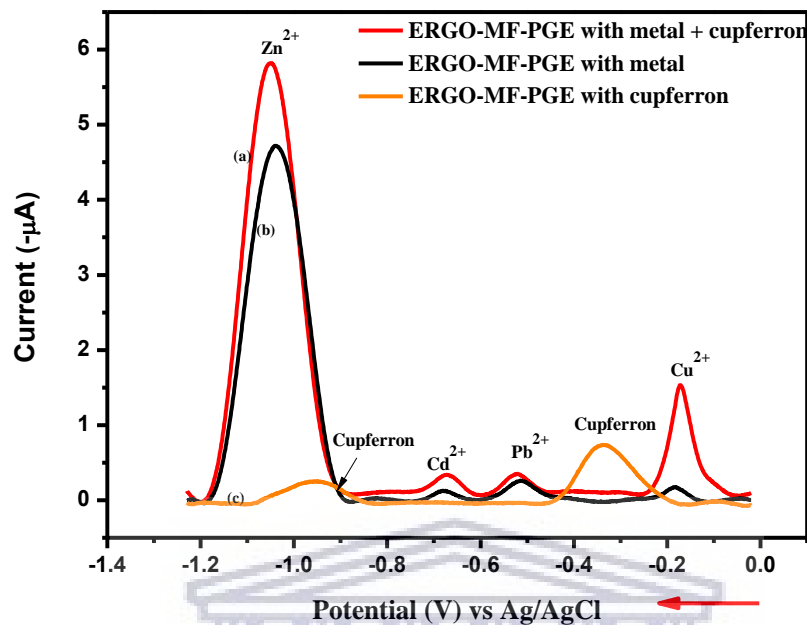
Figure 6.3 SW-AdCSV for (a) 0.04 mM cupferron, (b) 50 µg.L^{-1} Cd^{2+}, Pb^{2+}, Cu^{2+} and 20 µg.L^{-1} Zn^{2+} at the ERGO-HgF-PGE, (c) 0.04 mM cupferron and trace metals at the ERGO-HgF-PGE.

6.4. Influence of mercury film

The influence of the mercury film on the stripping peak currents of Cd^{2+}, Pb^{2+}, Cu^{2+}and Zn^{2+}-cupferron complexes was studied in 0.1 M acetate buffer solution (pH 4.6) at the ERGO-HgF-PGE for 60 s accumulation time. Figure 6.4(a) shows that in the absence of mercury film and metal ions, only the characteristic two distinct cupferron reduction peaks are observed. Upon addition of 50 µg.L^{-1} Cd^{2+}, Pb^{2+}, Cu^{2+}and Zn^{2+}, no peaks attributed to the reduction of each metal cation can be observed. This phenomenon indicates the lack of adsorption of suitable concentrations of metal-cupferron complexes at the bare-PGE surface in the absence of metal film. However, an increase in the two cupferron reduction peak currents is observed, as seen in Figure 6.4(b). In the presence of an electroplated mercury film as shown in Figure 6.4(c), four sharp and well-resolved peaks due to the reduction of the target metal ions from the formed metal-cupferron complexes were observed. This thereby proves the preferential accumulation of

70

the metal-chelate complexes at the metal film. The use of in-situ plated mercury film and cupferron complexing agents are therefore both needed to improve electrode sensitivity by increasing the solubility of the metal ions at the electrode surface.
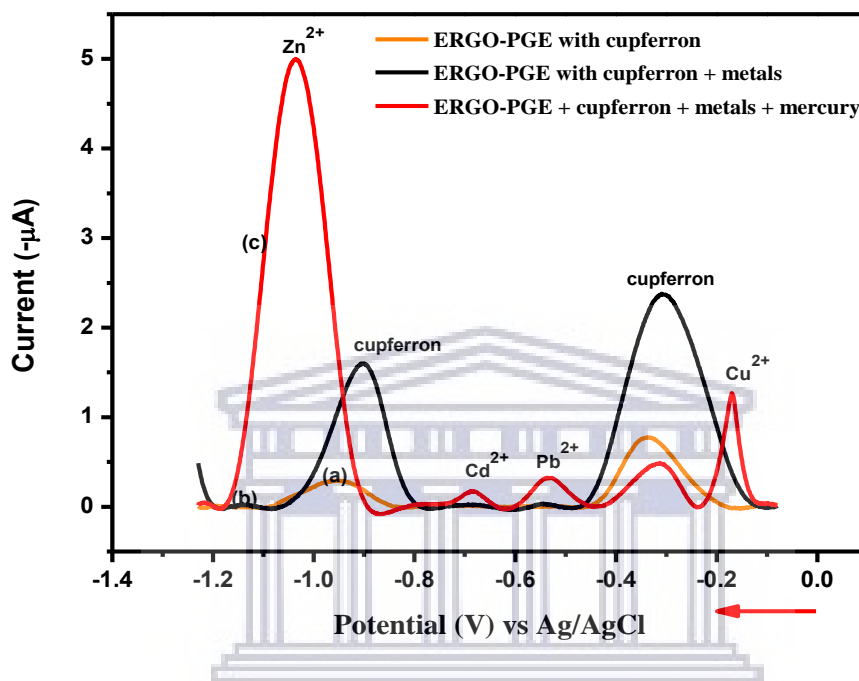
Figure 6.4 SW-AdCSV for (a) 0.04 mM cupferron at the ERGO-PGE, (b) 50 µg.L^{-1} Cd^{2+}, Pb^{2+}, Cu^{2+} and 20 µg.L^{-1} Zn^{2+} + (a), (c) 0.04 mM cupferron and Cd^{2+}, Pb^{2+}, Cu^{2+} and Zn^{2+} at the ERGO-HgF-PGE.

6.5. Optimization of various experimental conditions

Optimization of experimental conditions is crucial for better sensitivity of the simultaneous determination of Cd^{2+}, Pb^{2+}, Cu^{2+} and Zn^{2+} in the presence of cupferron ligand at the ERGO-HgF-PGE in 0.1 M acetate buffer solution (pH 4.6). Various experimental conditions for SW-AdCSV were optimized such as the effect of cupferron concentration, supporting electrolyte, pH of the buffer solution and instrumental parameters such as deposition time, amplitude, frequency and voltage step.

71

6.5.1 Effect of cupferron concentration

Ligand concentration plays an important role on adsorptive stripping peak current, cupferron is essential for the formation of adsorptive complex. The effect of cupferron concentration on the sensitivity of the simultaneous determination of Cd^{2+}, Pb^{2+}, Cu^{2+} and Zn^{2+} at the ERGO-HgF-PGE was studied from 0.04 to 4 mM. The cathodic peak currents of Cd^{2+}, Pb^{2+}, Cu^{2+} and Zn^{2+}-cupferron complexes increased with an increase in cupferron concentration up to 4 mM as shown in Figure 6.5.1. It was found that the peak currents decreased at higher cupferron concentrations from 0.2 to 4 mM due to competition between free cupferron ligand and trace metal- cupferron complexes for active-sites on the electrode surface. In addition, higher cupferron concentrations might have cause difficulties in reducing metal ion-cupferron complexes. For this reason, cupferron concentration of 0.04 mM was found to be ideal for further experiments to ensure maximum stripping peak response for the simultaneous determination of all four metals.
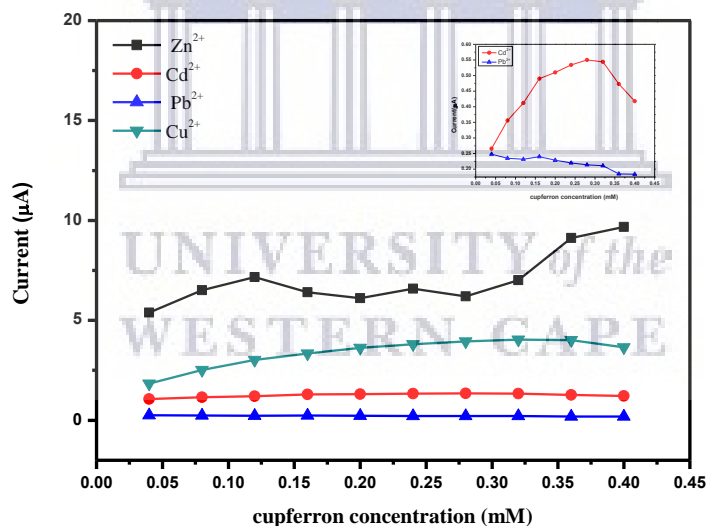
Figure 6.5.1 SW-AdCSV for the effect of various cupferron concentration on the peak current of 50 µg.L^{-1} Cd^{2+}, Pb^{2+}, Cu^{2+} and 20 µg.L^{-1} Zn^{2+} in 0.1 M acetate buffer solution (pH 4.6) at the ERGO-HgF-PGE.

72

6.5.2 Effect of supporting electrolyte

SW-AdCSV voltammograms of Cd^{2+}, Pb^{2+}, Cu^{2+} and Zn^{2+} in the presence of 0.04 mM cupferron were recorded in various supporting electrolytes such as 0.1 M of ammonia-ammonium chloride buffer solution (pH 9.6), 0.1 M acetate buffer solution (pH 4.6) and 0.1 M phosphate buffer solution (pH 7.0) following the pre-concentration of cupferron complexes onto the ERGO-HgF-PGE by adsorptive accumulation at 0.1 V for 60 s. Figure 6.5.2. Illustrates the influence of three different supporting electrolytes on the cupferron complexes at the ERGO-HgF-PGE, well-resolved and sharp reduction peak currents of metal ion-cupferron complexes with highly enhanced sensitivity were observed in 0.1 M acetate buffer solution (pH 4.6) compare to other electrolytes. In ammonia-ammonium chloride buffer solution (pH 9.6) and 0.1 M phosphate buffer solution (pH 7.0) no stripping peak of Zn^{2+} was observed, only weak reduction peak currents of Cd^{2+}, Pb^{2+} and Cu^{2+} with a negative shift in the peak potential were observed. Thus, 0.1 M acetate buffer solution (pH 4.6) was used for further experiments as it gave sharper and enhanced peak current response.
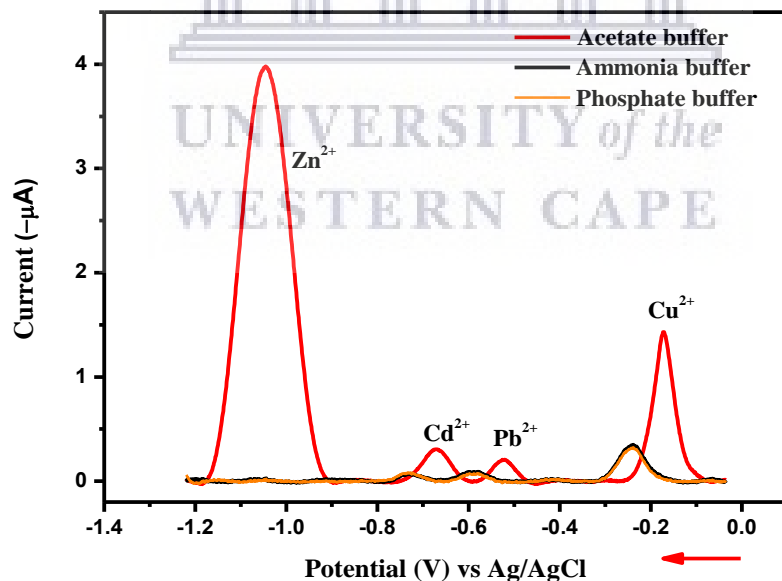
Figure 6.5.2 SW-AdCSV for simultaneous determination of 50 µg.L^{-1} Cd^{2+}, Pb^{2+}, Cu^{2+} and 20 µg.L^{-1} Zn^{2+} at the ERGO-HgF-PGE with supporting electrolyte: (red line) 0.1 M acetate buffer

73

solution (pH 4.6), (green line) 0.1 M ammonia-ammonium chloride buffer solution (pH 9.6) and (blue line) phosphate buffer solution (pH 7.0).

6.5.3. Influence of pH value

pH is very crucial for the formation of stable cupferron complexes, the potential of reduction and adsorption properties of the ERGO-HgF-PGE [21, 88]. The influence of pH on the cathodic peak currents of Cd^{2+}, Pb^{2+}, Cu^{2+} and Zn^{2+} at the ERGO-HgF-PGE was studied in the range of pH 3 to 6 in 0.1 M acetate buffer solution. As shown in Figure 6.5.3 it was found that at lower pH values the reduction peak currents decreased due to protonation of cupferron binding-sites, thereby reducing the adsorption of cupferron complexes on the electrode surface and excess protons resulted in competition of each metal-ions in forming a bond with ligand. Whereas, at high pH values from 5.0 to 6.0 the stripping peak currents decreased owing to hydrolysis of cupferron complexes as they are not adequately protonated to form cations, due to more hydroxide (OH⁻) ions formation therefore hindering the adsorption process on the electrode surface [37, 206, 207]. Hence, pH 4.6 was chosen for all subsequent experiments in order to achieve maximum sensitivity.
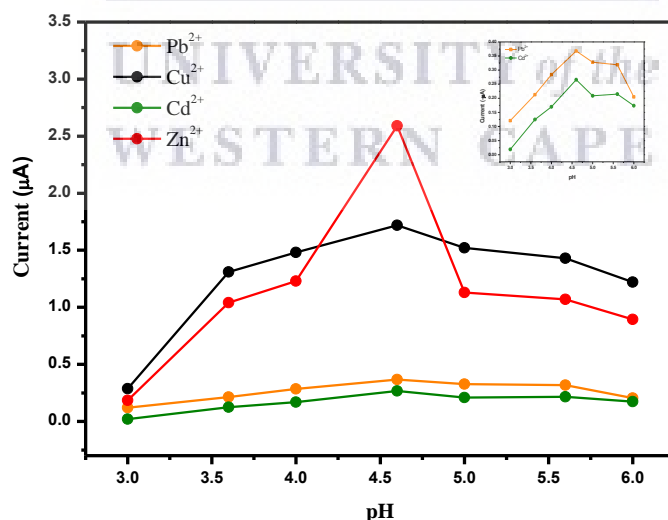
Figure 6.5.3 The effect of pH on adsorptive peak currents of 50 µg.L^{-1} Cd^{2+}, Pb^{2+}, Cu^{2+} and 20 µg.L^{-1} Zn^{2+}-cupferron complexes in 0.1 M acetate buffer solution at the ERGO-HgF-PGE.

74

6.5.4. Effect of deposition time

Pre-concentration time plays an important role in stripping voltammetry, as it can affect the sensitivity of SW-AdCSV, detection limit and analysis time of the measurements. The deposition time for Cd^{2+}, Pb^{2+}, Cu^{2+} and Zn^{2+} at the ERGO-HgF-PGE was studied in 0.1 M acetate buffer solution (pH 4.6) between 10 and 90 s. Figure 6.5.4 shows cathodic peak currents of trace-metals which increased with an increase in deposition time up to 60 s for all metal ions due to increased adsorption of metal-cupferron complexes and a larger concentration of analytes at the electrode surface. However, a plateau appears at a deposition times between 60 and 90 s suggesting that the electrode surface might be saturated by metal ions. Thus, a shorter deposition time of 60 s was chosen and used throughout as it enhanced the sensitivity and relatively shorten the analysis time.
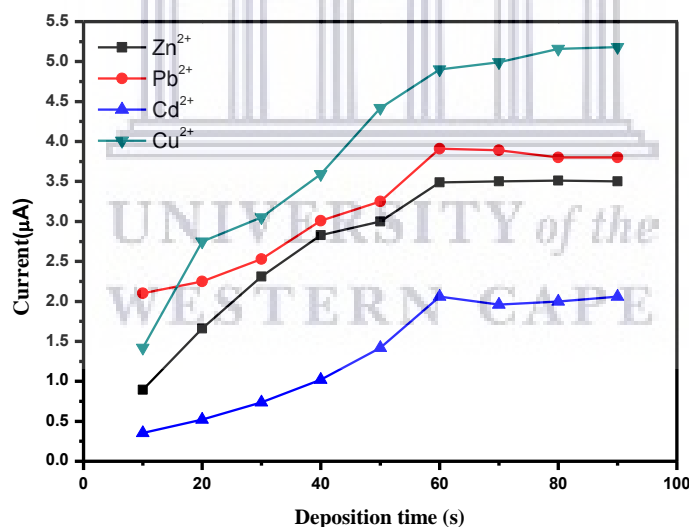
Figure 6.5.4 The effect of deposition time on the peak current of 50 µg.L^{-1} Cd^{2+}, Pb^{2+}, Cu^{2+} and 20 µg.L^{-1} Zn^{2+} in 0.1 M acetate buffer solution (pH 4.6) at the ERGO-HgF-PGE.

75

6.5.5. Effect of amplitude

Figure 6.5.5, shows the effect of amplitude on the cathodic peak currents of Cd^{2+}, Pb^{2+}, Cu^{2+} and Zn^{2+} at the ERGO-HgF-PGE varied from 10 to 50 mV in 0.1 M acetate buffer solution, a significant increase in cathodic stripping peak currents was observed and 30 mV amplitude was selected for subsequent experiments.
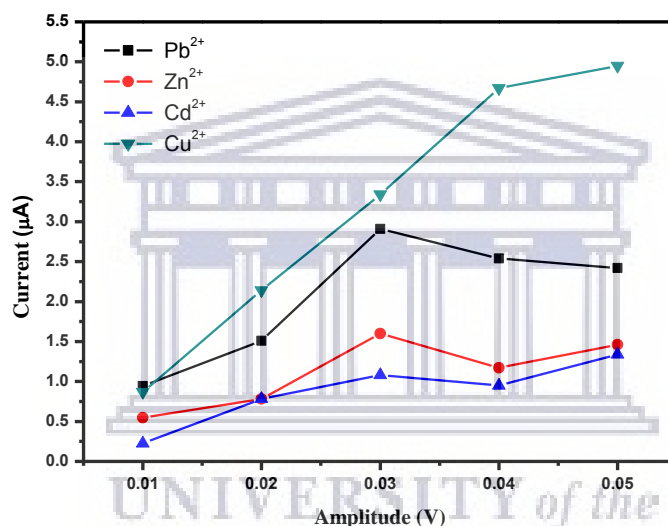
Figure 6.5.5 The effect of deposition time on the peak currents of 50 µg.L^{-1} Cd^{2+}, Pb^{2+}, Cu^{2+} and 20 µg.L^{-1} Zn^{2+} in 0.1 M acetate buffer solution (pH 4.6) at the ERGO-HgF-PGE.

6.5.6. Effect of frequency (Hz)

The influence of frequency on the cathodic peak currents of Cd^{2+}, Pb^{2+}, Cu^{2+} and Zn^{2+} at the ERGO-HgF-PGE was studied in the range of 15 to 85 Hz in 0.1 M acetate buffer solution. As shown in Figure 6.5.6 it was found that the cathodic peak currents increased with an increase in frequency from 15 to 65 Hz for Cd^{2+} and Cu^{2+}, at high frequency above 45 a drastic decreased in the peak currents of Pb^{2+} and Zn^{2+} was observed. A 35 Hz was selected for subsequent experiment.

76
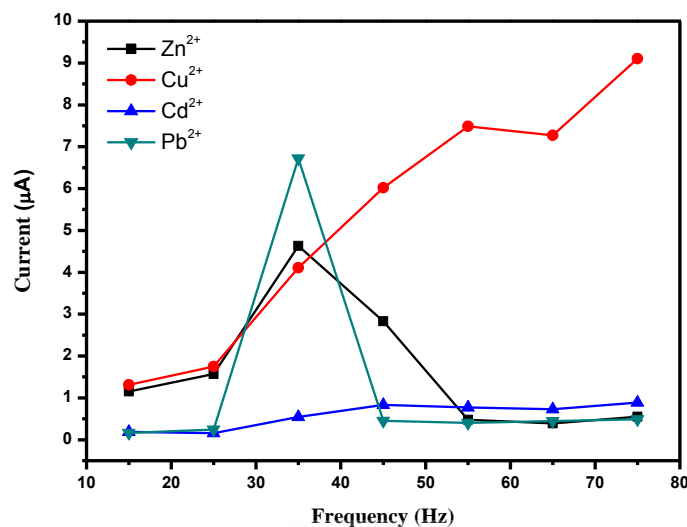
Figure 6.5.6 The effect of frequency on adsorptive peak currents of 50 µg.L^{-1} Cd^{2+}, Pb^{2+}, Cu^{2+} and 20 µg.L^{-1} Zn^{2+}-cupferron complexes in 0.1 M acetate buffer solution at the ERGO-HgF-PGE.

6.6. Analytical performance of the ERGO-HgF-PGE

Under optimum conditions, the individual and simultaneous determination of Cd^{2+}, Pb^{2+}, Cu^{2+} and Zn^{2+} were performed at the ERGO-HgF-PGE using SW-AdCSV and four calibration curves were constructed using standard addition method of successive metal ion aliquots to the electrochemical cell. Figure 6.6(a) displays SW-AdCSV peak current responses for simultaneous detection of Cd^{2+}, Pb^{2+}, Cu^{2+} and Zn^{2+}-cupferron and their corresponding calibration curves. The calibration curves are linear over the range of 20 to 200 µg.L^{-1} for simultaneous detection of Cd^{2+}, Pb^{2+} and Cu^{2+}. The sensitivity of the ERGO-HgF-PGE differed for all metal ions of interest with Cu^{2+} showing the best detection sensitivity. It can be clearly seen that Zn^{2+}-cupferron complex behaved differently compared to other metal ions with a distinct decrease in linearity. At higher concentrations a decrease in peak currents were observed due to competition of ligand and saturation of the ERGO-HgF-PGE. Individual detection of Cd^{2+}, Pb^{2+}, Cu^{2+} and Zn^{2+} was performed at the ERGO-HgF-PGE in the presence of cupferron over the same linear range of 20 to 200 µg.L^{-1}. Square-wave cathodic stripping voltammograms and corresponding calibration

77

curves for individual detection of Cd^{2+}, Pb^{2+}, Cu^{2+} and Zn^{2+}-cupferron complexes at the ERGO-HgF-PGE in 0.1 M acetate buffer solution (pH 4.6) using SW-AdCSV is shown in Figure 6.6b. For SW-AdCSV measurements, three replicates of each calibration curves for both individual and simultaneous analysis were tested. For both individual and simultaneous detection, good sensitivity is found at the ERGO-HgF-PGE validating the method used.
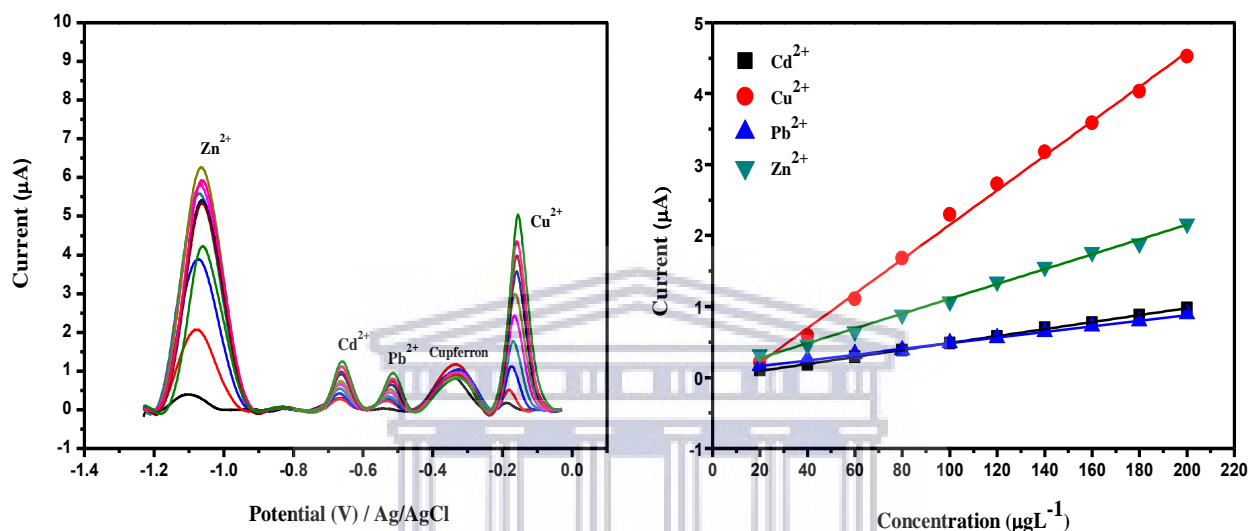
Figure 6.6a SW-AdCSV and corresponding calibration curve for simultaneous analysis of Cd^{2+}, Pb^{2+}, Cu^{2+} and Zn^{2+} obtained at the ERGO-HgF-PGE in concentration range 20 to 200 µg.L^{-1} in 0.1 M acetate buffer solution (pH 4.6) in the presence of cupferron (0.04 mM).

Table 6. Linear equations for the simultaneous determination of Pb^{2+}, Cd^{2+}, Zn^{2+} and Cu^{2+} from calibration plot.

Metal ions	Linear equations	R^2
Cu^{2+}	2.43E-8x – 2.78E-7	0.997
Cd^{2+}	4.92E-9x – 6.27E-9	0.999
Pb^{2+}	3.97E-9x – 8.37E-8	0.997
Zn^{2+}	5.21E-9x + 7.42E-8	0.915

78

(A)

(B)
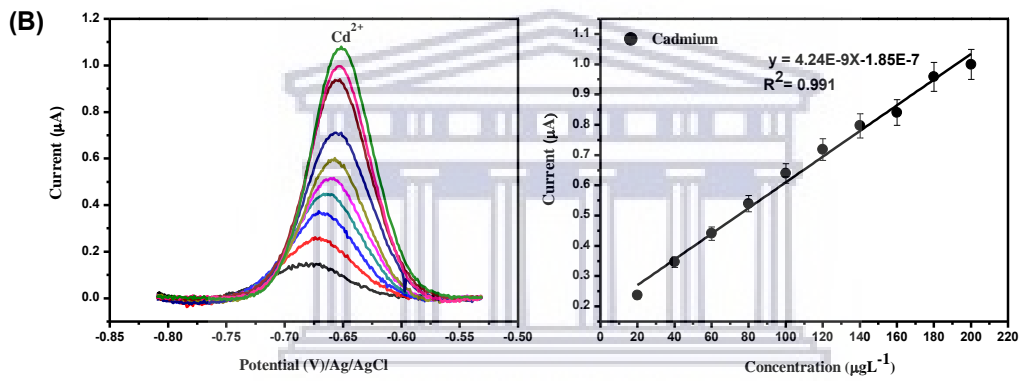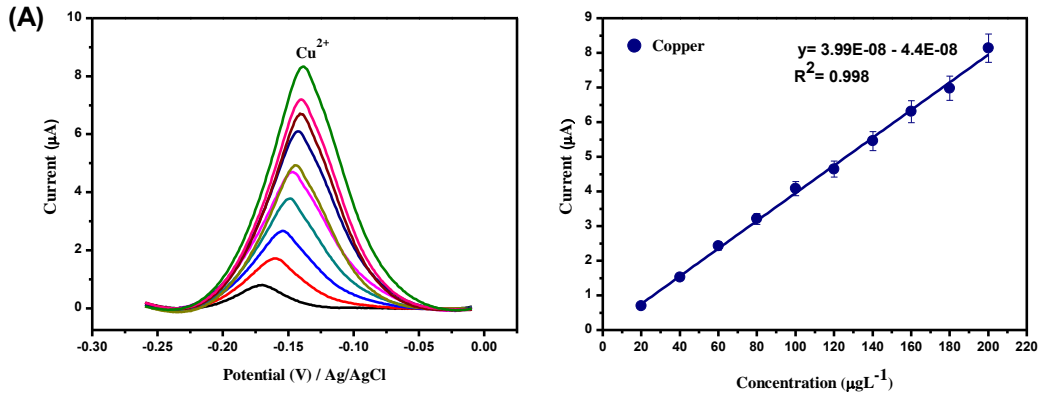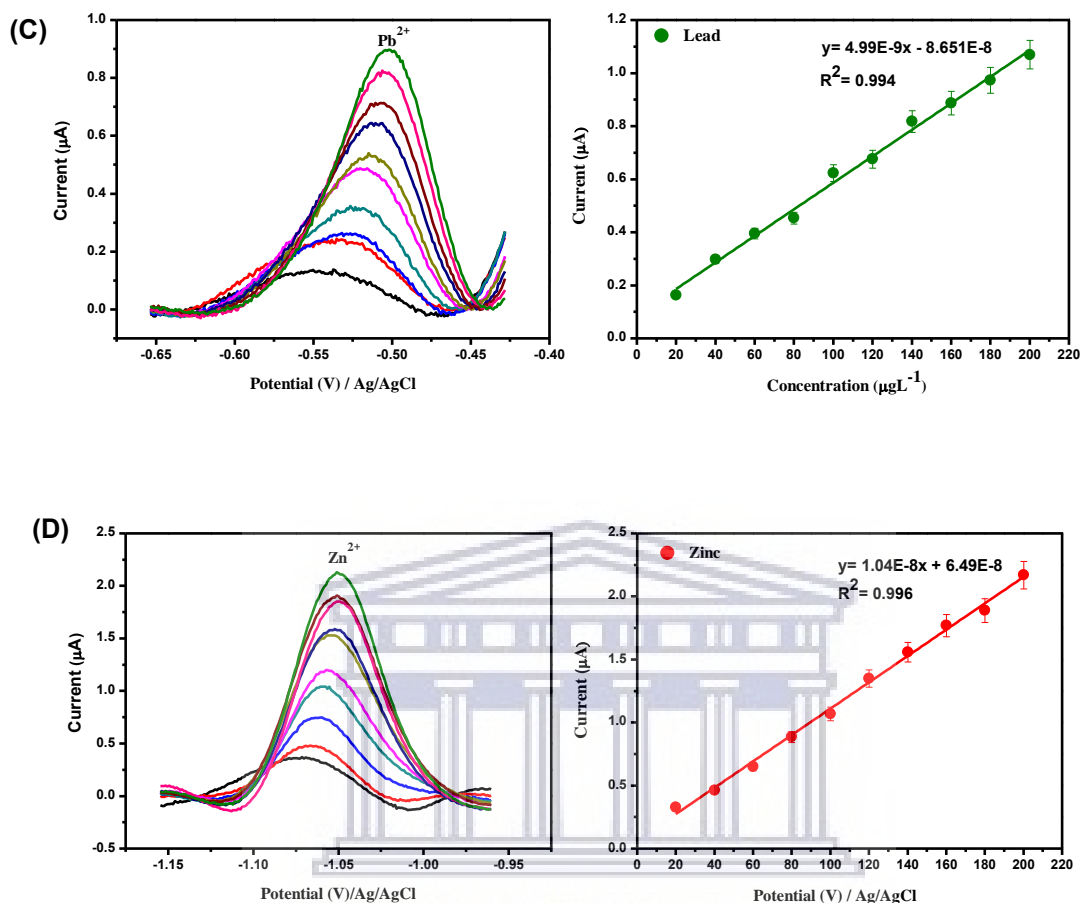
Figure 6.6b SW-AdCSVs and corresponding calibration curves for individual analysis of Cu^{2+}, Cd^{2+}, Pb^{2+} and Zn^{2+} (A-D) obtained at the ERGO-HgF-PGE in concentration range 20 to 200 $\mu g.L^{-1}$ in 0.1 M acetate buffer solution (pH 4.6) in the presence of cupferron (0.04 mM).

Table 7 summarizes the values for correlation coefficient (r), intercepts, standard deviation, sensitivity and limits of detection and quantitation for both simultaneous and individual analysis of all four metal ions at the ERGO-HgF-PGE in the presence of cupferron at 60 s deposition time. The limits of detection (LOD) and quantitation (LOQ) were calculated using the following equations: $LOD = \frac{3\sigma blanks}{Slope(Sensitivity)}$ described as three times (σ) the standard deviation of the blanks divides by the slope of calibration curve. LOQ described as the lowest concentration that

80

can be measured, calculated by 10 times LOD. From the table it can be seen that simultaneous analysis of Zn^{2+} in the presence of other target metal ions was not possible due to low linearity of its current response. It may also be observed that for all metal ions, LODs well below the WHO maximum contamination levels were possible. Individual analysis further demonstrated improved LODs for each of the metal ions of interest over simultaneous analysis due to lack of competition for active sites at the electrode surface thereby improving sensitivity.

Table 7. Comparison of simultaneous and individual analysis at the ERGO-HgF-PGE in 0.1 M acetate buffer solution (pH 4.6) at deposition time 60 s.

	Metal ions	LOD $(\mu g.L^{-1})$	LOQ $(\mu g.L^{-1})$	Correlation coefficient (R^2)	Sensitivity $(\mu A L.\mu g^{-1})$
Simultaneous analysis 20 – 200 µg.L^{-1}	Pb^{2+}	0.17	1.7	0.997	3.97×10^{-9}
	Cd^{2+}	0.17	1.7	0.999	4.92×10^{-9}
	Cu^{2+}	0.02	0.2	0.997	2.43×10^{-8}
Individual analysis 20 – 200 µg.L^{-1}	Pb^{2+}	0.13	1.3	0.994	4.99×10^{-9}
	Cd^{2+}	0.20	2	0.991	4.24×10^{-9}
	Cu^{2+}	0.01	0.1	0.998	3.99×10^{-8}
	Zn^{2+}	0.14	1.4	0.996	1.04×10^{-8}

n = 3, **Where:** n = number of replications

Table 8 summarizes the recent work done for the determination of metal ions at various electrode substrates in the presence of cupferron ligand. The bulk of work done in this field to date has been performed at hanging mercury disk electrodes (HMDE). Cd^{2+} has presented the focus of recent studies with no work done to date for Cu^{2+} detection. Furthermore, this work presented the first study done for the simultaneous detection of more than two metal ions using cupferron complexes. HMDEs exhibited the lowest detection limits as a result of the high solubility of metal-cupferron complexes within the mercury drop forming an amalgam. A study was performed for the use of a bismuth film as alternative to the HMDE, however, a lower LOD was found due to the alloy formation. This work presented the first approach using a lower volume of mercury as a greener approach in conjunction with graphene at a disposable PGE. The study showed comparable results and even improved LODs when compared to the other studies conducted.

Table 8. Comparison between proposed method and previously reported detection limits for Cd^{2+}, Pb^{2+}, Cu^{2+} and Zn^{2+} at various electrode substrates.

Electrode substrate	Method	Deposition time (s)	Analytes	Linear range µg.L^{-1}	Detection limits µg.L^{-1}	Reference
HMDE simultaneous	AdCSV	60 s	Zn^{2+} Cd^{2+}	0.15 - 250 0.4 - 175	0.058 0.092	[47]
Bi/poly(p-ABSA) film simultaneous	DPASV	100 s	Zn^{2+} Cd^{2+} Pb^{2+}	1 – 110 1 – 110 1 – 130	0.62 0.63 0.80	[206]
HMDE	AdSV	30 s	Cd^{2+}	0.11 - 22	0.033	[15]
SnFEs simultaneous	SWASV	120 s	Zn^{2+} Cd^{2+}	10 – 200 10 - 200	0.9 0.7	[207]
HMDE simultaneous	AdCSV	60 s	Cu^{2+} Mo^{6+}	0.1 - 20 0.1 - 20	0.2 0.06	[46]
µPEDs/SPCE	SWASV	120s	Pb^{2+} Cd^{2+}	0-100 0-100	2 2.3	[208]
HMDE simultaneous	AdSV	30 s	Cd^{2+} U^{6+}	0.28 – 22.48 2.38 – 119	0.096 0.833	[43]
HMDE simultaneous	AdSV	30 s	Cd^{2+} Bi^{3+}	0.28 – 22.48 0.42 – 41.80	0.11 0.2	[16]
HMDE	AdSV	30 s	Pb^{2+}	0.21– 31.93	0.05	[21]
BI/MWNT-IL/SPCE	SWASV		Zn^{2+} Cd^{2+}	1– 60 1– 60	0.12 0.5	[209]
HMDE	AdSV	60 s	Zn^{2+}	0.85 - 320	-	[24]
Nafion-BiFE	AdSV	60 s	Cd^{2+}	3 - 40	0.38	[37]
ERGO-PG-MFE Simultaneous	SW-AdCSV	60 s	Pb^{2+} Cd^{2+} Cu^{2+}	20 – 200	0.17 0.17 0.02	This work
ERGO-PG-MFE Individual analysis	SW-AdCSV	60 s	Pb^{2+} Cd^{2+} Cu^{2+} Zn^{2+}	20 – 200	0.13 0.20 0.01 0.14	This work

As observed in the table above, the working concentration range for the developed sensor was performed between 20 and 200 µg.L^{-1} in order to keep the concentration range for all four metal ions consistent. It is clear that by improving the analysis time, more analytes are able to accumulate at the electrode surface, as discussed in section 6.5.4. The individual analysis of Cd^{2+}, Pb^{2+}, Cu^{2+} and Zn^{2+}-cupferron complexes were therefore performed in 0.1 M acetate buffer solutions (pH 4.6) in the presence of cupferron ligand (0.04 mM) using a 360 s deposition time at the ERGO-HgF-PGE under optimized conditions as seen in Figure 6.6c. It was found that a longer deposition time of 360 s enabled the detection of metal ion-cupferron complexes at lower concentration of 3 µg.L^{-1} due to increasing adsorption of metal ion-complexes on the surface of the ERGO-HgF-PGE thus improving the selectivity and sensitivity of the electrode. This significant decrease in concentration demonstrates the feasibility of the sensor to operate at concentrations well below the WHO standards. For future work, we aim to repeat the calibration and standard addition method studies in this lower concentration range for comparative purposes.
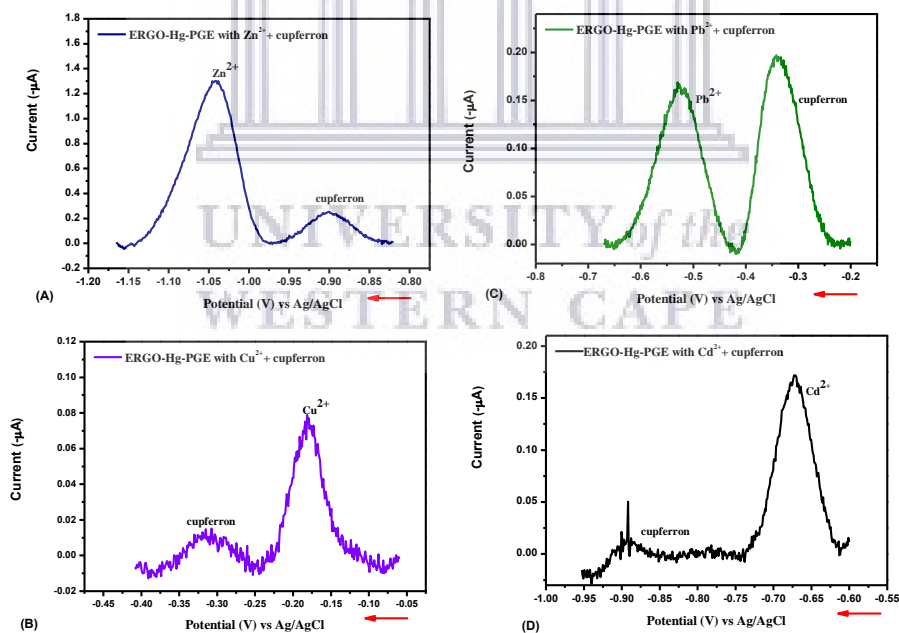
Figure 6.6c SW-AdCSVs for individual analysis of 3 µg.L^{-1} Cu^{2+}, Cd^{2+}, Pb^{2+}and Zn^{2+} (A-D) obtained at the ERGO-HgF-PGE in 0.1 M acetate buffer solution (pH 4.6) in the presence of cupferron (0.04 mM) for 360 s.

84

6.6.1. Recovery studies of the ERGO-HgF-PGE in test solutions

A standard addition method was used to determine the accuracy and precision of the SW-AdCSV method for the simultaneous determination of Cd^{2+}, Pb^{2+}, Cu^{2+} and Zn^{2+}-cupferron complexes at the ERGO-HgF-PGE by calculating recovery percentages for three replicates (n= 3). Recovery studies of the proposed method were performed in spiked solutions of known concentrations of 20 $\mu g.L^{-1}$ Cd^{2+}, Pb^{2+}, Cu^{2+} and Zn^{2+}, prepared in 20 ml of 0.1 M acetate buffer solutions (pH 4.6) in the presence of cupferron (0.04 mM) and recovery percentages calculated based on the peak current responses. Figure 6.6.1 (a-d) shows the standard addition curves obtained for Zn^{2+}, Cu^{2+}, Cd^{2+} and Pb^{2+} respectively at the ERGO-HgF-PGE. The results for the performed recovery studies are displayed in Table 9, below. As can be observed, recovery percentages between 95 and 100 % were found (< 5 % error) for all metal ions of interest. These results show that accurate detection of each metal was possible using the proposed sensor and method of detection.

Cu²⁺ graph (b): $y = 8.08\text{E-}08x + 1.61\text{E-}06$, $R^2 = 9.84\text{E-}01$

Cd²⁺ graph (c): $y = 6.73\text{E-}09x + 1.30\text{E-}07$, $R^2 = 9.87\text{E-}01$
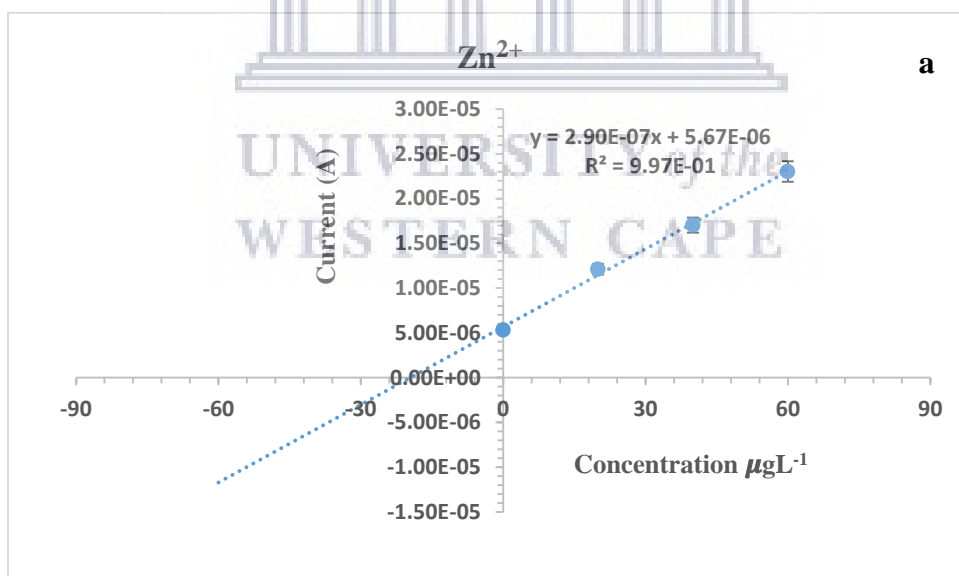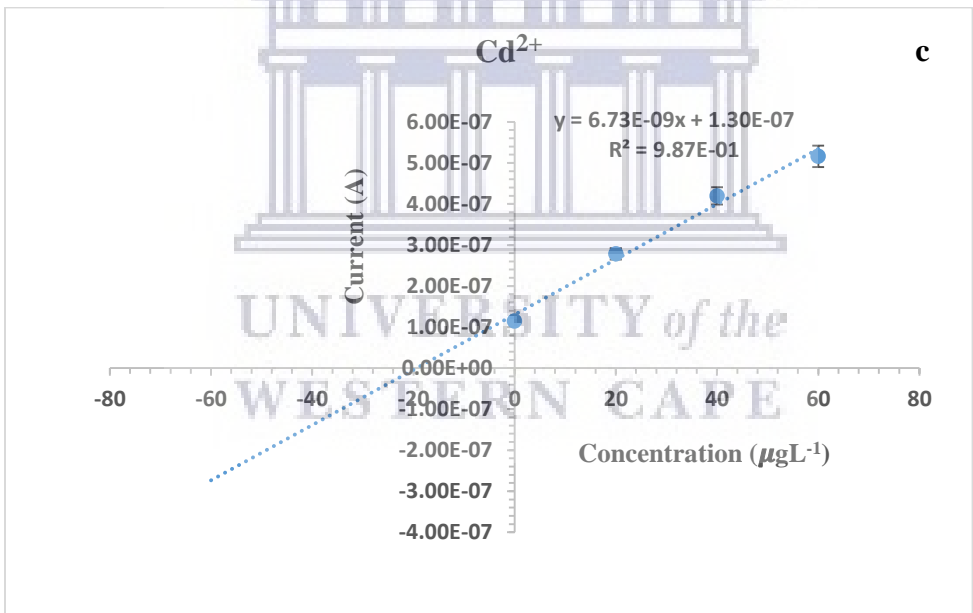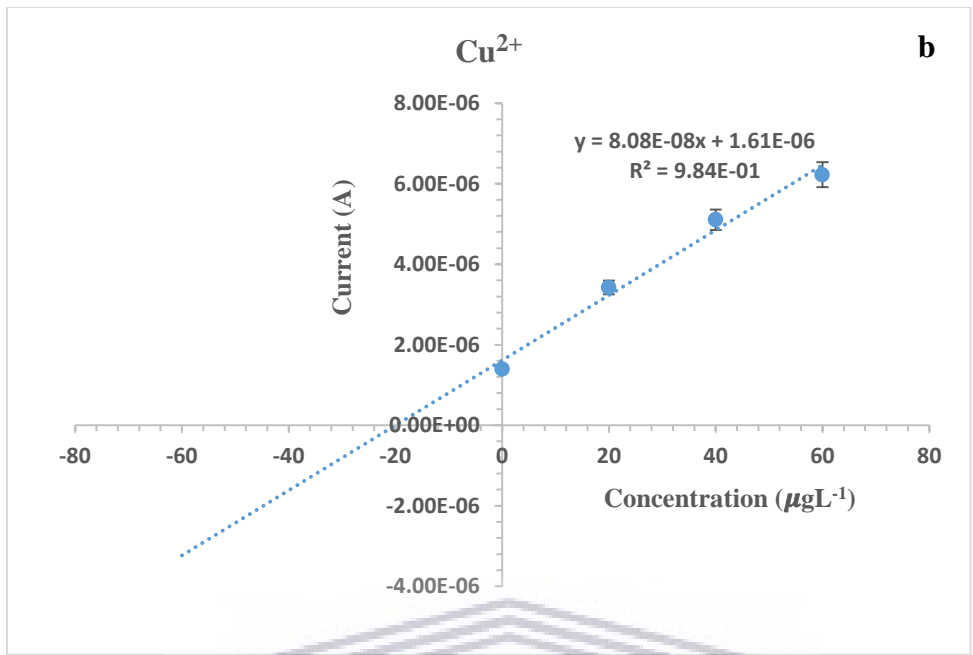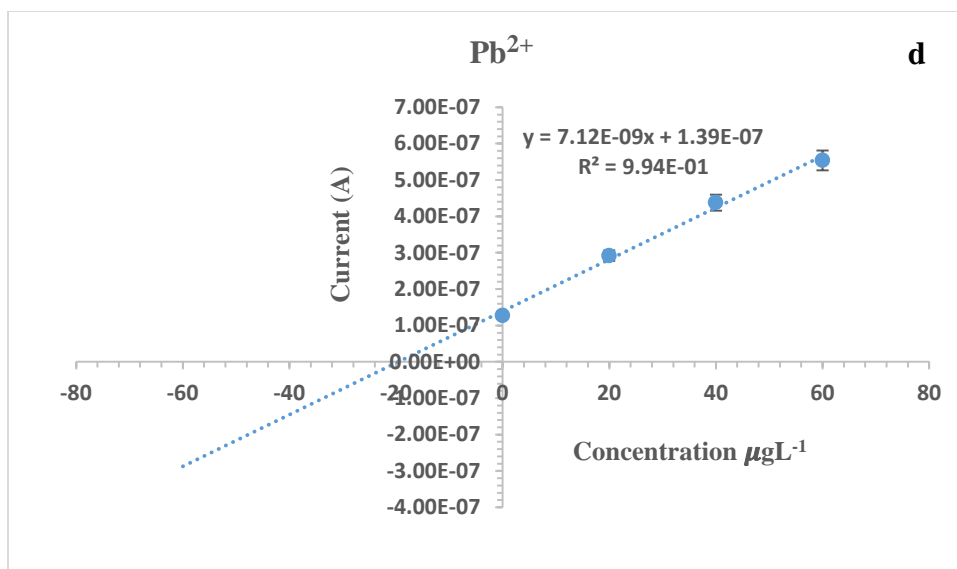
Figure 6.6.1 Standard addition calibration curves for simultaneous analysis spiked with 20 µg.L⁻¹ of Zn²⁺ (a), Cu²⁺(b), Cd²⁺(c), and Pb²⁺ (d) at 60 s.

Table 9. Recovery studies for the simultaneous determination of Pb^{2+}, Cd^{2+}, Zn^{2+} and Cu^{2+} in test solutions on the ERGO-HgF-PGE at 60 s.

Metal ions	Original (µg.L⁻¹)	Spiked (µg.L⁻¹)	Found (µg.L⁻¹)	RSD (%)	Recovery (%)
Zn^{2+}	ND	20	19.55	0.44	97.75
Cu^{2+}	ND	20	19.93	0.18	99.63
Pb^{2+}	ND	20	19.52	0.22	97.61
Cd^{2+}	ND	20	19.32	0.13	96.58

6.6.2. Interference studies

In order to study the selectivity of SW-AdCSV method, the effect of the intermetallic interferences on the simultaneous determination of Cd^{2+}, Pb^{2+}, Cu^{2+} and Zn^{2+} in 0.1 M acetate buffer solution (pH 4.6) were investigated under optimum experimental conditions. The inter-metallic interference study was performed by addition of possible interferent ions such as Ni^{2+}, Co^{2+}, Ga^{3+}, and As^{3+} at 100 μg.L^{-1} to a solution containing 50 μg.L^{-1} of Cd^{2+}, Pb^{2+}, Cu^{2+} and Zn^{2+}. The addition of these species may result in competition between interferent ions and trace-metals for either ligand complexation, complex adsorption or by producing reducible potential that can result in direct or partial overlap with trace-metal peaks on the ERGO-HgF-PGE thereby increasing or decreasing the peak currents of trace metals. Figure 6.6.2 shows the results obtained from the interference studies. The tolerance limit was defined as the highest concentration of the interfering ions that caused relative error above $\pm$ 5 %. The experimental results indicated that the interferent metal ions influenced the stripping peak currents of trace metals as seen in Figure 6.6.2, a significant increase of Zn^{2+} peak was observed in the presence of Ga^{3+}, due to the formation of zinc-gallium complexes, but only a slight change in the peak currents of Cu^{2+}, Cd^{2+} and Pb^{2+} occurred. Furthermore, decrease in the peak height of Zn^{2+} was observed for all other metal ions of interest. The decrease in peak current occurs due to the similar reduction potentials of Co^{2+}, Ni^{2+} and As^{3+}, respectively resulting in an overlap of stripping peaks and competitive interaction for the electrode surface. It can also be seen that detection of Cu^{2+} is significantly influence by As^{3+}. Whereas Cd^{2+} and Pb^{2+} signals were slight affected by the presence of the interferent ions, such interferences can be suppressed by the addition of excess amounts of the complexing agent in the solution.
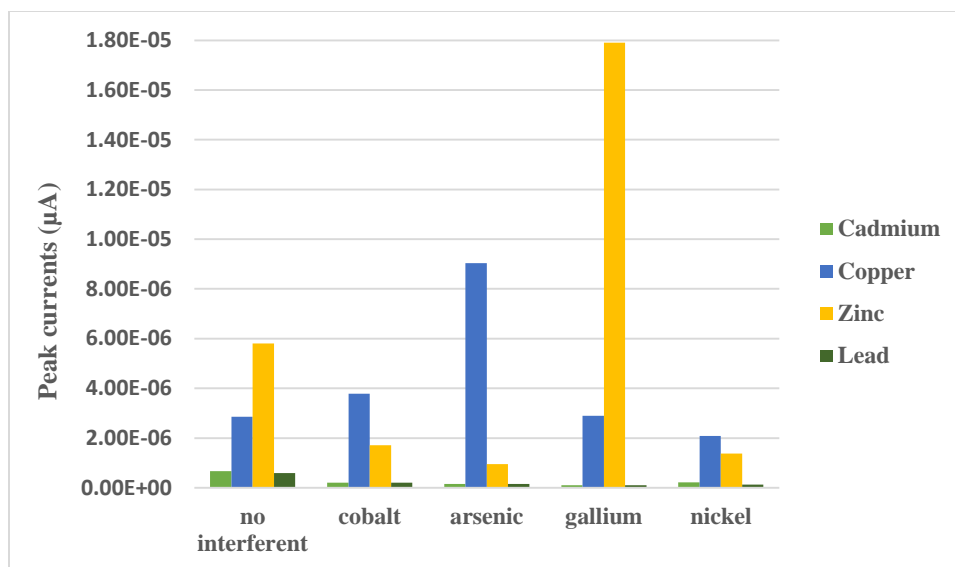
Figure 6.6.2 Interference studies for the simultaneous determination of Pb^{2+}, Cd^{2+}, Zn^{2+} and Cu^{2+} in on the ERGO-HgF-PGE sensor.

6.6.3. Sensor stability, repeatability and reproducibility

The stability and reproducibility of the developed ERGO-HgF-PGE sensor was investigated over a period of seven days. The reproducibility and repeatability of three individual ERGO-HgF-PGE sensors (n=3) were studied on different days with five repetitive measurements of 50 µg.L^{-1} Cd^{2+}, Pb^{2+}, Cu^{2+} and Zn^{2+} in 0.1 M acetate buffer solution (pH 4.6) was evaluated. The average current signals are shown. Moreover, results obtained were reported in Table 10 the relative standard deviation (RSD) < 5 % values were observed for the five measurements taken on the fresh (day1) and four-day old electrodes for each metal ion. A large RSD, > 5 % was observed on day 7. The RSD values on day 1 showed more reproducible results of the ERGO-HgF-PGE sensor towards Cd^{2+}, Pb^{2+}, Cu^{2+} and Zn^{2+} than day 4 and day 7, therefore it is best to use electrodes prepared on day 1. In addition, the stability of the ERGO-PGE was carried out by measuring stripping peak currents of trace-metals when the ERGO-PGEs were stored in a refrigerator for 7 days, then tested in 0.1 M acetate buffer solution (pH 4.6) containing 50 µg.L^{-1} of trace metals for two-day interval under same optimal conditions. It was observed that peak currents were higher on day 1 to 4 indicating longer stability of the developed sensor and on day

89

7 a significant decreased in current response was observed as seen in Figure 6.6.3. The findings confirm that the electrodes have a lifetime of 1week before deterioration takes place. Future work may involve investigating methods of electrode activation after this time.

Table 10. Reproducibility and repeatability of the ERGO-HgF-PGE sensor during seven days

	RSD (%)		
Metal cations	Day 1	Day 4	Day 7
Cu^{2+}	0.77	4.79	7.75
Zn^{2+}	0.83	3.79	6.99
Pb^{2+}	0.93	1.59	8.12
Cd^{2+}	1.29	3.07	9.04
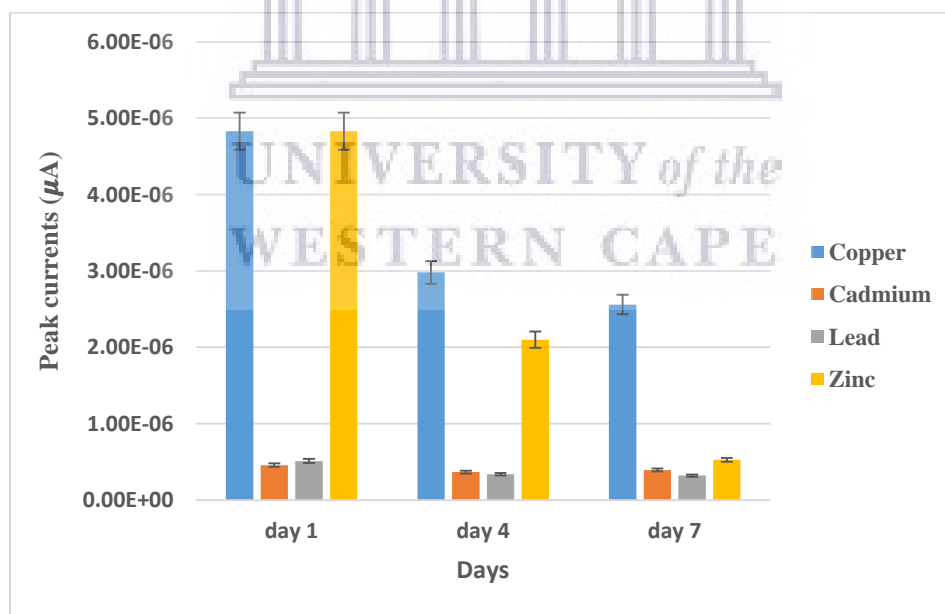
Figure 6.6.3 Stability of the ERGO-HgF-PGE sensor response during seven days.

90

6.6.4. Application of the ERGO-HgF-PGE in tap water samples

ERGO-HgF-PGE was applied to the simultaneous determination of Cd^{2+}, Pb^{2+}, Cu^{2+} and Zn^{2+} in tap water samples collected in our laboratory. 19 ml of tap water was added to 1 ml of 2 M acetate buffer solution (pH 4.6) followed by *in-situ* deposition of thin mercury film and metal ions performed at 60 s. The standard addition method was used to quantify metal ions present in tap water for three replicate measurements using SW-AdCSV. In order to evaluate the accuracy of the proposed method, tap water samples were spiked with known concentrations of 20 $\mu g.L^{-1}$ for each metal ions. No Cd^{2+}, Pb^{2+}, Cu^{2+} and Zn^{2+} were detected in the real tap water samples suggesting that concentrations of metal ions were below the detection limit of proposed procedure or not present in the water sample. The obtained percentage recovery with their relative standard deviations in tap water samples are shown in Table 11.

Table 11. Simultaneous determination of metal ions in tap water samples using the ERGO-HgF-PGE at 60 s.

Metal ions	Original ($\mu g.L^{-1}$)	Spiked ($\mu g.L^{-1}$)	Found ($\mu g.L^{-1}$)	RSD(%)	Recovery(%)
Zn^{2+}	ND	20	19.77	0.20	98.86
Cu^{2+}	ND	20	19.91	0.22	99.56
Pb^{2+}	ND	20	19.55	0.73	97.76
Cd^{2+}	ND	20	20.23	1.72	101.19

n = 3

where: n = three replicates of each experiment

ND = not detected

91
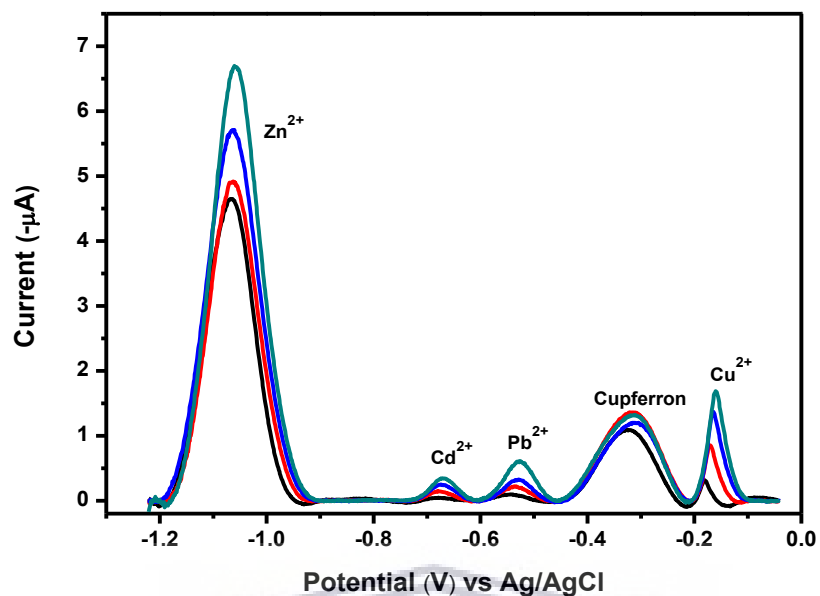
Figure 6.6.4 Square-wave voltammogram for simultaneous analysis of tap water (pH 4.6) spiked with 20 µg.L^{-1} of Cd^{2+}, Pb^{2+}, Cu^{2+} and Zn^{2+} at 60 s.
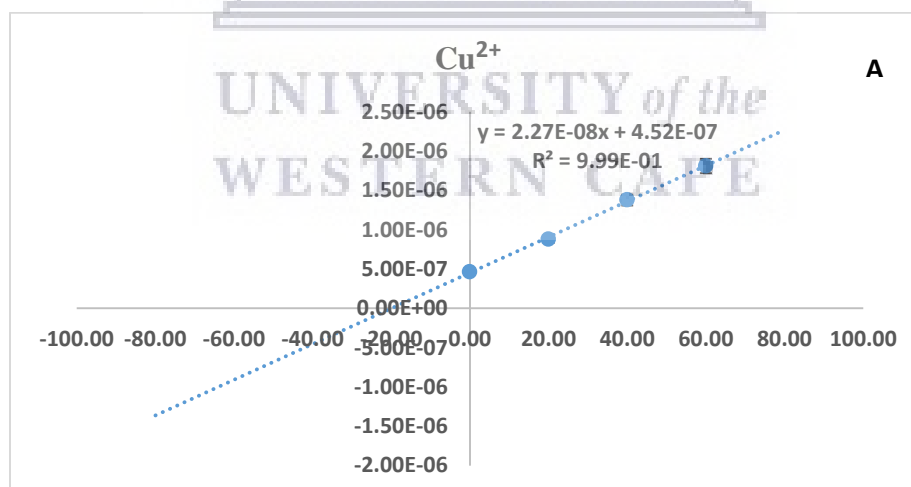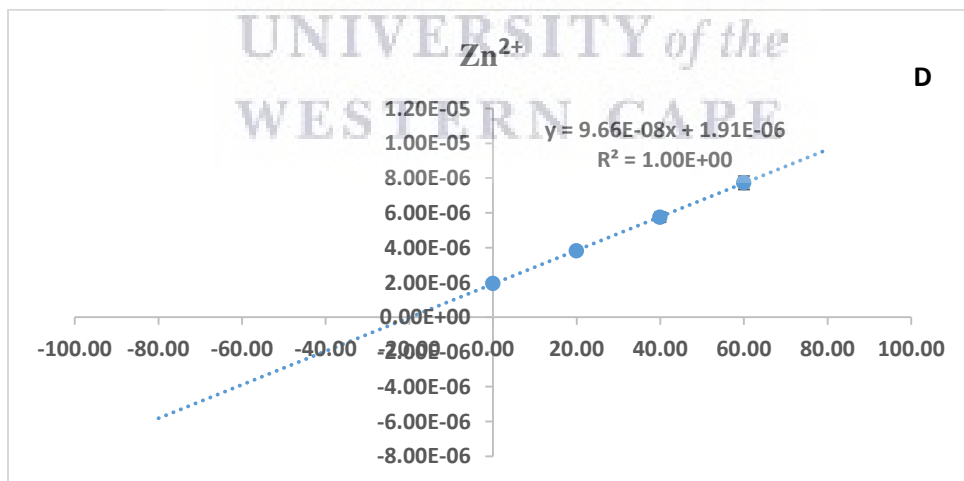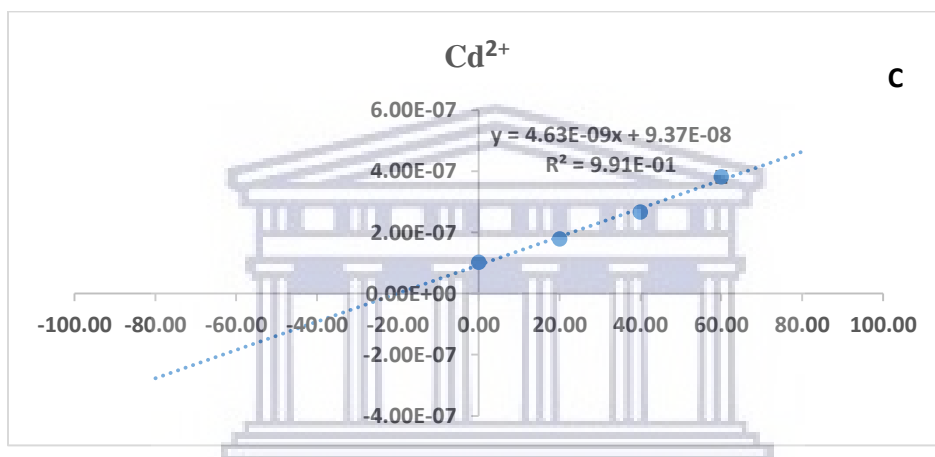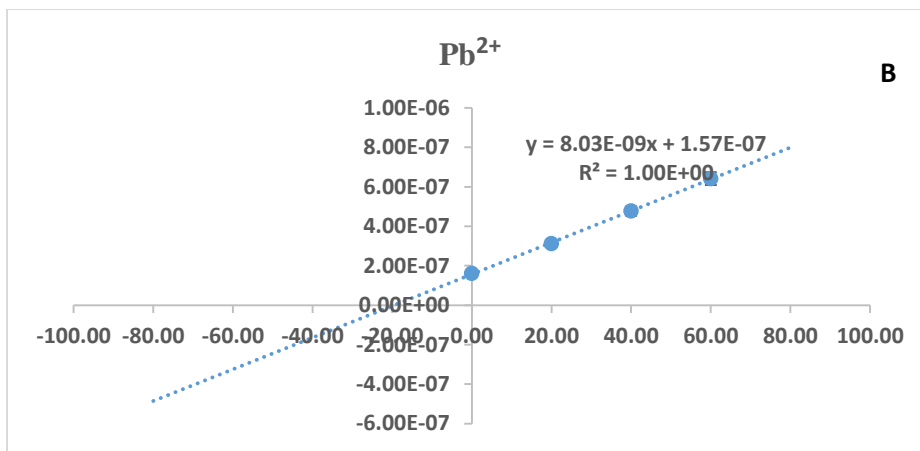
Figure 6.6.5 Standard addition calibration curves for simultaneous analysis of tap water (pH 4.6) spiked with 20 µg.L^{-1} of Cu^{2+} (a), Pb^{2+}(b), Cd^{2+}(c) , and Zn^{2+} (d) at 60 s.

93

CHAPTER SEVEN

Conclusions and Future work

7. Introduction

This chapter concludes key findings and achievements of the research study and presents suggestions for further investigations and future work related to this study.

7.1. Conclusions

An electrochemically reduced graphene oxide *in-situ* plated mercury film pencil graphite electrode (ERGO-HgF-PGE) as fast, sensitive and inexpensive sensing platform was successfully developed for simultaneous detection of Cd^{2+}, Pb^{2+}, Cu^{2+} and Zn^{2+} with cupferron chelating agent in tap water by square-wave adsorptive cathodic stripping voltammetry. The graphene nanosheets were successfully prepared by oxidizing graphite to graphene oxide using potassium permanganate ($KMnO_4$) and sulfuric acid (H_2SO_4) and successfully characterized by using Fourier transform infrared spectroscopy, X-ray diffraction, Ultraviolet-visible spectroscopy, electrochemical impedance spectroscopy, High resolution transmission electron microscopy and High-resolution scanning electron microscopy. The study outcomes have shown that the surface of the pencil graphite electrode (PGEs) can be modified through electrochemically reduction of graphene oxide (GO) colloidal solution at the PGEs. The ERGO-HgF-PGE showed enhanced sensitivity and selectivity compare to mercury film electrode, this was highly influenced using ERGO in conjunction with thin mercury film due to improved electron transfer rate and surface to volume ratio of the sensor. The simultaneous detection of Cd^{2+}, Pb^{2+}, Cu^{2+} and Zn^{2+} was successfully entailed by using cupferron chelating agent to form complexes, interestingly it was found that the formation of stable metal ion-cupferron complexes were highly dependent upon the pH and nature of the buffer solution. The ERGO-HgF-PGE showed improved and comparable detection limits with other reported studies in literature, the detection limits (LOD) were calculated below the US-EPA maximum contaminant level for zinc (5 mg.L^{-1}), cadmium (0.003 mg.L^{-1}), lead (0.02 mg.L^{-1}) and copper (0.05 mg.L^{-1}) in drinking water. The recovery percentages for the ERGO-HgF-PGE were between 95 and 100 % were

94

found (< 5 % error) for all metal ions of interest. The obtained results showed that the ERGO-HgF-PGE can serve as enhanced electrochemical sensor with improved detection limits for determination of Cd^{2+}, Pb^{2+}, Cu^{2+} and Zn^{2+} in tap water by SW-AdCSV.

7.2. Future work

This study gave insight into the use of other metal films previously studied in literature on other substrates for the simultaneous detection of metal ion-cupferron complexes, by implementing the same principles used in this study to observe if there could be an improved selectivity and sensitivity of the electrode. Similarly, a more detailed evaluation of different metal ions other than Cd^{2+}, Pb^{2+}, Cu^{2+} and Zn^{2+} at the ERGO-HgF-PGE in the presence of cupferron chelating agent is another field of interest. The use of *in-situ* method for simultaneous detection of metal ion-cupferron chelating agent complexes was successfully demonstrated in this study, therefore further research could be explored by using *ex-situ* method to provide other possible way to detect heavy metal ions. Future work may also involve the reinvestigation of intermetallic interferences on the simultaneous determination of Cd^{2+}, Pb^{2+}, Cu^{2+} and Zn^{2+} to ensure that similar interfering effect caused by the interferent ions can be obtained. It is also intended to further investigate organic interferences previously reported in literature, including humic acid and fluvic acid as they were found in literature to interfere with the selected metal ions used in this study. The results obtained in this study inspire other area of interest like the use of other electrodes such as glassy carbon, screen-printed or microfluidics to detect Cd^{2+}, Pb^{2+}, Cu^{2+} and Zn^{2+}. Lastly, it is envisaged that the analytical performance of the sensor maybe significantly improved and operated in a lower concentration range of 3 to 30 $\mu g.L^{-1}$ using an accumulation time of 360 s. These calibration studies will be conducted to compare to the existing sensor.

References

[1]   G. March, T.D. Nguyen, B. Piro, Modified electrodes used for electrochemical detection of metal ions in environmental analysis, Biosensors. 5 (2015) 241–275. doi:10.3390/bios5020241.

[2]   J. Kudr, L. Richtera, L. Nejdl, K. Xhaxhiu, P. Vitek, B. Rutkay-Nedecky, D. Hynek, P. Kopel, V. Adam, R. Kizek, Improved electrochemical detection of zinc ions using electrode modified with electrochemically reduced graphene oxide, Materials (Basel). 9 (2016) 1–12. doi:10.3390/ma9010031.

[3]   S. Muhammad, M.T. Shah, S. Khan, Health risk assessment of heavy metals and their source apportionment in drinking water of Kohistan region, northern Pakistan, Microchem. J. 98 (2011) 334–343. doi:10.1016/j.microc.2011.03.003.

[4]   C. V Mohod, J. Dhote, Review of Heavy Metals in Drinking Water and Their Effect on Human Health, Int. J. Innov. Res. Sci. Eng. Technol. 2 (2013) 2992–2996.

[5]   T.O. Kolawole, A.S. Olatunji, M.T. Jimoh, O.T. Fajemila, Heavy metal contamination and ecological risk assessment in soils and sediments of an industrial area in Southwestern Nigeria, J. Heal. Pollut. 8 (2018). doi:10.5696/2156-9614-8.19.180906.

[6]   C. Ariño, N. Serrano, J.M. Díaz-Cruz, M. Esteban, Voltammetric determination of metal ions beyond mercury electrodes. A review, Anal. Chim. Acta. 990 (2017) 11–53. doi:10.1016/j.aca.2017.07.069.

[7]   A. Hardberger, Life, Liberty, and the Pursuit of Water: Evaluating Water as a Human Right and the Duties and Obligations it Creates, Northwest. J. Int. Hum. Rights. 4 (2006) 32.

[8]   D. J.O, O. M.O.C, E. J.N, Heavy metal pollution and human biotoxic effects, Int. J. Phys. Sci. 2 (2007) 112–118.

96

[9]   E. Flores, J. Pizarro, F. Godoy, R. Segura, A. Gómez, N. Agurto, P. Sepúlveda, An electrochemical sensor for the determination of Cu(II) using a modified electrode with ferrocenyl crown ether compound by square wave anodic stripping voltammetry, Sensors Actuators, B Chem. 251 (2017) 433–439. doi:10.1016/j.snb.2017.05.058.

[10]   R. Nazir, M. Khan, M. Masab, H.U. Rehman, N.U. Rauf, S. Shahab, N. Ameer, M. Sajed, M. Ullah, M. Rafeeq, Z. Shaheen, Accumulation of heavy metals (Ni, Cu, Cd, Cr, Pb, Zn, Fe) in the soil, water and plants and analysis of physico-chemical parameters of soil and water collected from Tanda Dam Kohat, J. Pharm. Sci. Res. 7 (2015) 89–97.

[11]   B. Ayenew, T. Ahmad, Assessment of Heavy Metals Concentration in Togona River of Goba Town , Oromia Region , 14 (2016) 3207–3214.

[12]   S. Muhammad, M.T. Shah, S. Khan, Health risk assessment of heavy metals and their source apportionment in drinking water of Kohistan region, northern Pakistan, Microchem. J. 98 (2011) 334–343. doi:10.1016/j.microc.2011.03.003.

[13]   O.A. Farghaly, Direct and simultaneous voltammetric analysis of heavy metals in tap water samples at Assiut city: An approach to improve the analysis time for nickel and cobalt determination at mercury film electrode, Microchem. J. 75 (2003) 119–131. doi:10.1016/S0026-265X(03)00090-0.

[14]   A. Sarkar, G. Ravindran, V. Krishnamurthy, K.K.B.G. Campus, A brief review on the effect of cadmium toxicity : from cellular to organ level, Int. J. Bio-Technology. 3 (2013) 17–36.

[15]   M. Grabarczyk, A. Koper, Direct Determination of Cadmium Traces in Natural Water by Adsorptive Stripping Voltammetry in the Presence of Cupferron as a Chelating Agent, Electroanalysis. 24 (2012) 33–36. doi:10.1002/elan.201100357.

[16]   A. Koper, M. Grabarczyk, Simultaneous voltammetric determination of trace bismuth(III) and cadmium(II) in water samples by adsorptive stripping voltammetry in the presence of cupferron, J. Electroanal. Chem. 681 (2012) 1–5. doi:10.1016/j.jelechem.2012.05.020.

97

[17]   Nordic Council of Ministers, Cadmium Review, UNEP Gov. Counc. (2003) 26.

[18]   K. Zinoubi, H. Majdoub, H. Barhoumi, S. Boufi, N. Jaffrezic-Renault, Determination of trace heavy metal ions by anodic stripping voltammetry using nanofibrillated cellulose modified electrode, J. Electroanal. Chem. 799 (2017) 70–77. doi:10.1016/j.jelechem.2017.05.039.

[19]   M. Kaji, Role of experts and public participation in pollution control: The case of Itai-itai disease in Japan, Ethics Sci. Environ. Polit. 12 (2012) 99–111. doi:10.3354/esep00126.

[20]   M. Grabarczyk, A. Koper, Simultaneous Determination of Trace Uranium(VI) and Cadmium(II) by Adsorptive Stripping Voltammetry in the Presence of Cupferron as a Complexing Agent, Electroanalysis. 24 (2012) 907–910. doi:10.1002/elan.201100665.

[21]   M. Grabarczyk, Sensitive adsorptive stripping voltammetric method for direct determination of trace concentration of lead in the presence of cupferron in natural water samples, Int. J. Environ. Anal. Chem. 93 (2013) 1008–1018. doi:10.1080/03067319.2012.702275.

[22]   S. Tiwari, I.P. Tripathi, H. Tiwari, Effects of Lead on Environment, Emerg. Res. Manag. Technol. Echnology. 2 (2013) 1–5.

[23]   G. Flora, D. Gupta, A. Tiwari, Toxicity of lead : A review with recent updates, 5 (2012) 47–58. doi:10.2478/v10102-012-0009-2.

[24]   S. Abbasi, A. Farmany, M. Roushani, S.S. Mortazavi, Sensitive quantification of trace zinc in water samples by adsorptive stripping voltammetry, Water Sci. Technol. 69 (2014) 438–442. doi:10.2166/wst.2013.704.

[25]   L.M. Plum, L. Rink, H. Hajo, The essential toxin: Impact of zinc on human health, Int. J. Environ. Res. Public Health. 7 (2010) 1342–1365. doi:10.3390/ijerph7041342.

[26]   A.S. PRASAD, J.A. HALSTED, M. NADIMI, Syndrome of Iron Deficiency Anemia , Dwarfism and Geophagia, Am. J. Med. 31 (1961) 532–546.

[27] A. Dorsey, L. Ingerman, S. Swarts, Relevance To Public Health Background and Environmental Exposures To Copper in the United States, Agency Toxic Subst. Dis. Regist. (2004) 11–19. http://www.atsdr.cdc.gov/toxprofiles/tp132.pdf.

[28] B.R. Stern, M. Solioz, D. Krewski, P. Aggett, T.C. Aw, S. Baker, K. Crump, M. Dourson, L. Haber, R. Hertzberg, C. Keen, B. Meek, L. Rudenko, R. Schoeny, W. Slob, T. Starr, Copper and human health: Biochemistry, genetics, and strategies for modeling dose-response relationships, 2007. doi:10.1080/10937400600755911.

[29] Dr. Paul C. Eck and Dr. Larry Wilson, Copper Toxicity, Eck Inst. Appl. Nutr. Bioenerg. Ltd. (1989) 1–308.

[30] A. Badiye, N. Kapoor, H. Khajuria, Copper Toxicity: A Comprehensive Study, Res. J. Recent Sci. 2 (2013) 58–67. http://www.isca.in/rjrs/archive/special_issue2012/12.ISCA-ISC-2012-4CS-93.pdf.

[31] G. Berg, L. Kohlmeier, H. Brenner, Effect of oral contraceptive progestins on serum copper concentration, Eur. J. Clin. Nutr. 52 (1998) 711–715. doi:10.1038/sj.ejcn.1600631.

[32] J. Polio, R.E. Enriquez, A. Chow, W.M. Wood, C.E. Atterburry, Hepatocellular Carcinoma in Wilsom's Disease, J Clin Gastroenterol. 11 (1989) 220–224.

[33] J.M. Walshe, History of Wilson's disease: 1912 to 2000, Mov. Disord. 21 (2006) 142–147. doi:10.1002/mds.20694.

[34] W.S. Zhong, T. Ren, L.J. Zhao, Determination of Pb (Lead), Cd (Cadmium), Cr (Chromium), Cu (Copper), and Ni (Nickel) in Chinese tea with high-resolution continuum source graphite furnace atomic absorption spectrometry, J. Food Drug Anal. 24 (2016) 46–55. doi:10.1016/j.jfda.2015.04.010.

[35] B. Feist, B. Mikula, K. Pytlakowska, B. Puzio, F. Buhl, Determination of heavy metals by ICP-OES and F-AAS after preconcentration with 2,2′-bipyridyl and erythrosine, J. Hazard. Mater. 152 (2008) 1122–1129. doi:10.1016/j.jhazmat.2007.07.095.

[36] S. Zhou, Z. Yuan, Q. Cheng, Z. Zhang, J. Yang, Rapid in situ determination of heavy metal concentrations in polluted water via portable XRF: Using Cu and Pb as example, Environ. Pollut. 243 (2018) 1325–1333. doi:10.1016/j.envpol.2018.09.087.

[37] N. Meepun, S. Siriket, S. Dejmanee, Adsorptive stripping voltammetry for determination of cadmium in the presence of cupferron on a nafion-coated bismuth film electrode, Int. J. Electrochem. Sci. 7 (2012) 10582–10591.

[38] S. Chaiyo, E. Mehmeti, K. Žagar, W. Siangproh, O. Chailapakul, K. Kalcher, Electrochemical sensors for the simultaneous determination of zinc, cadmium and lead using a Nafion/ionic liquid/graphene composite modified screen-printed carbon electrode, Anal. Chim. Acta. 918 (2016) 26–34. doi:10.1016/j.aca.2016.03.026.

[39] J.A. Barón-jaimez, J.L. Marulanda-arévalo, J.J. Barba-ortega, Electrodos amistosos con el medio ambiente para detectar metales pesados, 81 (2014) 122–128.

[40] Deswati, H. Pardi, H. Suyani, R. Zein, Adsorptive cathodic stripping voltammetric method with alizarin for the simultaneous determination of cadmium, and zinc in water samples, Orient. J. Chem. 32 (2016) 3071–3080. doi:10.13005/ojc/320628.

[41] J.A. Rodrigues, C.M. Rodrigues, P.J. Almeida, I.M. Valente, L.M. Gonçalves, R.G. Compton, A.A. Barros, Increased sensitivity of anodic stripping voltammetry at the hanging mercury drop electrode by ultracathodic deposition, Anal. Chim. Acta. 701 (2011) 152–156. doi:10.1016/j.aca.2011.05.031.

[42] O.A. Farghaly, R.S.A. Hameed, A.- Alhakeem, H. Abu-Nawwas, Analytical Application Using Modern Electrochemical Techniques, Int. J. Electrochem. Sci. 9 (2014) 3287–3318. doi:10.4172/2155-9872.1000192.

[43] M. Grabarczyk, A. Koper, Simultaneous Determination of Trace Uranium(VI) and Cadmium(II) by Adsorptive Stripping Voltammetry in the Presence of Cupferron as a Complexing Agent, Electroanalysis. 24 (2012) 907–910. doi:10.1002/elan.201100665.

[44]   Deswati, H. Pardi, H. Suyani, R. Zein, Adsorptive cathodic stripping voltammetric method with alizarin for the simultaneous determination of cadmium, and zinc in water samples, Orient. J. Chem. 32 (2016) 3071–3080. doi:10.13005/ojc/320628.

[45]   S. Abbasi, M. Roushani, S.B. Mortazavi, Sensitive quantification of trace zinc in water samples by adsorptive stripping voltammetry, 69 (2013) 438–442.

[46]   A.A. Ensafi, T. Khayamian, M. Atabati, Simultaneous voltammetric determination of molybdenum and copper by adsorption cathodic differential pulse stripping method using a principal component artificial neural network, Talanta. 57 (2002) 785–793. doi:10.1016/S0039-9140(02)00103-0.

[47]   S. Abbasi, A. Farmany, S.S. Mortazavi, Ultrasensitive Simultaneous Quantification of Nanomolar Level of Cd and Zn by Cathodic Adsorptive Stripping Voltammetry in Some Real Samples, Electroanalysis. 22 (2010) 2884–2888. doi:10.1002/elan.201000359.

[48]   M. Grabarczyk, Sensitive adsorptive stripping voltammetric method for direct determination of trace concentration of lead in the presence of cupferron in natural water samples, 93 (2013) 1008–1018.

[49]   S. Dutta, G. Strack, P. Kurup, Gold nanostar electrodes for heavy metal detection, Sensors Actuators, B Chem. 281 (2019) 383–391. doi:10.1016/j.snb.2018.10.111.

[50]   T. Bassie, K. Siraj, T.E. Tesema, Determination of Heavy Metal Ions on Glassy Carbon Electrode Modified with Antimony, Adv. Sci. Eng. Med. 5 (2012) 275–284. doi:10.1166/asem.2013.1251.

[51]   K. Pokpas, N. Jahed, P.G. Baker, E.I. Iwuoha, Complexation-based detection of nickel(II) at a graphene-chelate probe in the presence of cobalt and zinc by adsorptive stripping voltammetry, Sensors (Switzerland). 17 (2017) 1–22. doi:10.3390/s17081711.

[52]   Z. Koudelkova, T. Syrovy, P. Ambrozova, Z. Moravec, L. Kubac, D. Hynek, L. Richtera, V. Adam, Determination of zinc, cadmium, lead, copper and silver using a carbon paste

101

electrode and a screen printed electrode modified with chromium(III) oxide, Sensors (Switzerland). 17 (2017). doi:10.3390/s17081832.

[53] P.K.Q. Nguyen, S.K. Lunsford, Electrochemical response of carbon paste electrode modified with mixture of titanium dioxide/zirconium dioxide in the detection of heavy metals: Lead and cadmium, Talanta. 101 (2012) 110–121. doi:10.1016/j.talanta.2012.09.004.

[54] R. Tekenya, K. Pokpas, N. Jahed, E.I. Iwuoha, Enhanced Specificity and Sensitivity for the Determination of Nickel(II) by Square-wave Adsorptive Cathodic Stripping Voltammetry at Disposable Graphene-modified Pencil Graphite Electrodes, Anal. Lett. 52 (2019) 373–398. doi:10.1080/00032719.2018.1469139.

[55] K. Pokpas, S. Zbeda, N. Jahed, N. Mohamed, P.G. Baker, E.I. Iwuoha, Electrochemically Reduced Graphene Oxide Pencil-Graphite in situ Plated Bismuth-film Electrode for the Determination of Trace Metals by Anodic Stripping Voltammetry, Int. J. Electrochem. Sci. 9 (2014) 736–759.

[56] I.G. David, D.-E. Popa, M. Buleandra, Pencil Graphite Electrodes: A Versatile Tool in Electroanalysis, J. Anal. Methods Chem. (2017) 1–22. doi:10.1155/2017/1905968.

[57] X. Guo, Q. Wang, J. Li, J. Cui, S. Zhou, S. Hao, D. Wu, A mini-electrochemical system integrated micropipet tip and pencil graphite electrode for detection of anticancer drug sensitivity in vitro, Biosens. Bioelectron. 64 (2015) 594–596. doi:10.1016/j.bios.2014.09.086.

[58] F. Kuralay, T. Vural, C. Bayram, E.B. Denkbas, S. Abaci, Carbon nanotube-chitosan modified disposable pencil graphite electrode for Vitamin B 12 analysis, Colloids Surfaces B Biointerfaces. 87 (2011) 18–22. doi:10.1016/j.colsurfb.2011.03.030.

[59] J. Wang, A.N. Kawde, E. Sahlin, Renewable pencil electrodes for highly sensitive stripping potentiometric measurements of DNA and RNA, Analyst. 125 (2000) 5–7. doi:10.1039/a907364g.

[60] J.D. Gale, A.K. Geim, K.S. Novoselov, A.H. Castro Neto, N.M.R. Peres, K.S. Novoselov, A.K. Geim, M.E. Tuckerman, A. Tomadin, A. Loya, J.L. Stair, G. Ren, A.K. Geim, K.S. Novoselov, Geim A. K., Novoselov K. S., M.A.N. Dewapriya, J. a. Barker, D. Henderson, T.L. Anderson, M.P. Ariza, M. Ortiz, M.C. Wang, C. Yan, L. Ma, N. Hu, M.W. Chen, A. Carpio, L.L. Bonilla, F. De Juan, M.A.H. Vozmediano, The rise of graphene., Rev. Mod. Phys. 58 (2012) 710–734. doi:10.1016/j.jmps.2010.02.008.

[61]   the royal swedish academy of Science, GRAPHENE, R. Swedish Acad. Sci. (2010) 1–10. doi:10.1038/news.2010.620.

[62] H. Gürsu, M. Gençten, Y. Şahin, One-step electrochemical preparation of graphene-coated pencil graphite electrodes by cyclic voltammetry and their application in vanadium redox batteries, Electrochim. Acta. 243 (2017) 239–249. doi:10.1016/j.electacta.2017.05.065.

[63] J. Zhu, D. Yang, Z. Yin, Q. Yan, H. Zhang, Graphene and graphene-based materials for energy storage applications, Small. 10 (2014) 3480–3498. doi:10.1002/smll.201303202.

[64] G. Jo, M. Choe, S. Lee, W. Park, Y.H. Kahng, T. Lee, The application of graphene as electrodes in electrical and optical devices, Nanotechnology. 23 (2012) 1–19. doi:10.1088/0957-4484/23/11/112001.

[65] N. Meepun, S. Siriket, S. Dejmanee, Adsorptive stripping voltammetry for determination of cadmium in the presence of cupferron on a nafion-coated bismuth film electrode, Int. J. Electrochem. Sci. 7 (2012) 10582–10591.

[66] A. Koper, M. Grabarczyk, Simultaneous voltammetric determination of trace bismuth(III) and cadmium(II) in water samples by adsorptive stripping voltammetry in the presence of cupferron, J. Electroanal. Chem. 681 (2012) 1–5. doi:10.1016/j.jelechem.2012.05.020.

[67] M. Grabarczyk, A. Koper, Direct Determination of Cadmium Traces in Natural Water by Adsorptive Stripping Voltammetry in the Presence of Cupferron as a Chelating Agent, Electroanalysis. 24 (2012) 33–36. doi:10.1002/elan.201100357.

[68] A.A. Ensafi, T. Khayamian, M. Atabati, Simultaneous voltammetric determination of molybdenum and copper by adsorption cathodic differential pulse stripping method using a principal component artificial neural network, Talanta. 57 (2002) 785–793. doi:10.1016/S0039-9140(02)00103-0.

[69] K. Mahato, S. Kumar, A. Srivastava, P.K. Maurya, R. Singh, P. Chandra, Electrochemical Immunosensors: Fundamentals and Applications in Clinical Diagnostics, Elsevier Inc., 2018. doi:https://doi.org/10.1016/B978-0-12-811762-0.00014-1.

[70] E.P. Achterberg, M. Gledhill, K. Zhu, Voltammetry—Cathodic Stripping ☆, Elsevier Inc., 2018. doi:10.1016/b978-0-12-409547-2.00553-9.

[71] A. Economou, S.D. Bolis, C.E. Efstathiou, G.J. Volikakis, A "virtual" electroanalytical instrument for square wave voltammetry, 467 (2002) 179–188.

[72] S.P. Kounaves, Voltammetric Techniques, n.d.

[73] K.C. Honeychurch, Printed thick-film biosensors, Print. Film. Mater. Sci. Appl. Sensors, Electron. Photonics. (2012) 366–409. doi:10.1533/9780857096210.2.366.

[74] F. Zhao, R.C.T. Slade, J.R. Varcoe, Techniques for the study and development of microbial fuel cells: An electrochemical perspective, Chem. Soc. Rev. 38 (2009) 1926–1939. doi:10.1039/b819866g.

[75] R. Chen, C. Yang, W. Cai, H.Y. Wang, J. Miao, L. Zhang, S. Chen, B. Liu, Use of Platinum as the Counter Electrode to Study the Activity of Nonprecious Metal Catalysts for the Hydrogen Evolution Reaction, ACS Energy Lett. 2 (2017) 1070–1075. doi:10.1021/acsenergylett.7b00219.

[76] J. Wang, J. Lu, S.B. Hocevar, P.A.M. Farias, Bismuth- Coated Carbon Electrodes for Anodic Stripping Voltammetry, Anal. Chem. 72 (2000) 3218–3222.

[77] J. Wang, J. Lu, D. Luo, J. Wang, B. Tian, Simultaneous Adsorptive Stripping

Voltammetric Measurements of Trace Chromium, Uranium, and Iron in the Presence of Cupferron, Electroanalysis. 9 (1997) 1247–1251. doi:10.1002/elan.1140091606.

[78]   A.A. Ensafi, A. Benvidi, T. Khayamian, Determination of Cadmium and Zinc in Water and Alloys by Adsorption Stripping Voltammetry, Anal. Lett. 37 (2004) 449–462. doi:10.1081/AL-120028618.

[79]   M. Grabarczyk, M. Adamczyk, A Simple, Fast, and Inexpensive Simultaneous Determination of Trace Bismuth(III) and Lead(II) in Water Samples by Adsorptive Stripping Voltammetry, J. Anal. Methods Chem. 2017 (2017) 1–6. doi:10.1155/2017/1486497.

[80]   M. Grabarczyk, J. Wasag, Adsorptive Cathodic Stripping Voltammetric Method for Determination of Gallium Using an In Situ Plated Lead Film Electrode, Electroanalysis. 27 (2015) 2596–2600. doi:10.1002/elan.201500235.

[81]   N.M. Thanh, N.D. Luyen, T. Thanh Tam Toan, N. Hai Phong, N. Van Hop, Voltammetry determination of Pb(II), Cd(II), and Zn(II) at bismuth film electrode combined with 8-hydroxyquinoline as a complexing agent, J. Anal. Methods Chem. (2019) 1–11. doi:10.1155/2019/4593135.

[82]   G. Kefala, A. Economou, A. Voulgaropoulos, Adsorptive stripping voltammetric determination of trace uranium with a bismuth-film electrode based on the U(VI) → U(V) reduction step of the uranium-cupferron complex, Electroanalysis. 18 (2006) 223–230. doi:10.1002/elan.200503386.

[83]   D.A. Bessonova, V.D. Ivanov, Catalytic polarographic wave in the vanadium-cupferron system, J. Electroanal. Chem. 759 (2015) 72–76. doi:10.1016/j.jelechem.2015.10.028.

[84]   M. Grabarczyk, C. Wardak, A new voltammetric strategy for sensitive and selective determination of gallium using cupferron as a complexing agent, J. Environ. Sci. Heal. - Part A Toxic/Hazardous Subst. Environ. Eng. 49 (2014) 1142–1148. doi:10.1080/10934529.2014.897156.

105

[85]   C.M.G. van den Berg, O. Abollino, C. Sarzanini, E. Mentasti, M. Aceto, Determination of trace europium by adsorptive cathodic stripping voltammetry after complexation with cupferron, Electroanalysis. 9 (1997) 444–448. doi:10.1002/elan.1140090603.

[86]   M. Grabarczyk, J. Wasag, Determination of trace amounts of Ga(III) by adsorptive stripping voltammetry with in situ plated bismuth film electrode, Talanta. 144 (2015) 1091–1095. doi:10.1016/j.talanta.2015.07.083.

[87]   N. Hui, J. Wang, W. Sun, A new electrochemical method for the determination of proteins with cupferron-cadmium(II) complex, Electroanalysis. 22 (2010) 536–541. doi:10.1002/elan.200900326.

[88]   K. Pokpas, N. Jahed, P.G. Baker, E.I. Iwuoha, N. Mohamed, S. Zbeda, Nafion-graphene nanocomposite in situ plated bismuth-film electrodes on pencil graphite substrates for the determination of trace heavy metals by anodic stripping voltammetry, Int. J. Electrochem. Sci. 9 (2014) 736–759.

[89]   A. Chen, B. Shah, Electrochemical sensing and biosensing based on square wave voltammetry, Anal. Methods. 5 (2013) 2158–2173. doi:10.1039/c3ay40155c.

[90]   J.J. O'Dea, J. Osteryoung, R.A. Osteryoung, Theory of Square Wave Voltammetry for Kinetic Systems, Anal. Chem. 53 (1981) 695–701. doi:10.1021/ac00227a028.

[91]   B. Dogan-Topal, S.. Ozkan, B. Uslu, The Analytical Applications of Square Wave Voltammetry on Pharmaceutical Analysis, Open Chem. Biomed. Methods J. 3 (2010) 56–73. doi:10.2174/1875038901003010056.

[92]   J. Barton, M. Begoña, G. García, D.H. Santos, P. Fanjul-bolado, A. Ribotti, M. Mccaul, D. Diamond, P. Magni, Screen-printed electrodes for environmental monitoring of heavy metal ions : a review, 183 (2015) 503–517. doi:10.1007/s00604-015-1651-0.

[93]   L.G. Dias, S.G. Meirinho, A.C.A. Veloso, L.R. Rodrigues, A.M. Peres, Electronic tongues and aptasensors, Elsevier Ltd., 2017. doi:10.1016/B978-0-08-100741-9.00013-9.

106

[94]   J. P.S., D.S. Sutrave, A Brief Study of Cyclic Voltammetry and Electrochemical Analysis, Int. J. ChemTech Res. 11 (2018) 77–88. doi:10.20902/ijctr.2018.110911.

[95]   E.P. Achterberg, C. Braungardt, Stripping voltammetry for the determination of trace metal speciation and in-situ measurements of trace metal distributions in marine waters, Anal. Chim. Acta. 400 (1999) 381–397.

[96]   J. Osteryoung, P. Chandresekhar, o'Dea. J. J, Kounaves. p. S, Square Wave Voltammetry at the Mercury Film Electrode :Theoretical treatment, Anal. Chem. 58 (1986) 3199–3202.

[97]   S. Chaiyo, E. Mehmeti, K. Žagar, W. Siangproh, O. Chailapakul, K. Kalcher, Electrochemical sensors for the simultaneous determination of zinc, cadmium and lead using a Nafion/ionic liquid/graphene composite modified screen-printed carbon electrode, Anal. Chim. Acta. 918 (2016) 26–34. doi:10.1016/j.aca.2016.03.026.

[98]   P.J. Almeida, L.M. Gonçalves, A.A. Barros, J.A. Rodrigues, R.G. Compton, I.M. Valente, C.M. Rodrigues, Increased sensitivity of anodic stripping voltammetry at the hanging mercury drop electrode by ultracathodic deposition, Anal. Chim. Acta. 701 (2011) 152–156. doi:10.1016/j.aca.2011.05.031.

[99]   B. Zagar, H. Parham, A. Hatamie, Mercury Thin Film at Glassy Carbon Electrode for Captopril in Pharmaceutical Samples, Anal. Bioanal. Electrochem. 7 (2015) 344–357.

[100] O. Abollino, M. Aceto, E. Mentasti, C. Sarzanini, C.M.G. Van Den Berg, Determination of Trace Europium by Adsorptive Cathodic Stripping Voltammetry after Complexation with Cupferron, Electroanalysis. 9 (1997) 444–448. doi:10.1002/elan.1140090603.

[101] J. Limson, T. Nyokong, Substituted catechols as complexing agents for the determination of bismuth, lead, copper and cadmium by adsorptive stripping voltammetry, Anal. Chim. Acta. 344 (1997) 87–95. doi:10.1016/S0003-2670(96)00585-5.

[102] S. Abbasi, A. Farmany, S.S. Mortazavi, Ultrasensitive Simultaneous Quantification of Nanomolar Level of Cd and Zn by Cathodic Adsorptive Stripping Voltammetry in Some

107

Real Samples, Electroanalysis. 22 (2010) 2884–2888. doi:10.1002/elan.201000359.

[103] S. Abbasi, A. Farmany, M. Roushani, S.S. Mortazavi, Sensitive quantification of trace zinc in water samples by adsorptive stripping voltammetry, Water Sci. Technol. 69 (2014) 438–442. doi:10.2166/wst.2013.704.

[104] Pomeroy.S.R, B.M. Denton, R.. Armstrong, Voltammetry at the thin film mercury electrode(TFME), (1989) 877–880.

[105] S. Lee, S. Park, E. Choi, Y. Piao, Voltammetric determination of trace heavy metals using an electrochemically deposited graphene / bismuth nanocomposite fi lm-modi fi ed glassy carbon electrode, J. Electroanal. Chem. 766 (2016) 120–127. doi:10.1016/j.jelechem.2016.02.003.

[106] S.B. Hocevar, I. Švancara, B. Ogorevc, K. Vytřas, Antimony film electrode for electrochemical stripping analysis, Anal. Chem. 79 (2007) 8639–8643. doi:10.1021/ac070478m.

[107] A.M. Ashrafi, K. Vytřas, Codeposited antimony-bismuth film carbon paste electrodes for electrochemical stripping determination of trace heavy metals, Int. J. Electrochem. Sci. 8 (2013) 2095–2103.

[108] D. Yang, L. Wang, Z. Chen, M. Megharaj, R. Naidu, Voltammetric Determination of Lead (II) and Cadmium (II) Using a Bismuth Film Electrode Modified with Mesoporous Silica Nanoparticles, Electrochim. Acta. 132 (2014) 223–229. doi:10.1016/j.electacta.2014.03.147.

[109] Z. Wang, H. Wang, Z. Zhang, G. Liu, Electrochemical determination of lead and cadmium in rice by a disposable bismuth/electrochemically reduced graphene/ionic liquid composite modified screen-printed electrode, Sensors Actuators, B Chem. 199 (2014) 7–14. doi:10.1016/j.snb.2014.03.092.

[110] M. Frena, I. Campestrini, O.C. De Braga, A. Spinelli, In situ bismuth-film electrode for

108

square-wave anodic stripping voltammetric determination of tin in biodiesel, Electrochim. Acta. 56 (2011) 4678–4684. doi:10.1016/j.electacta.2011.02.111.

[111] E.A. Hutton, S.B. Hočevar, L. Mauko, B. Ogorevc, Bismuth film electrode for anodic stripping voltammetric determination of tin, Anal. Chim. Acta. 580 (2006) 244–250. doi:10.1016/j.aca.2006.07.075.

[112] J. Ping, Y. Wang, J. Wu, Y. Ying, Development of an electrochemically reduced graphene oxide modified disposable bismuth film electrode and its application for stripping analysis of heavy metals in milk, FOOD Chem. 151 (2014) 65–71. doi:10.1016/j.foodchem.2013.11.026.

[113] M. Morfobos, A. Economou, A. Voulgaropoulos, Simultaneous determination of nickel(II) and cobalt(II) by square wave adsorptive stripping voltammetry on a rotating-disc bismuth-film electrode, Anal. Chim. Acta. 519 (2004) 57–64. doi:10.1016/j.aca.2004.05.022.

[114] U. Kurgoz, H. Tural, S. Timur, N. Pazarlioglu, A. Telefoncu, Laccase Biosensors Based on Mercury Thin Film Electrode, (2005) 447–456.

[115] Ping Wu.H, Nature and Stability of Mercury Thin Films on Glassy Carbon Electrodes under Fast-Scan Anodic Stripping Voltammetry, (1994) 3151–3157.

[116] D. Demetriades, A. Economou, A. Voulgaropoulos, A study of pencil-lead bismuth-film electrodes for the determination of trace metals by anodic stripping voltammetry, Anal. Chim. Acta. 519 (2004) 167–172. doi:10.1016/j.aca.2004.05.008.

[117] R.R. Nair, P. Blake, A.N. Grigorenko, K.S. Novoselov, T.J. Booth, T. Stauber, N.M.R. Peres, A.K. Geim, Fine structure constant defines visual transparency of graphene, Science (80-.). 320 (2008) 1308. doi:10.1126/science.1156965.

[118] P.S. Karthik, A.L. Himaja, S.P. Singh, Carbon-allotropes: Synthesis methods, applications and future perspectives, Carbon Lett. 15 (2014) 219–237. doi:10.5714/CL.2014.15.4.219.

109

[119] S. Nasir, M.Z. Hussein, Z. Zainal, N.A. Yusof, Carbon-based nanomaterials/allotropes: A glimpse of their synthesis, properties and some applications, Materials (Basel). 11 (2018) 1–24. doi:10.3390/ma11020295.

[120] K.S. Novoselov, V.I. Fal'Ko, L. Colombo, P.R. Gellert, M.G. Schwab, K. Kim, A roadmap for graphene, Nature. 490 (2012) 192–200. doi:10.1038/nature11458.

[121] K.S. Novoselov, A.K. Geim, S. V. Morozov, D. Jiang, Y. Zhang, S. V. Dubonos, I. V. Grigorieva, A.A. Firsov, Electric Field Effect in Atomically Thin Carbon Films, Science (80-.). 306 (2004) 666–669. doi:10.1126/science.aab1343.

[122] S. Iijima, Carbon nanotubes: Past, present, and future, Phys. B Condens. Matter. 323 (2002) 1–5. doi:10.1016/S0921-4526(02)00869-4.

[123] H.W. Kroto, J.R. Heath, S.C. O'Brien, R.F. Curl, R.E. Smalley, C60 : Buckminsterfullerene, Nature. 318 (1985) 162–163.

[124] B. Garg, T. Bisht, Y.C. Ling, Graphene-based nanomaterials as heterogeneous acid catalysts: A comprehensive perspective, Molecules. 19 (2014) 14582–14614. doi:10.3390/molecules190914582.

[125] U.K. Sur, Graphene: A Rising Star on the Horizon of Materials Science, Int. J. Electrochem. (2012) 1–12. doi:10.1155/2012/237689.

[126] N.A.A. Ghany, S.A. Elsherif, H.T. Handal, Revolution of Graphene for different applications: State-of-the-art, Surfaces and Interfaces. 9 (2017) 93–106. doi:10.1016/j.surfin.2017.08.004.

[127] W. Choi, I. Lahiri, R. Seelaboyina, Y.S. Kang, Synthesis of graphene and its applications: A review, Crit. Rev. Solid State Mater. Sci. 35 (2010) 52–71. doi:10.1080/10408430903505036.

[128] C. Schafhaeutl, On the combinations of carbon with silicon and iron , and other metals , forming the different species of cast iron , steel , and malleable, Philos. Mag. Ser. 16

110

(1840) 570–590.

[129] Brodie, On the Atomic Weight of Graphite, Philos. Trans. R. Soc. B Biol. Sci. 149 (1859) 249–259. doi:10.1098/rstb.1983.0080.

[130] E.P. Randviir, D.A.C. Brownson, C.E. Banks, A decade of graphene research: Production, applications and outlook, Mater. Today. 17 (2014) 426–432. doi:10.1016/j.mattod.2014.06.001.

[131] A.H.C. Neto, F. Guinea, N.M.R. Peres, K.S. Novoselov, A.K. Geim, The electronic properties of graphene, 81 (2009) 109–162. doi:10.1103/RevModPhys.81.109.

[132] P. Avouris, C. Dimitrakopoulos, Graphene: Synthesis and applications, Mater. Today. 15 (2012) 86–97. doi:10.1016/S1369-7021(12)70044-5.

[133] V. Gupta, N. Sharma, U. Singh, M. Arif, A. Singh, Higher oxidation level in graphene oxide, Optik (Stuttg). 143 (2017) 115–124. doi:10.1016/j.ijleo.2017.05.100.

[134] P. Blake, E.W. Hill, A.H. Castro Neto, K.S. Novoselov, D. Jiang, R. Yang, T.J. Booth, A.K. Geim, Making graphene visible, Appl. Phys. Lett. 91 (2007). doi:10.1063/1.2768624.

[135] Y. Zhu, S. Murali, W. Cai, X. Li, W. ji Suk, R.J. Potts, R.S. Ruoff, Graphene and Graphene Oxide: Synthesis, Properties, and Applications, 22 (2010) 3906–3924.

[136] M. Anthony Xavior, H.G. Prashantha Kumar, Processing and Characterization Techniques of Graphene Reinforced Metal Matrix Composites (GRMMC); A Review, Mater. Today Proc. 4 (2017) 3334–3341. doi:10.1016/j.matpr.2017.02.220.

[137] Q. Zheng, J.-K. Kim, Graphene for Transparent Conductors, (2015). doi:10.1007/978-1-4939-2769-2.

[138] R. Muñoz, C. Gómez-Aleixandre, Review of CVD synthesis of graphene, Chem. Vap. Depos. 19 (2013) 297–322. doi:10.1002/cvde.201300051.

111

[139] F. Pendolino, N. Armata, Graphene Oxide in Environmental Remediation Process, 2017. http://www.springer.com/series/8884.

[140] W.S. Hummers, R.E. Offeman, Preparation of Graphitic Oxide, J. Am. Chem. Soc. 80 (1958) 1339. doi:10.1021/ja01539a017.

[141] F. Pendolino, N. Armata, Graphene Oxide in Environmental Remediation Process, (2017). doi:10.1007/978-3-319-60429-9.

[142] A. Adetayo, D. Runsewe, Synthesis and Fabrication of Graphene and Graphene Oxide : A Review, Compos. Mater. 9 (2019) 207–229. doi:10.4236/ojcm.2019.92012.

[143] B.C. Smith, Fundamentals of TRANSFORM FOURIER SPECTROSCOPY INFRARED, 2011.

[144] S. Ruiz, J.A. Tamayo, J.D. Ospina, D.P.N. Porras, M.E.V. Zapata, J.H.M. Hernandez, C.H. Valencia, F. Zuluaga, C.D.G. Tovar, Antimicrobial films based on nanocomposites of chitosan/poly(Vinyl alcohol)/graphene oxide for biomedical applications, Biomolecules. 9 (2019) 1–17. doi:10.3390/biom9030109.

[145] P. Dakshinamoorthy, S. Vaithilingam, Platinum-copper doped poly(sulfonyldiphenol/cyclophosphazene/benzidine)-graphene oxide composite as an electrode material for single stack direct alcohol alkaline fuel cells, RSC Adv. 7 (2017) 34922–34932. doi:10.1039/c7ra04525e.

[146] A.H. Wazir, I.W. Kundi, Synthesis of graphene nano sheets by the rapid reduction of electrochemically exfoliated graphene oxide induced by microwaves, J. Chem. Soc. Pakistan. 38 (2016) 11–16.

[147] D. Titus, E. James Jebaseelan Samuel, S.M. Roopan, Nanoparticle characterization techniques, Elsevier Inc., 2019. doi:10.1016/b978-0-08-102579-6.00012-5.

[148] W.L. Bragg, The Structure of Some Crystals as Indicated by their Diffraction, 89 (1913) 248–277.

[149] M.S. Braga, O.F. Gomes, R. Flavia, V. Villamil, E.R. Braga, W. Borysow, W.J. Salcedo, Multispectral colorimetric portable system for detecting metal ions in liquid media, Circuits and Transducers. (2019) 1–6. doi:10.1109/INSCIT.2019.8868861.

[150] C.D. Joy, B.J. Pawley, High resolution scanning electron microscopy, J. Sci. Instrum. 47 (1992) 80–100. doi:10.1088/0950-7671/42/2/305.

[151] B.D. Williams, B.C. Carter, The Transmission Electron Microscope, (1996) 1–17.

[152] E. Ruska, The development of the electron microscope and of electron microscopy, 59 (1987) 627–638.

[153] X. Jiang, T. Higuchi, H. Jinnai, Transmission Electron Microscopy, Springer Japan, 2019. doi:10.1007/978-4-431-56877-3.

[154] M. Joshi, A. Bhattacharyya, S.W. Ali, Characterization techniques for nanotechnology applications in textiles, Indian J. Fibre Text. Res. 33 (2008) 304–317.

[155] M. Joshi, A. Bhattacharyya, Characterization techniques for nanotechnology applications in textiles, Fibre Text. 33 (2008) 304–317.

[156] D. Yang, A. Velamakanni, G. Bozoklu, S. Park, M. Stoller, R.D. Piner, S. Stankovich, I. Jung, D.A. Field, C.A. Ventrice, R.S. Ruoff, Chemical analysis of graphene oxide films after heat and chemical treatments by X-ray photoelectron and Micro-Raman spectroscopy, Carbon N. Y. 47 (2009) 145–152. doi:10.1016/j.carbon.2008.09.045.

[157] M. Bera, Chandravati, P. Gupta, P.K. Maji, Facile One-Pot Synthesis of Graphene Oxide by Sonication Assisted Mechanochemical Approach and Its Surface Chemistry, J. Nanosci. Nanotechnol. 18 (2018) 902–912. doi:10.1166/jnn.2018.14306.

[158] V. Ţucureanu, A. Matei, A.M. Avram, FTIR Spectroscopy for Carbon Family Study, Crit. Rev. Anal. Chem. 46 (2016) 502–520. doi:10.1080/10408347.2016.1157013.

[159] J. Sun, L. Yu, C. Seung, K. Shin, J. Hun, Liquid-phase exfoliation of expanded graphites

113

into graphene nanoplatelets using amphiphilic organic molecules, J. Colloid Interface Sci. 417 (2014) 379–384. doi:10.1016/j.jcis.2013.11.066.

[160] J.A. Luceño-Sánchez, G. Maties, C.G. Gonzalez-Arellano, M. Díez-Pascual, Synthesis and Characterization of Graphene Oxide Derivatives via Functionalization Reaction with Hexamethylene Diisocyanate †, 3 (2019) 1–6. doi:10.3390/IOCN.

[161] N. Pan, D. Guan, T. He, R. Wang, I. Wyman, Y. Jin, C. Xia, Removal of Th4+ ions from aqueous solutions by graphene oxide, J. Radioanal. Nucl. Chem. 298 (2013) 1999–2008. doi:10.1007/s10967-013-2660-2.

[162] V. Ţucureanu, A. Matei, A.M. Avram, V. Ţucureanu, A. Matei, A. Marius, A. Ftir, A. Matei, A.M. Avram, FTIR Spectroscopy for Carbon Family Study FTIR Spectroscopy for Carbon Family Study, Crit. Rev. Anal. Chem. 46 (2016) 502–520. doi:10.1080/10408347.2016.1157013.

[163] H. He, J. Klinowski, M. Forster, A. Lerf, A new structural model for graphite oxide, Chem. Phys. Lett. 287 (1998) 53–56. doi:10.1016/S0009-2614(98)00144-4.

[164] G. Vinodha, L. Cindrella, P.D. Shima, Graphene oxide based highly sensitive electrochemical sensor for detection of environmental pollutants and biomolecules, Mater. Res. Express. 6 (2019). doi:10.1088/2053-1591/ab2852.

[165] V. Kumar, V. Singh, S. Umrao, V. Parashar, S. Abraham, A.K. Singh, G. Nath, P.S. Saxena, A. Srivastava, Facile, rapid and upscaled synthesis of green luminescent functional graphene quantum dots for bioimaging, RSC Adv. 4 (2014) 21101–21107. doi:10.1039/c4ra01735h.

[166] J. Theerthagiri, R. Sudha, K. Premnath, P. Arunachalam, J. Madhavan, A.M. Al-Mayouf, Growth of iron diselenide nanorods on graphene oxide nanosheets as advanced electrocatalyst for hydrogen evolution reaction, Int. J. Hydrogen Energy. 42 (2017) 13020–13030. doi:10.1016/j.ijhydene.2017.04.042.

114

[167] E. Rommozzi, M. Zannotti, R. Giovannetti, C.A. D'amato, S. Ferraro, M. Minicucci, R. Gunnella, A. Di Cicco, Reduced graphene oxide/TiO2 nanocomposite: From synthesis to characterization for efficient visible light photocatalytic applications, Catalysts. 8 (2018) 1–14. doi:10.3390/catal8120598.

[168] F. Sima, C. Ristoscu, L. Duta, O. Gallet, K. Anselme, I.N. Mihailescu, Laser thin films deposition and characterization for biomedical applications, Elsevier Ltd, 2016. doi:10.1016/B978-0-08-100883-6.00003-4.

[169] R. Kohli, Methods for Monitoring and Measuring Cleanliness of Surfaces, Elsevier, 2012. doi:10.1016/B978-1-4377-7883-0.00003-1.

[170] M. Vanitha, N. Balasubramanian, I.M. Joni, C. Panatarani, Detection of mercury ions using L-cysteine modified electrodes by anodic stripping voltammetric method, AIP Conf. Proc. (2018). doi:10.1063/1.5021194.

[171] R. Siburian, H. Sihotang, S. Lumban Raja, M. Supeno, C. Simanjuntak, New route to synthesize of graphene nano sheets, Orient. J. Chem. 34 (2018) 182–187. doi:10.13005/ojc/340120.

[172] S.N. Alam, N. Sharma, L. Kumar, Synthesis of Graphene Oxide (GO) by Modified Hummers Method and Its Thermal Reduction to Obtain Reduced Graphene Oxide (rGO)*, Graphene. 06 (2017) 1–18. doi:10.4236/graphene.2017.61001.

[173] A. Shalaby, D. Nihtianova, P. Markov, A. Staneva, Structural analysis of reduced graphene oxide by transmission electron microscopy, 47 (2015) 291–295.

[174] C.A. Ávila-Orta, F. Soriano Corral, H.A. Fonseca-Florido, F.I. Estrada Aguilar, S.G. Solís Rosales, J.M. Mata Padilla, P. González Morones, S. Fernández Tavizón, E. Hernández-Hernández, Starch-graphene oxide bionanocomposites prepared through melt mixing, J. Appl. Polym. Sci. 135 (2018). doi:10.1002/app.46037.

[175] M. Perween, D.B. Parmar, G.R. Bhadu, D.N. Srivastava, Polymer–graphite composite: A

115

versatile use and throw plastic chip electrode, Analyst. 139 (2014) 5919–5926. doi:10.1039/c4an01405g.

[176] M. Lv, X. Wang, J. Li, X. Yang, C. Zhang, J. Yang, H. Hu, Cyclodextrin-reduced graphene oxide hybrid nanosheets for the simultaneous determination of lead(II) and cadmium(II) using square wave anodic stripping voltammetry, Electrochim. Acta. 108 (2013) 412–420. doi:10.1016/j.electacta.2013.06.099.

[177] L. Chen, Y. Tang, K. Wang, C. Liu, S. Luo, Direct electrodeposition of reduced graphene oxide on glassy carbon electrode and its electrochemical application, Electrochem. Commun. 13 (2011) 133–137. doi:10.1016/j.elecom.2010.11.033.

[178] P. Tan, J. Sun, Y. Hu, Z. Fang, Q. Bi, Y. Chen, J. Cheng, Adsorption of Cu2+, Cd2+ and Ni2+ from aqueous single metal solutions on graphene oxide membranes, J. Hazard. Mater. 297 (2015) 251–260. doi:10.1016/j.jhazmat.2015.04.068.

[179] Z. Zhang, H.C. Schniepp, D.H. Adamson, Characterization of graphene oxide: Variations in reported approaches, Carbon N. Y. 154 (2019) 510–521. doi:10.1016/j.carbon.2019.07.103.

[180] M.T.. Aunkor, I.M. Mahbubul, R. Saidur, C.S.. Metselaar, RSC Advances, RSC Adv. 86 (2015) 1–32. doi:10.1039/C5RA10520J.This.

[181] X. Wang, I. Kholmanov, H. Chou, R.S. Ruoff, Simultaneous Electrochemical Reduction and Delamination of Graphene Oxide Films, ACS Nano. 9 (2015) 8737–8743. doi:10.1021/acsnano.5b03814.

[182] K. Chen, D. Xue, S. Komarneni, Nanoclay assisted electrochemical exfoliation of pencil core to high conductive graphene thin-film electrode, J. Colloid Interface Sci. 487 (2017) 156–161. doi:10.1016/j.jcis.2016.10.028.

[183] R. Hack, C.H.G. Correia, R.A.D.S. Zanon, S.H. Pezzin, Characterization of graphene nanosheets obtained by a modified hummer's method, Rev. Mater. 23 (2018).

116

doi:10.1590/s1517-707620170001.0324.

[184] T. Somanathan, K. Prasad, K.K. Ostrikov, A. Saravanan, V.M. Krishna, Graphene oxide synthesis from agro waste, Nanomaterials. 5 (2015) 826–834. doi:10.3390/nano5020826.

[185] R. Kumar, R.M. Kumar, P. Bera, S. Ariharan, D. Lahiri, I. Lahiri, Temperature-time dependent transmittance, sheet resistance and bonding energy of reduced graphene oxide on soda lime glass, Appl. Surf. Sci. 425 (2017) 558–563. doi:10.1016/j.apsusc.2017.06.224.

[186] R. Navratil, A. Kotzianova, V. Halouzka, T. Opletal, I. Triskova, L. Trnkova, J. Hrbac, Polymer lead pencil graphite as electrode material: Voltammetric, XPS and Raman study, J. Electroanal. Chem. 783 (2016) 152–160. doi:10.1016/j.jelechem.2016.11.030.

[187] R.M. Alonso, M.I. San-Martín, A. Sotres, A. Escapa, Graphene oxide electrodeposited electrode enhances start-up and selective enrichment of exoelectrogens in bioelectrochemical systems, Sci. Rep. 7 (2017) 1–10. doi:10.1038/s41598-017-14200-7.

[188] E. Alipour, M.R. Majidi, A. Saadatirad, S.M. Golabi, A.M. Alizadeh, Simultaneous determination of dopamine and uric acid in biological samples on the pretreated pencil graphite electrode, Electrochim. Acta. 91 (2013) 36–42. doi:10.1016/j.electacta.2012.12.079.

[189] B. Devadas, M. Rajkumar, S.M. Chen, R. Saraswathi, Electrochemically reduced graphene oxide/ Neodymium hexacyanoferrate modified electrodes for the electrochemical detection of paracetomol, Int. J. Electrochem. Sci. 7 (2012) 3339–3349.

[190] M. Zaib, M.M. Athar, Electrochemical evaluation of Phanerocheaete chrysosporium based carbon paste electrode with potassium ferricyanide redox system, Int. J. Electrochem. Sci. 10 (2015) 6690–6702.

[191] L. Fotouhi, M. Fatollahzadeh, M.M. Heravi, Electrochemical behavior and voltammetric determination of sulfaguanidine at a glassy carbon electrode modified with a multi-walled

117

carbon nanotube, Int. J. Electrochem. Sci. 7 (2012) 3919–3928.

[192] N. Ramalakshmi, S. Muthukumar, B. Marichamy, Preparation and Characterization of 4-hydroxybenzylidencarbamide-CTAB modified Glassy Carbon Electrode by using [Fe (CN) 6] 4-/[Fe (CN) 6] 3-redox system, J. Chem. Phys. Sci. 2 (2013) 16–24. www.ijcps.org.

[193] B.S. He, W.B. Chen, Voltammetric determination of sulfonamides with a modified glassy carbon electrode using carboxyl multiwalled carbon nanotubes, J. Braz. Chem. Soc. 27 (2016) 2216–2225. doi:10.5935/0103-5053.20160114.

[194] M. Puttaiah, A.N. Yanjerappa, Development of Gold Modified Disposable Pencil Graphite Electrode for the Electrochemical Investigation of Acetaminophen Present in Pharmaceutical formulations and biological samples, Anal. Bioanal. Electrochem. 9 (2017) 841–861.

[195] B.K. Shrestha, R. Ahmad, S. Shrestha, C.H. Park, C.S. Kim, Globular Shaped Polypyrrole Doped Well-Dispersed Functionalized Multiwall Carbon Nanotubes/Nafion Composite for Enzymatic Glucose Biosensor Application, Sci. Rep. 7 (2017) 1–13. doi:10.1038/s41598-017-16541-9.

[196] M. Sakthivel, S. Ramaraj, S.M. Chen, B. Dinesh, Synthesis of rose like structured LaCoO 3 assisted functionalized carbon nanofiber nanocomposite for efficient electrochemical detection of anti-inflammatory drug 4-aminoantipyrine, Electrochim. Acta. 260 (2018) 571–581. doi:10.1016/j.electacta.2017.11.122.

[197] E. Eksin, E. Zor, A. Erdem, H. Bingol, Electrochemical monitoring of biointeraction by graphene-based material modified pencil graphite electrode, Biosens. Bioelectron. 92 (2017) 207–214. doi:10.1016/j.bios.2017.02.016.

[198] S. Xiong, M. Wang, D. Cai, Y. Li, N. Gu, Z. Wu, Electrochemical Detection of Pb(II) by Glassy Carbon Electrode Modified with Amine-Functionalized Magnetite Nanoparticles, Anal. Lett. 46 (2013) 912–922. doi:10.1080/00032719.2012.747094.

[199] X. Cui, R. Lv, R.U.R. Sagar, C. Liu, Z. Zhang, Reduced graphene oxide/carbon nanotube hybrid film as high performance negative electrode for supercapacitor, Electrochim. Acta. 169 (2015) 342–350. doi:10.1016/j.electacta.2015.04.074.

[200] H. Cui, W. Sun, X. Li, H. Zou, Z. Yuan, Determination of trace titanium(iv) by differential pulse catalytic adsorptive stripping voltammetry at a bismuth film electrode, Anal. Methods. 5 (2013) 1784–1789. doi:10.1039/c3ay26249a.

[201] R. Tekenya, K. Pokpas, N. Jahed, E.I. Iwuoha, Enhanced Specificity and Sensitivity for the Determination of Nickel(II) by Square-wave Adsorptive Cathodic Stripping Voltammetry at Disposable Graphene-modified Pencil Graphite Electrodes, Anal. Lett. 52 (2019) 373–398. doi:10.1080/00032719.2018.1469139.

[202] G. Kefala, A. Economou, M. Sofoniou, Determination of trace aluminium by adsorptive stripping voltammetry on a preplated bismuth-film electrode in the presence of cupferron, Talanta. 68 (2006) 1013–1019. doi:10.1016/j.talanta.2005.07.001.

[203] Y. Wei, C. Gao, F.L. Meng, H.H. Li, L. Wang, J.H. Liu, X.J. Huang, SnO 2/reduced graphene oxide nanocomposite for the simultaneous electrochemical detection of cadmium(II), lead(II), copper(II), and mercury(II): An interesting favorable mutual interference, J. Phys. Chem. C. 116 (2012) 1034–1041. doi:10.1021/jp209805c.

[204] T.M. Reddy, K. Balaji, S. Reddy, J. Reddy, Differential Pulse Adsorptive Stripping Voltammetric Determination of Benzocaine and Butacaine with Nafion Modified Glassy Carbon Electrode, 79 (2006) 253–259.

[205] M. Lv, X. Wang, J. Li, X. Yang, C. Zhang, J. Yang, H. Hu, Cyclodextrin-reduced graphene oxide hybrid nanosheets for the simultaneous determination of lead(II) and cadmium(II) using square wave anodic stripping voltammetry, Electrochim. Acta. 108 (2013) 412–420. doi:10.1016/j.electacta.2013.06.099.

[206] Y. Wu, N.B. Li, H.Q. Luo, Simultaneous measurement of Pb, Cd and Zn using differential pulse anodic stripping voltammetry at a bismuth/poly(p-aminobenzene sulfonic acid) film

119

electrode, Sensors Actuators, B Chem. 133 (2008) 677–681. doi:10.1016/j.snb.2008.04.001.

[207] E. Czop, A. Economou, A. Bobrowski, A study of in situ plated tin-film electrodes for the determination of trace metals by means of square-wave anodic stripping voltammetry, Electrochim. Acta. 56 (2011) 2206–2212. doi:10.1016/j.electacta.2010.12.017.

[208] J. Shi, F. Tang, H. Xing, H. Zheng, L. Bi, W. Wang, Electrochemical detection of Pb and Cd in paper-based microfluidic devices, J. Braz. Chem. Soc. 23 (2012) 1124–1130. doi:10.1590/S0103-50532012000600018.

[209] H. Wang, G. Zhao, Z. Zhang, Y. Yi, Z. Wang, G. Liu, A portable electrochemical workstation using disposable screen-printed carbon electrode decorated with multiwall carbon nanotube-ionic liquid and bismuth film for Cd(II) and Pb(II) determination, Int. J. Electrochem. Sci. 12 (2017) 4702–4713. doi:10.20964/2017.06.73.

120